Power System Oscillations

Detection Estimation & Control

Morten Hemmingsson

LUND UNIVERSITY

Doctoral Dissertation in Industrial Automation
Department of Industrial Electrical Engineering
and Automation

Department of
Industrial Electrical Engineering and Automation
Lund Institute of Technology
Lund University
P.O. Box 118
S-221 00 LUND
SWEDEN

http://www.iea.lth.se

ISBN 91-88934-27-6
CODEN:LUTEDX/(TEIE-1035)/1-158/(2003)

Printed in Sweden by Universitetstryckeriet, Lund University

Abstract

The topic of this thesis is the electro-mechanical oscillations which to some extent always are present in a power system. The demand of electric power is ever increasing. At the same time, the tolerance of disruptions in the power supply is decreasing. The deregulated market together with distributed generation have then pushed the system to operate during circumstances for which it was not designed. To this we can then add that getting concessions for new lines becomes more and more difficult in densly populated areas. All these factors makes the electric power system operate with smaller safety margins. Decreasing these margins limits with sustained availability is achieved by the application of advanced monitoring and control methods.

This thesis deals with this in several time-scales. When a large oscillation occurs it is important to detect it as fast as possible as the remedial action depends on if the current operating is due to a fault or an oscillation. In the thesis, a new method to distinguish these incidents from each other is presented.

In a slower time-scale it is important to monitor the dynamics of the electromechanical modes. This information can be used to verify that simulations correspond to the real world behaviour. Real-time methods can also be used to alarm operators or arm special protection schemes if the power system enters undesired operating conditions. A number of methods are studied and then evaluated on three case studies.

Finally, load modulation for damping enhancement is studied. It has previously been shown that modulation of active power at the transmission level increases the damping of the power system when correctly performed. Loads suitable for load modulation at the transmission level are rare and using actuators at the distribution level creates new problems. It is shown that it is possible to detect poor damping at the distribution level, thus reducing the need of communications. It is also shown how the variation of active and reactive power at

the transmission level, caused by modulation of active power at the distribution level can be estimated without knowledge of the complete distribution network. This is most important as the active and reactive variations counteract each other. Finally load modulation at distribution level is evaluated on two test systems. It is shown that the damping is increased and that the influence of the reactive variation decreases the performance of load modulation. The degradation of the control scheme is, however, small in the studied cases.

Acknowledgements

This thesis, although written by me, would not have been possible without the cooperation and aid of several persons. My supervisors, Gustaf Olsson and Olof Samuelsson deserves a great thank for guiding me through the traps and pitfalls of research. Gustaf's open mind and vast knowledge of various fields is invaluable when working in the cross-lands of different areas. His reading of the manuscript has also improved the final product a lot. Olof was the one who introduced me to power systems and showed me that it could be so much more than asymmetric faults in phase quantities. I also appreciate his view that results should be possible to explain by using the basic mechanisms behind different phenomena. Both of them has been invaluable for keeping me on the track, broaden my view and preventing me to stare too much at the same spot.

Having Sture Lindahl at hand has been a great asset. I am most grateful to him for introducing me to the world of relay protection. Sture has revealed the interesting things behind the seemingly boring name. His encyclopedic knowledge has also been of great help for making rough but realistic estimates of power system behaviour.

Lars Gertmar, Daniel Karlsson, Kenneth Walve, Bo Eliasson, Jan Rønne-Hansen (†2002), György Sárosi and Sture Lindahl have all been part of the project steering committee and provided many interesting comments and suggestions.

A good theory is a nice starting point but it is even better if it can be verified by measurements and experiments. Obtaining measurements is simple, at least in theory. When the requirements on equipment turned out to be extreme it was not easy even in theory. At that time, Arne Hejde Nielsen and Knud Ole Helgesen Pedersen at the technical university of Denmark showed up and offered to perform measurements with their newly developed equipment. Thanks to their measurements it was possible to see the electro-mechanical dy-

namics in a wall-outlet in their lab! Some time later, Daniel Karlsson at ABB asked if I was interested in time synchronized measurements from their new equipment. Again, this was an extraordinary offer and thanks to Daniel and his coworkers I did not have to do anything other than to copy 8 GB of collected data onto my computer.

Measurements are good but there are events that we would not like to experience. Tweaking a simulator to simulate these cases can be difficult due to the complexity of a power system. Kenneth Walve at Svenska Kraftnät performed simulations in ARISTO, mimicing the behaviour I wanted to study without any hesitation on how to accomplish the desired behaviour. Thanks also to Anders Fransson and Dag Ingemansson for interesting discussions and fault recorder measurements.

Not having to perform measurements oneself often implies heavy use of computers to analyze the data. Thanks to Gunnar Lindstedt, Olof Strömstedt (†2002) and Ulf Jeppsson I have yet to experience any computer problems.

Ulf together with Gustaf, Anita Borné and Christina Rentschler has also prevented a lot of frustration from my side by taking care of all the bureaucracy. Thanks also to Bengt Simonsson, Getachew Darge and Carina Lindström for help with various practical things.

I would like to express my gratitude to all persons at the department for providing the nice and stimulating environment in which I work. Among my colleagues I would especially like to mention Christian Rosén, the department chief opinionist, for always sharing his thoughts about good and bad taste when it comes to design and typesetting.

Still, this help in my profession is nothing compared to the love and support I have got from my family. My parents, Sten and Margareta, thank you for your encouragement, support and guidance. My dear and beloved Malin has enhanced my life to a large extent especially during the last weeks which I hope I can return someday. I also admire Astrid for always knowing what is most important in life, herself!

This project has been supported by Elforsk and ABB Automation Technology Products AB whos financial support is greatly acknowledged.

Lund March 2003
Morten Hemmingsson

Contents

Chapter 1

Introduction

Electricity consumed in outlets is extremely perishable. At the same time the switch is turned on, the exact amount of extra electric power is produced. When the switch is turned off, the production of the power required for that device ceases. The ability to meet the required power demand for a complete network, possibly covering several countries, requires an advanced control system for the generating units. The increased requirement of electric power combined with the reluctance to build new transmission lines implies that the transmission systems are more stressed and are operating closer to the stability limits than they were designed for. The introduction of the deregulated market in several countries has further stressed the situation as the power systems are not operated during the circumstances for which they were designed.

Whereas research and development on control and protection of individual components as well as the power system in itself has been ongoing ever since the first power systems were put into service, this is not true for monitoring and surveillance. The use of advanced control is based on extensive simulations. The models used for these simulations can, however, not be assured to always be correct. Furthermore, the number of cases studied can not always be guaranteed to be enough. This brings up the need for early warning systems as well as online monitoring and detection of the potentially dangerous situations that will not show up in simulations because of errors in the models or by omitting some operating conditions in the simulation studies. The main topic of this

thesis is to some extent remedy this lack of online knowledge by investigating different detection and warning schemes, preferably based on local measurements. Detection of a dangerous situation can then enable the use of special protection schemes.

1.1 Motivation

The motivation for online monitoring and early waring systems is perhaps best viewed by an actual example.

> The cascade of events on the very hot August 10, 1996 started when a 500 kV line in Oregon sagged into a tree and tripped. The load was shifted to other lines, and forty-six minutes later another 500 kV line sagged into a tree and was tripped. An hour later yet another 500 kV line was lost. The situation still seemed acceptable, but voltage support was critical. Three minutes later, when another line tripped and generators were taken off-line by over-excitation protection, the northern and southern parts of the WSCC (Western Systems Coordinating Council) system began to oscillate against each other. When the growing oscillations on the Pacific AC Intertie reached an amplitude of 1 000 MW, the AC and DC interties finally opened and the WSCC system broke apart into four islands. A total of 30 000 MW load and 27 000 MW generation was lost and 7.5 million customers were without power.
>
> The aftermath of August 10 was mainly about "How could this happen?" The key point regarding August 10 was that the WSCC planning models predicted the operating point as stable, when oscillations in fact broke the system apart, see Figure 1.1. Operators acted in agreement with experience of the system as described by the planning model, giving little reason for concern about instability. As the outages progressed, they did not study the data from the newly installed Portable Power System Monitor (PPSM), which actually was very close at hand, yet not routinely displayed (upper part of Figure 1.1).
>
> The August 10 breakup demonstrated how much of power system

reliability was based on the planning models. They were immediately reviewed and adjusted to replicate the PPSM data. With the updated model, the events on August 10, 1996, could now be accurately predicted knowing the operating point. There is still the question, however, if the behaviour will be correctly predicted also under other extreme conditions. Direct measurements here serve as a guarantee that, whatever models are used, the true behaviour of the system can always be observed. The phasor measurement system now in operation supplying data to the control centre in real-time is particularly valuable for this purpose.

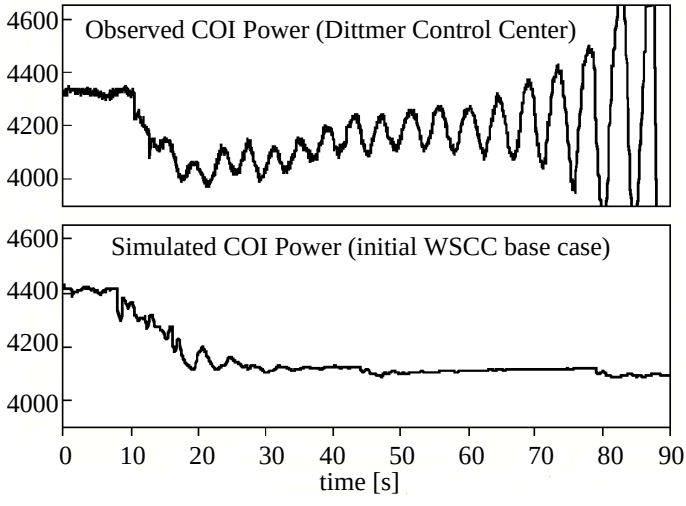

Figure 1.1: Power measurements on the California Oregon Intertie (COI) of the August 10, 1996 event and simulations of the same event with the models in use at the time of the event (picture from Samuelsson (1999)).

The lesson from this is that although there were measurements capturing the course of events that lead to separation of the system, no one looked at the signals. In order to be efficient, a warning system should present data that is easier to "consume" for the operators than raw measurements. One such thing to present can be system damping and oscillation frequencies, preferably as time trends.

It should be noted that Dynamic Security Assessment (DSA) tools would not have been able to help in this case. The reason is that the DSA tools rely on massive simulations starting at the current operating point. The consequences of a number of contingencies are then evaluated and the operation is eventually classified as secure or insecure. DSA tools thus require accurate models. Whereas the generating part of a system can be assumed to be well known this is not the case for the loads. It is pointed out in Hiskens and Milanovic (1997) that the type of load and the time-constants for dynamic loads influence the damping substantially. With incorrect models, the result from DSA tools is, however, highly questionable.

The consequences of an event need not be as severe as in the example to be interesting to monitor. Also lightly damped oscillations are of interest. In the case of a lightly damped oscillation, decisions to change operation or to enable special protection/control schemes can be based on the information from a dynamics monitoring system.

In the very short timescale (a few ms) there is also the need to quickly determine if the present situation is due to a powerswing or a fault. To minimize the consequences of either, it is important to know what caused the present situation as the remedial actions for a powerswing or a fault can differ substantially from each other. This requires a response time of an indicator to be in the timescale of the fundamental frequency or shorter.

1.2 Objectives

The primary objective of this work is to look at new protection and control systems with the aim to increase the operational safety. This is divided into (1) Investigation and evaluation of different methods for detection and classification of electro-mechanical oscillations from local measurements. This also involves studies of the different characteristics of different measurements. The result of this can be viewed as a virtual sensor. (2) Use measurements from the developed sensor for control of active end-use loads to damp electro-mechanical oscillations.

1.3 Contributions

The contributions of this work is summarized in Chapter 7 but the major contributions are summarized here:

A new idea for distinguishing faults from powerswings in distance protection relays is presented. The principle is based on a change of coordinate system to a system that is more suitable for distinguishing faults from powerswings. It should be noted that the proposed method only works for large powerswings, that is, when there is a chance to mix up faults with powerswings.

It is shown that real-time monitoring of electro-mechanical oscillation frequency and damping is possible, at least for a single mode system. Limits for transducer sensitivity is derived when using frequency measurements.

The change in feeding power to a distribution network, fed from one bus, when end-loads are changed is investigated. Neglecting tap changer control, it is shown that the change in feeding power can be accurately estimated without network knowledge by using the voltage angle between the feeding bus and the load bus. Accuracy is dependent on operating point and seems to decrease with increased stress of the distribution network. In normal operation, the accuracy for a load change of 10% is good.

Load modulation for damping enhancement by switching end-loads is studied with the aid of the previous result. The reactive covariation caused by the distribution network seems, in many cases, to have a limited influence on the results.

1.4 Outline of the thesis

The thesis is organised in time-scale order, going from fast to slow. In Chapter 2 detection of powerswings is studied. A brief review of methods used in distance protection relays are given and new results are presented. Chapter 3 discusses different methods to estimate frequency and damping of the electro-mechanical

oscillations. Some of the presented methods are applied to measurements and simulations in Chapter 4. Part of the results in these chapters has previously been published in Hemmingsson et al. (2001) and Hemmingsson (2001).

Chapter 5 discusses how reactive covariation caused by the distribution network can be estimated. These results together with Samuelsson (1997) are then used in simulation studies in order to show how distributed load control can be used to enhance the damping in a power system.

1.5 Power system fundamentals

This is a short section to provide the fundamentals of electric power systems to people not familiar with the area. People familiar with the topic will find this text to perhaps be a bit misleading as not all details are covered. The intention is, however, to describe the root and cause of the basic phenomena in a short and simple way.

Phase voltages and currents in a three phase system are described by:

$$\begin{aligned} v_a &= \hat{v}_a \cos(\omega t) & I_a &= \hat{I}_a \cos(\omega t + \varphi_a) \\ v_b &= \hat{v}_b \cos(\omega t - 2\pi/3) & I_b &= \hat{I}_b \cos(\omega t - 2\pi/3 + \varphi_b) \\ v_c &= \hat{v}_c \cos(\omega t - 4\pi/3) & I_c &= \hat{I}_c \cos(\omega t - 4\pi/3 + \varphi_c) \end{aligned}$$

A more common representation in power system analysis are the zero, positive and negative sequence voltages and currents.

$$\begin{aligned} V_0 &= v_a + v_b + v_c \\ V_+ &= v_a + v_b e^{j2\pi/3} + v_c e^{j4\pi/3} \\ V_- &= v_a + v_b e^{-j2\pi/3} + v_c e^{-j4\pi/3} \end{aligned}$$

If $\varphi_a = \varphi_b = \varphi_c$ then the system is called symmetric and $V_0 = V_- = 0$, which greatly simplifies calculations. In the sequel, it will be assumed that the system always operates under symmetric conditions.

Electric power is expressed as voltage times current. With sinusoidal voltages

this is divided into two parts, active power (P) and reactive power (Q).

$$S = v_a\, I_a = \frac{\hat{v}_a\, \hat{I}_a}{2}\left[\underbrace{((\cos(2\omega t)+1)\cos(\varphi))}_{p} + \underbrace{\sin(2\omega t)\sin(\varphi)}_{q}\right]$$

In the expression above P is identified as the mean value of p whereas Q is defined as the maximum value of q.

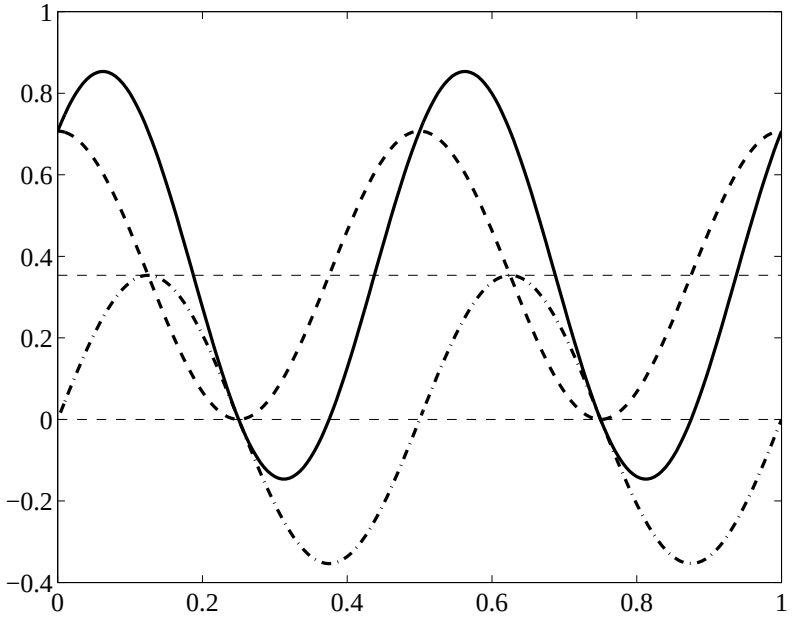

Figure 1.2: Instantaneous power (solid), active power (dashed), reactive power (dash dotted).

P is the power that can be used to perform actual work whereas Q corresponds to power required to move magnetic energy between the phase conductors in a transmission line.

The mechanical dynamics of a generator is given by

$$\omega\, J\frac{d\omega}{dt} = P_M - P_E$$

where ω is the angular velocity of the generator, J is the moment of inertia for the generator and the turbine driving the generator. P_M and P_E corresponds to the mechanical (from the turbine) and electrical power affecting the generator.

A generator delivering power to a large network is seen if Figure 1.3. Assuming

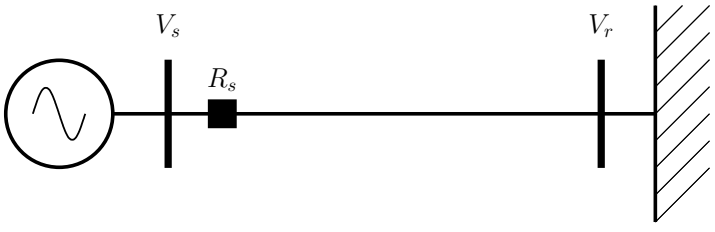

Figure 1.3: Generator delivering power to a large power system.

a purely reactive[1] line with reactance X, the active power transfered on the line can be written as:

$$P = \frac{V_s V_r}{X} \sin(\delta) \tag{1.1}$$

where δ is the phase angle between the the sending end voltage, V_s, and the receiving end voltage, V_r.

We can now make the following definitions:

Small-signal-stability has to do with torque affecting the generator that depends on $\dot{\delta}$.

Transient-stability has to do with the torque affecting the generator that depends on δ

The equations above do not contain any terms that are directly dependent on $\dot{\delta}$. Such terms exist although not in the simplified model above. Viscous damping is for example often included in the mechanical torque. Introducing voltage control on the generator, that is manipulating V_s, also introduces torque dependent on $\dot{\delta}$. The torque introduced by voltage control tends, however, often

[1] meaning voltage across the line and the current through the line having a phase shift of 90°

to decrease the damping of the system. To circumvent this to some extent the voltage controllers are equipped with Power System Stabilizers (PSS) which is an add-on control loop on top of the voltage controller. The PSS will increase the damping by adding an extra signal to the output from the voltage controller. The control authority of a PSS is limited to a few percent of the voltage controller output.

We can now see how system instability can occur in two different ways. In the small signal case generators will speed up/down because of the random load variations. The turbine control is not fast enough to always maintain an exact frequency. When more power is required, this is accomplished by taking some of the stored kinetic energy in the rotating masses of the generator and turbine and turn that into power. This will decrease the generator speed. In a power system the generators will respond differently to different load changes meaning that some will speed up/down more than others because of distance to loads. Having the generators changing their speed by a small amount will change the angle between the generators and thus change the powerflow between the generators. Once this imbalance has occured all generators will more or less move with or against each other. The goal is that the generators should be damped so that these oscillations will vanish. In case of low or negative damping the oscillations will sustain or even increase which in the end will damage the system. Small signal stability is thus concerned with lightly damped or undamped oscillations that in the end might break the system.

Transient stability stems from large external disturbances. The most common is when there is a fault on a transmission line. The voltage at the fault will be small and as seen in equation 1.1 no active power can be transported on the line. This will cause the generators that are unable to deliver electric power to speed up because the turbine governors are not able to decrease the mechanical power fast enough. For fixed V_s, V_r and X equation 1.1 will have two equilibriums, one stable when $\delta < 90°$ and one unstable when $\delta > 90°$. It can now be seen that if the fault is not cleared fast enough δ will grow until it reaches the unstable equilibrium leading to an out-of-step event. Out-of-step operation can severely damage the generator and must be inhibited, either by clearing the fault fast or by disconnecting the generator.

Chapter 2

Power swing detection

This chapter deals with fast detection of power swings. Fast detection of power swings is of interest in distance protection of transmission lines but can also serve as a starting mechanism for the methods described in Chapter 3. In distance protection, the main goal is to prevent high speed distance protection to operate. This requires the detection of a power swing to be done within milli-seconds The possibility to accurately determine the swing frequency and damping within such a short time is naturally limited.

The task of a power swing detector in a distance protection relay is to prevent unintended operation of the relay during a stable power swing. Ideally we would also like the detector to trip the relay when an unstable power swing is detected. Depending on when the unstable swing is detected we can choose to trip before or after a poleslip occurs. Normally, it is desirable to trip before the out-of-step condition occurs. If, however, the unstable swing is detected when the swinging machines are close to phase opposition it might be advantageous to trip after the pole slip has occured. The reason is that the wear and tear of the circuit breaker will be reduced when it does not have to operate at its maximum rating.

The rest of the chapter is organized as follows: First there is an overview of some different methods used for out-of-step protection and power swing blocking/tripping in distance protection. The methods are divided into sub-categories depending on their function. The three main categories are:

Swing detectors are meant to determine if a swing is present. This is often done by looking at the speed at which some variables move in certain operating regions. The problem is to define the limits for when the result should be interpreted as a swing and when it should be treated as a fault. The old and widespread technique of looking at how fast the impedance travels through a region belongs to this category of detectors. Because a swing is a much slower phenomenon than a fault it usually takes longer time to detect a swing than a fault. This has led to the use of fault detectors instead of swing detectors.

Fault detectors, look for special characteristics in the measured signals that indicate the inception of a fault. The presence of a fault then arms the relay so that it can operate. Basically this means that the relay is normally blocked and only enabled a short time at the fault inception.

Out-of-step detectors/predictors are, as the name suggests, devices that will alarm when they can detect or predict an out-of-step condition. These methods are often based on a two-machine model of the network where the input mechanical power to the generators has to be known. The R-Rdot algorithm belongs to this category but does not require knowledge of the mechanical power, see Taylor et al. (1983); Haner et al. (1986)

Following the review, a new method to distinguish faults from power swings is presented and analyzed. Finally the new method is tried on a number of simulated scenarios.

2.1 Power swing and detection variables

A common situation in which power swings should be detected is transmission line protection. Using static measurements it is impossible to distinguish faults from power swings, whereas the protection often is required to operate differently depending on if the current situation is caused by a fault or a power swing. Figure 2.1 depicts the situation in which the detection should operate. Detectors are located at R_s and R_r, V_s and V_r are sending and receiving end voltages. When the impedance measured at R_s or R_r enters one of the zones depicted to the right in Figure 2.1 a timer is started. The timer is preset with

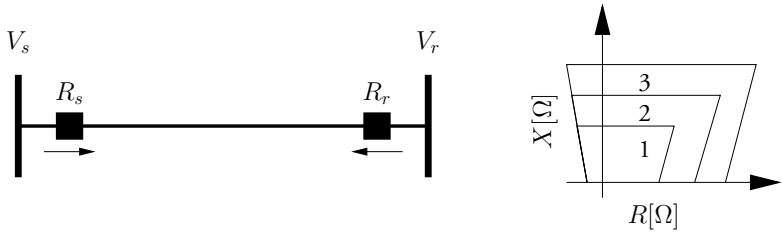

Figure 2.1: Model used for distance protection relays (left) and relay zones (right).

longer times the higher the zone number is. If the measured impedance still is in the zone when the timer has timed out, the relay is tripped. The ultimate task of a swing detector is now to distinguish faults in the forward direction from power swings. In the case of a power swing it is also advantageous if the detector can predict if the detected swing will be stable or if the system will reach out-of-step conditions.

Swing detectors

The oldest and perhaps most widespread technique to detect a power swing or an out-of-step condition is to use a directional impedance relay equipped with some additional logic. An impedance relay is a device that measures the apparent impedance at the relay location, that is the voltage divided by the current taking the phase shift between voltage and current into consideration. Directional merely means that when active power flows in the reference direction the resistance seen by the relay will be positive.

A relay located at the sending end (R_s) in Figure 2.1 will thus see an impedance that is the line impedance plus an impedance that models the load at the other end. The relay at the receiving end will see an impedance with negative real part corresponding to a generating unit at the sending end.

When a bolted (or metallic) fault occurs on the line the impedance seen by the relay will be the line impedance from the relay to the fault. Let us now compare this with the following two cases

1. V_s and V_r are in phase. In this case the apparent impedance

$$Z_a = \frac{|V_s|}{|V_s| - |V_r|} Z_{line}$$

   is large because $|V_s| - |V_r|$ should be a small number.

2. V_s and V_r are in phase-opposition. Here the apparent impedance

$$Z_a = \frac{|V_s|}{|V_s| + |V_r|} Z_{line}$$

   lies on the line impedance so it looks like a fault to the relay.

It is thus not possible to distinguish a swing from a fault by just looking at the apparent impedance.

It should also noticed that when $|V_s| \neq |V_r|$ the two extreme value impedances above form the endpoints of a circle diameter. For constant $|V_s|$ and $|V_r|$, all impedance values measured at R_s during a power swing will be located on this circle Poage et al. (1943); Clarke (1945).

A common way to distinguish a fault from a swing is to start a timer when the apparent impedance enters a specified area in the R-X plane. If the apparent impedance remains in this area after the timer has timed out, we consider the system to be in a faulted state. Another approach is to measure the time it takes for the apparent impedance to travel through one or several slices of the R-X plane. A short time is then interpreted as a fault and a long time as a swing. Typical areas/slices are depicted in Figure 2.2.

Another approach to swing detection is taken in the following algorithms. First we notice that the time derivative of a quantity q

$$\frac{dq}{dt} = \frac{dq}{d\delta}\frac{d\delta}{dt} = \frac{dq}{d\delta}\omega \tag{2.1}$$

is proportional to the rotor speed ω. For a quantity to be useful in swing detection it should thus have a derivative $\frac{dq}{d\delta}$ that is large, making it heavily dependent on ω. Furthermore, it should be monotonous preferably for $0 \leq \delta \leq 2\,\pi$ or at least in a wide interval around $\delta = \pi$. The detection of a swing is then made

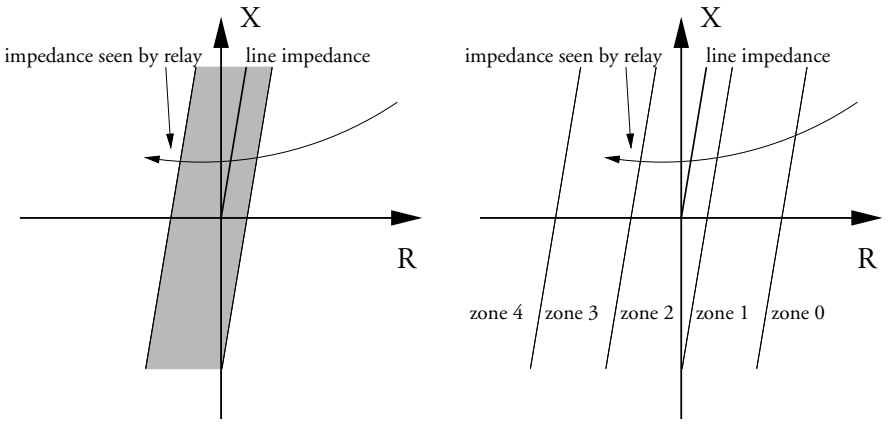

Figure 2.2: Areas/slices used for swing detection when using timers.

when the derivative $\frac{dq}{dt}$ exceeds a threshold value. One suitable candidate for q is

$$q = V \cos \varphi$$

where φ is the phase angle between voltage and current. This quantity was suggested in Ilar (1981); Ilar and Metzger (1984) and is used in the distance protection relays UP91 and UP92 from Brown Boveri Corporation. The behaviour is further studied in Machowski and Nelles (1997) where also some improvements are suggested. Other quantities which are suggested in Machowski and Nelles (1992) are

$$\begin{aligned} q &= \frac{d(Q-P)}{dt}\frac{1}{S} \\ q &= -\frac{dP}{dt}\frac{1}{S} \end{aligned}$$

both these signals should be multiplied with a sign function in order to be independent of being in the sending or receiving end.

Fault detectors

The basic idea behind the fault detectors is to look for information in the measured signals that is only present when a fault actually occurs. The presence of this information will then enable the main fault indicator in the relay to, if needed, trip the circuit breaker. With this setup the normal state of the relay is to be blocked and it is only enabled for a short time when the fault detector senses a fault or events that are interpreted as faults. Two different approaches will be discussed.

In Moore and Johns (1996) it is studied how the fault inception affects the estimated reactance. The occurrence of a fault in the relay protected zone will

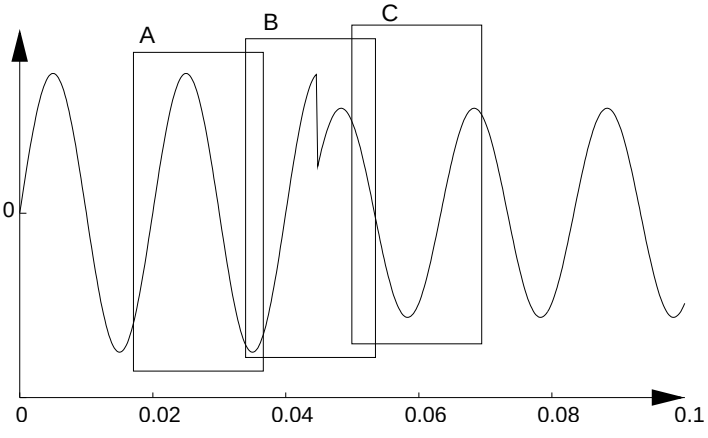

Figure 2.3: Waveform experienced at fault inception.

result in instantaneous changes in magnitude and phase of the relay input signals (Figure 2.3). Since the algorithm usually processes a fixed number of input samples at any point in time we have a time window moving one step to the right at each sampling instant. In positions A and C the window only contains prefault or postfault data and hence the impedance calculation works as expected. However, in position B the window contains both prefault and postfault data. This leads to error in the impedance calculations since the waveform present in window B does not represent a single frequency sinusoid, which is the requirement for the calculations. This effect, the fault transient effect, is usually regarded as a nuisance but here the authors use it to their advantage as

it something that only is present in the measurements when a fault occurs. The fault transient is not usable in itself but needs some additional processing in order to provide an accurate enable signal for the main relay indicators.

Another approach is taken in Jonsson and Daalder (2001) where the time derivative of the phase angle between voltage and current is used as an indicator of a fault occurrence. The idea here is that the phase angle between voltage and current is small during normal operation. Faults are mainly reactive so the phase angle between voltage and current will be close to 90° during the fault. The phase angle alone is not a sufficient indicator as we may have a large angle during low load operation and also during large power swings. Therefore the authors look at the derivative of the phase angle. As a fault is close to an instantaneous change while a power swing is a slow phenomenon it is now possible to distinguish faults from power swings.

Out-of-step predictors

The out-of-step predictor is a device that will tell us when the system has reached a state that inevitably will lead to the occurrence of a pole slip. The predictors can be used not only for equipment protection but also for system protection. In system protection we need to know that there will be loss of synchronism and we might need to split the system into several parts. Knowing that the system will have to be split we can select the points where to disconnect the systems in order to minimize the effects and to facilitate reconnection. The better prediction required the more knowledge about the system is needed. Often, the system is simplified to a two-machine system.

A method that does not rely on a two machine model is the R-Rdot algorithm Taylor et al. (1983); Haner et al. (1986) where the time derivative of the apparent resistance versus the apparent resistance is plotted in a diagram. The use of a time derivative enables some sort of prediction of the type of swing, stable or unstable. In Figure 2.4 we see the R-Rdot diagram for a single machine infinite bus system. For a system such as this we can define a line (here at $R = 0.4$) that will trip the relay when R-Rdot passes through the line. The basic principle behind the R-Rdot relay is that the apparent resistance is a measure of the angle between the swinging units. Consequently, Rdot is a measure of rotor speed between the swinging units. A high speed when the angle is large will then

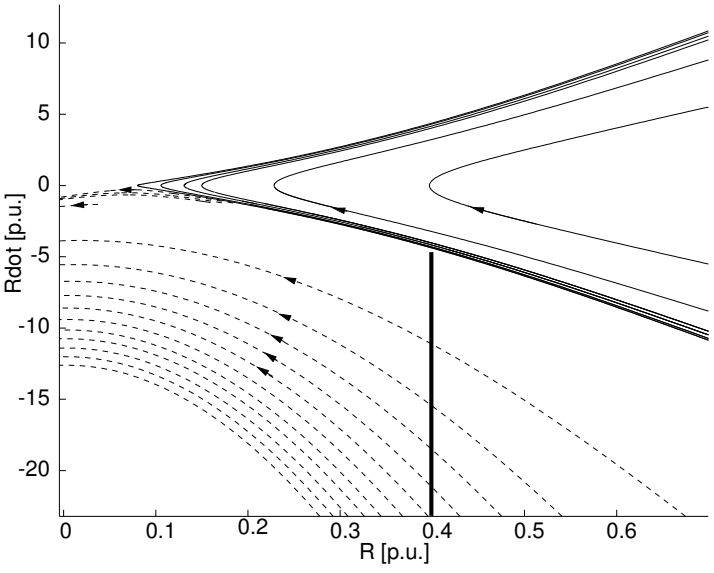

Figure 2.4: R-Rdot diagram for a single machine infinite bus system. Solid lines correspond to stable swings, dashed lines to unstable.

indicate that the system probably will lose synchronism. For a more complex system, automatic generation of trip-rules from massive amounts of simulations have successfully been tried in Rovnyak et al. (2000).

The idea behind the following methods is to use the equal-area criterion (Figure 2.6) for a single machine infinite bus system (Figure 2.5) to determine if a system is stable. For this kind of system to remain stable it is required that the accelerating area A in Figure 2.6 is smaller than the deaccelerating area D. This requires the knowledge of the mechanical power driving the generators. Unless the generators are equipped with special protection such as fast valving we can usually use the prefault power on the protected line as a pessimistic estimate of the mechanical power.

In Redfern and Checksfield (1995, 1998) it is noticed that $\frac{dP}{dt} < 0$ when passing the critical point 5 in Figure 2.6 from left to right. However, this is also the case when, for example, passing point 1 from right to left. It is then noticed

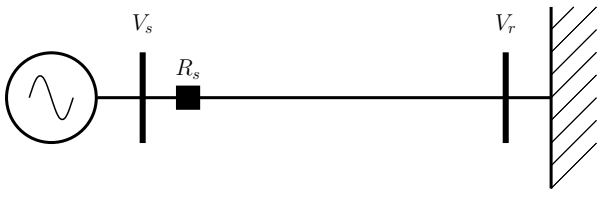

Figure 2.5: Single machine infinite bus system used in algorithms by Redfern and Checksfield (1995, 1998); Minakawa et al. (1999)

that the reactive power extracted at the receiving end, given by:

$$Q = \frac{V_s\, V_r}{X} \cos\delta - \frac{V_r^2}{X} \tag{2.2}$$

is smaller than $-\frac{V_r^2}{X}$ for $\delta \in [90°, 270°]$. Since point 5 occurs for load angles

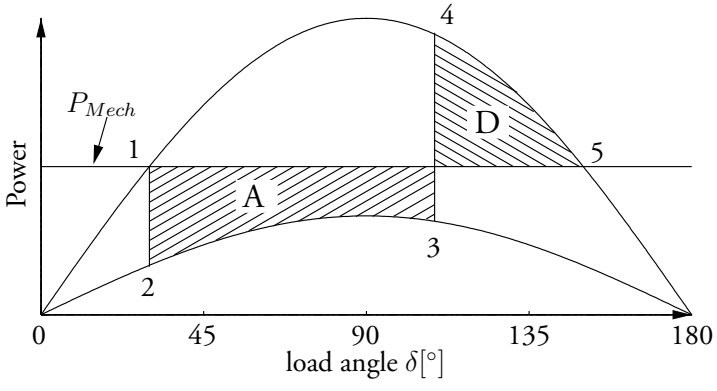

Figure 2.6: P-δ diagram used for equal-area calculations

greater than 90° then if:

$$Q \leq -\frac{V_r^2}{X} = Q_{trip} \tag{2.3}$$

the machine must be operating at point 5 and not point 1. For machine protection, we consider V_s the internal voltage in the generator and V_r the bus voltage

where the relay is located. An estimate of Q_{trip} is then given by:

$$Q_{trip} = -\frac{S_{gen}}{X_q} \tag{2.4}$$

where S_{gen} is the rated power of the generator and X_q is the quadrature axis synchronous reactance. The last requirement for being unstable is then that $P \leq P_{Mech}$. To summarize, we can conclude that the system will exhibit loss of synchronism if:

$$\begin{aligned} P &\leq P_{Mech} \\ Q &\leq Q_{trip} \\ \frac{dP}{dt} &\leq 0 \end{aligned}$$

In Minakawa et al. (1999) a similar approach is used but current is used instead of reactive power. The requirement on reactive power in the previous algorithm

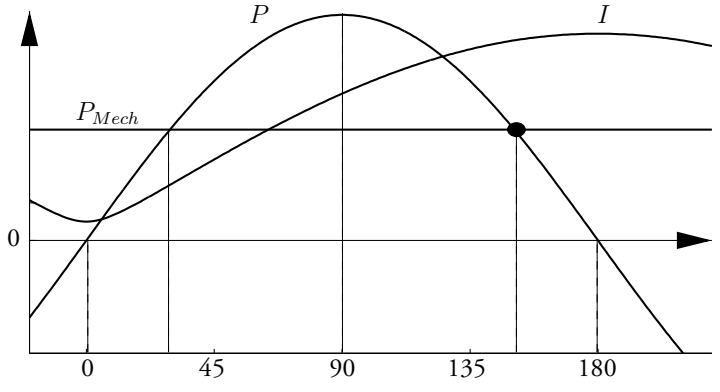

Figure 2.7: P and I versus δ

is now replaced with $\frac{dI}{dt} \geq 0$ to assure that the correct point is identified. Visual inspection of Figure 2.7 gives that the algorithm can the be summarized to

$$\begin{aligned} P &\leq P_{Mech} \\ \frac{dI}{dt} &\geq 0 \\ \frac{dP}{dt} &\leq 0 \end{aligned}$$

Both of the mentioned methods are detectors in that they detect when the unstable equilibrium point (5 in Figure 2.6) is passed from left to right. If the post-fault swing curve is known we can instead predict an out-of-step condition already at the last switching instant (3-4 in Figure 2.6). A possible scheme for this would then be

- During fault
  - Obtain the load angle by integrating the frequency difference given by the actual frequency minus the frequency at the fault inception.
  - Calculate the accelerating area (A) by integrating the prefault power minus the actual electric power.
- Postfault
  - Fit a sinusoid to the postfault swing curve. This includes calculating an additional angle as the estimated load angle is zero at the fault inception.
  - Based on the estimated swingcurve calculate the maximum deacclereating area (D). If D is smaller than A then trip.

In Centeno et al. (1993, 1997) real-time synchronized measurements of the voltage-phasors at each end of a two machine system is used to estimate the system parameters. The estimated system is then used to predict the swings and tell if they are stable or not. The method is elegant in that there is no need to supply model parameters as they are continuously estimated. However, the equipment is expensive and also requires communication between the measurement points.

2.2 Fault discrimination using circle fitting

In this section a new method to distinguish a fault from a power swing is presented. The method is based on the phenomenon that the apparent impedance seen by a relay moves on a circle during a power swing Poage et al. (1943); Clarke (1945). The characteristics of a circle (radius and centre) can then be used to distinguish a fault from a power swing.

The system used in the analysis is a two-machine system without shunt elements and with the generators represented by the classical model (Figure 2.8). Measurements and calculated values are valid for the point R in Figure 2.8

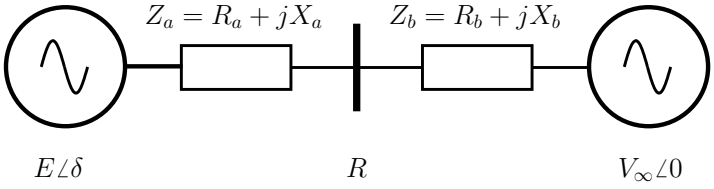

Figure 2.8: Two-machine system with relay located at R.

which is the relay location.

The apparent impedance at R is given by:

$$Z = \frac{\vec{V}_R}{\vec{I}} = \frac{\vec{E} - Z_a\vec{I}}{\vec{I}} = \frac{\vec{E}}{\vec{E} - V_\infty}(Z_a + Z_b) - Z_a \tag{2.5}$$

We notice that the impedance is divided into two parts; a voltage dependent part and a position dependent part. For $\vec{E}$ and $\vec{V}$ having constant magnitude the measured impedance Z will move on a circle (Figure 2.9).

The centre C is now calculated as the mean value of the impedances when the angle difference between E and V_∞ is 0, 180 degrees respectively. In the same way the diameter which is $2r$ where r is the radius of the circle is given by the difference of the impedances when the angle difference between E and V_∞ is 0 and 180 degrees respectively.

$$C = \frac{E^2}{E^2 - V_\infty^2}(Z_a + Z_b) - Z_a \tag{2.6}$$

$$r = \frac{E\,V_\infty}{|E^2 - V_\infty^2|}|Z_a + Z_b| \tag{2.7}$$

With Z defined as in equation (2.5), then for a solid fault ($V_\infty = 0$) we get $Z = Z_b$ where Z_b is the impedance from the measuring location to the fault. A solid fault will thus have radius 0 and the centre at the fault location.

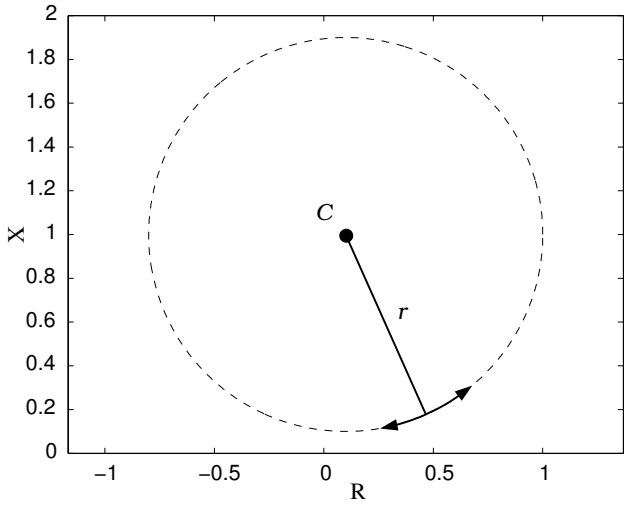

Figure 2.9: Impedance seen by relay.

In the more general case where shunt elements are allowed we can use the $ABCD$ parametrization of the circuit,

$$\begin{bmatrix} V_s \\ I_s \end{bmatrix} = \begin{bmatrix} \mathbf{A} & \mathbf{B} \\ \mathbf{C} & \mathbf{D} \end{bmatrix} \begin{bmatrix} V_r \\ I_r \end{bmatrix} \tag{2.8}$$

where $\mathbf{A}, \mathbf{B}, \mathbf{C}, \mathbf{D}$ are complex constants. Provided that we measure at the sending end then Poage et al. (1943) has derived the following expressions for the centre and radius:

$$C = \frac{BD\angle\beta - \Delta}{D^2 - \left(\frac{V_r}{V_s}\right)^2} \tag{2.9}$$

$$r = \left| \frac{B\left(\frac{V_r}{V_s}\right)}{D^2 - \left(\frac{V_r}{V_s}\right)^2} \right| \tag{2.10}$$

where $\mathbf{B} = B\angle\beta$ and $\mathbf{D} = D\angle\Delta$.

Either the centre or the radius can be used as a fault detector. The radius is preferred because of the property that it becomes zero when there is a solid fault

on the line. It is thus easier to find a suitable limit for a fault detector when using radius instead of centre.

The results shown above are valid when there is a fault on a line. For a system with parallel lines it is also interesting to look at behaviour on the healthy lines. A system with two parallel lines which have a fault on one line can be transformed to a single line system by converting the generator and the faulted part of the line to an equivalent two-pole as in Figure 2.10. If the fault occurs such

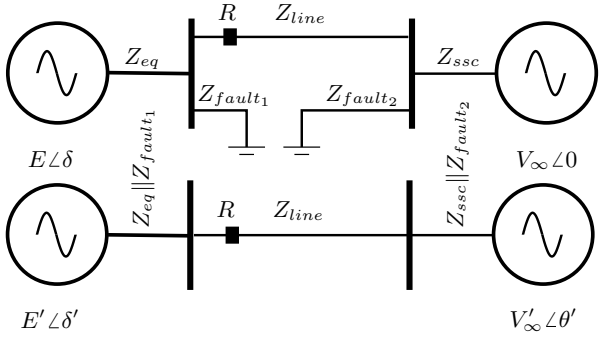

Figure 2.10: Faulted system and equivalent system seen by the relay.

that $E' \approx V'_\infty$, then we get a radius that is large or even infinite which in turn corresponds to a healthy condition of the line, see Figure 2.11. This is actually correct as the monitored line is healthy, the fault is on the parallel line. What we can conclude is that the proposed approach, sometimes will detect a fault on a parallel line as a power swing.

Estimation

The radius and centre can be calculated by fitting a circle to the impedance measurements and then identifying the different parts.

A circle in cartesian coordinates is described by:

$$r^2 = (R - R_0)^2 + (X - X_0)^2 \tag{2.11}$$

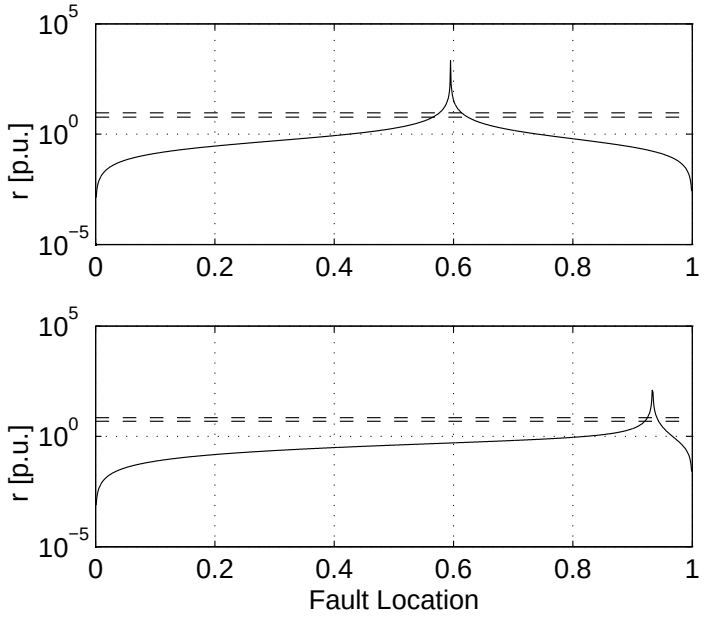

Figure 2.11: Radius (r) as a function of fault distance from the generator (E). The upper graph is for V_∞ having a much larger impedance than in the lower graph. The dashed lines are the radius for unfaulted system with one and two lines in operation.

where the centre $C = R_0 + jX_0$. With the change of variables:

$$Z^2 = r^2 - R_0^2 - X_0^2 \tag{2.12}$$

we get the regression model

$$R^2 + X^2 = Z^2 + 2RR_0 + 2XX_0 \tag{2.13}$$

where we estimate R_0, X_0, Z^2 and then calculates r from equation 2.12

This estimation can for example be done by using a sliding window, a Kalman filter or any other kind of recursive least squares method. The recursive versions should be equipped with some sort of change detector that restarts the estimator whenever there is a large jump in the data.

When applying a recursive method to equation 2.13, two problems are noticed.

- The estimates drift away during normal operation. This is probably due to that the measured impedances are located around a short segment of a circle. The estimator sees this as a circle with centre at the measured impedance.
- The convergence at changes is sometimes poor with lots of jumps in the estimated parameters before they settle. This will likely happen when there are to few points to make a good estimate. This can be cured if we can provide some extra information about the circle, such as an approximate location of the centre.

Both of these problems can be solved by restricting the values that the centre can have.

From equation 2.5 we find that the centre is located on a line. A first approach is thus to restrict the centre to be on a line. This will prevent the drift of the centre and will possibly speed up the convergence too. If, however, we can assume that the parameters of the line will change considerably, then restricting the centre to be on a specific line may deteriorate the performance of the estimator. In such a case it might be advantageous to restrict the centre to be within a restricted area of the impedance plane. Two possible area-restrictions are shown in Figure 2.12. The restriction shown to the left in Figure 2.12 is easier to implement because when the estimate is outside the admissible region, then the restricted estimate is located on the closest border. This can be accomplished without evaluating the loss-function itself. For the restriction to the right in Figure 2.12 we must choose between two lines and the intersection of the lines. This requires evaluation of the loss-function at several different points.

The restricted or constrained estimate can be obtained in the following way Goodwin and Payne (1977).

A normal least-squares problem

$$Y = \Phi\theta \tag{2.14}$$

where θ is the unknown parameter vector, Y is the measurement vector and Φ

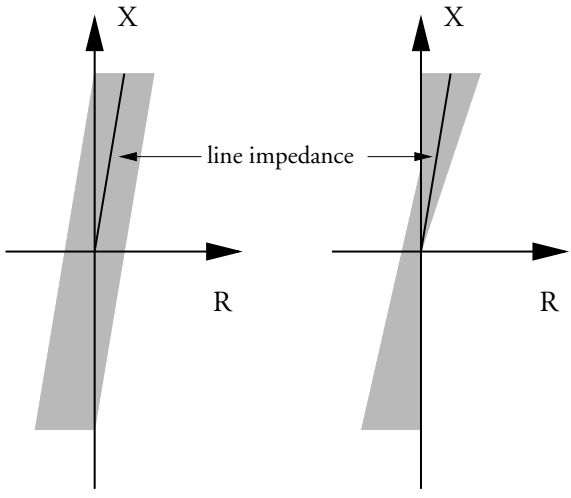

Figure 2.12: Possible area-restrictions for the centre.

is the regressor matrix we have the solution

$$\hat{\theta} = (\Phi^T\Phi)^{-1}\Phi^T Y \tag{2.15}$$

We now introduce linear constraints

$$L\theta = C \tag{2.16}$$

The minimum variance unbiased estimator $\tilde{\theta}$ subject to the constraints $L\tilde{\theta} = C$ is then given by:

$$\tilde{\theta} = \hat{\theta} - (\Phi^T\Phi)^{-1}L^T(L(\Phi^T\Phi)^{-1}L^T)^{-1}(L\hat{\theta} - C) \tag{2.17}$$

Here, the constraints C, are the boundaries of the admissible area for the centre.

What remains now is to incorporate the constrained estimate into the recursive algorithms. This is shown for the standard recursive least-squares method and is then applied in the same way on the methods which are suited for detection of varying parameters.

First we define our regressor, observation and parameter vectors

$$\varphi_k = \begin{bmatrix} 1 & 2R_k & 2X_k \end{bmatrix}^T \quad y_k = R_k^2 + X_k^2 \quad \theta = \begin{bmatrix} Z^2 & R_0 & X_0 \end{bmatrix}^T$$

Next we collect the regressors and measurement up to time k

$$\Phi_k = \begin{bmatrix} \varphi_1^T \\ \vdots \\ \varphi_k^T \end{bmatrix} \quad Y_k = \begin{bmatrix} y_1 \\ \vdots \\ y_k \end{bmatrix}$$

Introduce the matrix

$$\mathbf{P}_k = \left(\sum_{i=1}^{k} \varphi_i \varphi_i^T \right)^{-1} = (\Phi_k^T \Phi_k)^{-1}$$

Finally we can write the update of the estimates as

$$\mathbf{P}_k^{-1} = \mathbf{P}_{k-1}^{-1} + \varphi_k \varphi_k^T \tag{2.18}$$

$$\hat{\theta}_k = \hat{\theta}_{k-1} + \mathbf{P}_k \varphi_k (y_k - \varphi_k^T \hat{\theta}_{k-1}) \tag{2.19}$$

To constrain the estimates of a recursive least-squares type algorithm we thus have to use equation 2.17 when the estimates are outside the desired area, where we substitute $(\Phi^T \Phi)^{-1}$ with P_k.

A comparison between the constrained and the unconstrained algorithms can be seen in the lower part of Figure 2.13.

Choice of estimator

Among the vast number of estimators that can be used to solve 2.13 only a few have been tried. Their performance will be shortly reviewed.

Least Squares The least squares method applied on a sliding window with fixed length works but the performance is poor for abrupt changes. The performance for slow motion of the measured impedance is also poor. In both cases this depends on the fixed length of the sliding window. For the abrupt changes we wold like a short window so that we quickly change from prefault to postfault data in the window. For slow motion of the measured impedance however, we would like to use a long window so that the distance between the endpoints is large. A window that becomes

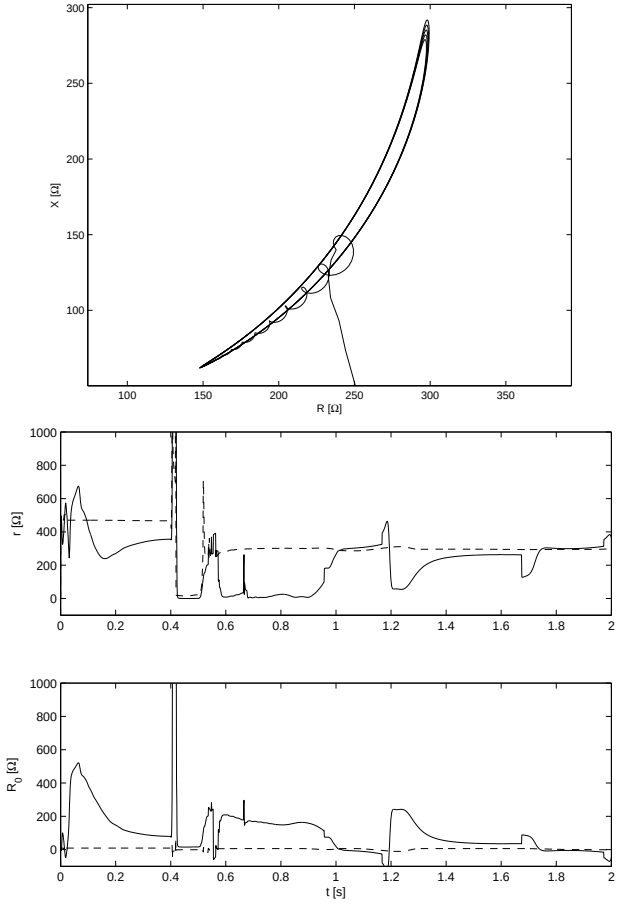

Figure 2.13: (Top),Measured resistance and reactance after a fault is removed (after 0.5s). (Bottom), Estimated radius (top) and real part of centre (bottom). Solid line is unconstrained algorithm and dashed line is the constrained algorithm.

small at abrupt changes and then grows with each sample will probably solve most of these problems. If the solution needs to be constrained the obtained estimates are often "noisy". The reason for this is that there is no "memory" in the algorithm, at each time a completely new estimate is calculated. Compare this to the recursive estimators where the new estimate is obtained as the old estimate plus a correction,

Recursive Least Squares The behaviour of the recursive least squares estimator is better than the normal least squares estimator. Most problematic is when there is lack of excitation, that is when we operate at or close to steady state. If we use forgetting, then the estimates start to drift after some time. It is a well known problem and can be solved by using conditional updating. The performance when the estimates are constrained is better than for the normal least squares algorithm but is still "noisy".

Kalman Filter The behaviour of the Kalman filter is better than the recursive least squares. In particular we can take advantage of that the estimates of the centre (resistance and reactance) are correlated. The degree of correlation will change with operating and fault conditions. Even if the degree of correlation is wrong there is a clear improvement in the result when correlated process noise is used compared to uncorrelated process noise. The behaviour when the estimates are constrained is much better than for the previous algorithms with a smooth estimate when the constraint is encountered.

Directional Forgetting The algorithm in Cao and Schwartz (2000) which is shown in equation 3.38 on page 66 has been used. The algorithm has been somewhat modified so that the choice of updating is not only based on the norm of the regressor but on the size of the prediction error. The results are comparable to the results obtained with a Kalman filter. The behaviour when the estimates are constrained is also similar with a smooth estimate when the constraint is encountered.

For the reasons described above the Kalman filter and the directional forgetting algorithms have been the most used estimators in the case studies.

Numerical considerations

When the sending and receiving voltage magnitudes are equal, then the centre and the radius as given by (2.6,2.7) approaches infinity. This of course leads to numerical problems. Furthermore, the impedance itself is large or infinite when a line is disconnected.

Looking for other parametrizations of the problem we find that if using power instead of impedance then the measurements are limited. The trajectories are, however, not longer limited to circles but are instead ellipses. Using admittance instead of impedance we find that the trajectories are circles and the admittance will only be "infinite" for bus-faults. To investigate the behaviour of the admittance we notice that the admittance is given by

$$Y = \frac{1}{Z} \tag{2.20}$$

but (2.20) is also a Möbius transform which has the property that it maps circles onto circles. Here, straight lines are considered as circles with infinite radius. Impedance "circles" that will be transformed to lines are thus those that pass through the origin. From (2.5) we get that this is when

$$Z = 0 \quad \rightarrow \quad \frac{\vec{E}}{V_\infty} = -\frac{Z_a}{Z_b} \tag{2.21}$$

that is for any system that has

$$\frac{E}{V_\infty} = \frac{|Z_a|}{|Z_b|} \tag{2.22}$$

This is equivalent to the potential at the measuring point being zero when $\vec{E}$ and V_∞ are in phase opposition.

By working with admittance instead of impedance, potential problems when $E \approx V_\infty$ are circumvented. On the other hand, a new case for potential numeric problems has appeared. A major drawback with circle estimation in the admittance plane is that the technique to restrict the permitted values of the centre requires *linear* constraints. Even a simple constraint such as the one to the left in Figure 2.12 will be translated into an area between two circles. Restricting the centre to be on a line through the origin will however still work.

Estimator resetting

The applied recursive estimators are designed to follow slowly varying parameters. For large changes, however, they might lose track of the parameters. The common way to resolve this is to restart the estimator when an abrupt change in the parameters is detected. Here, the prediction error is the detection variable. A large prediction error would then indicate that the used model is no longer correct. Using a fixed value for the resetting showed to be difficult. This can be explained by referring to Figure 2.15. A larger error can be tolerated for measurements that are far from the origin than for measurements close to the origin. One way to solve this is to make the reset limit dependent on the impedance plus an additional constant that defines the smallest required accuracy. Simulations have shown that making the limit 5%-10% of the measured impedance gives a good result.

In Figure 2.15 it can also be noted that the fault occurs at 0.4 s but the impedance does not move directly to the new value. Instead a large detour is made which depends on how the impedance is calculated. Here, voltages and currents are evaluated over a whole cycle of the fundamental frequency to get the rms value and phase. The correct value is thus not available until 0.42 s. Trying to estimate a circle on the detour is not of much use so the criteria for resetting have to be changed.

Several possible change detectors can now be used to solve this problem. The CUSUM (Cumulated Sum) detector will signal a change when the monitored variable, here the prediction error, has had the same sign and been too large so that the cumulated sum of the prediction errors reaches a specified value. Since the limit on prediction errors were adjustable it is hard to find a limit for the detector. An alternative approach is to raise an alarm when the prediction errors have had the same sign and been larger than the limit for a fixed number of samples. This will result in a delayed resetting. Simplifying this we can choose to just schedule the resetting of the estimator with a fixed delay when the prediction error is sufficiently large. Scheduling of another reset is then inhibited until the reset has taken place. The latter approach is implemented and has worked satisfactory.

2.3 Case studies

The studies are performed on a system that consists of a generator connected to an infinite bus through a double line. At 0.4 s a fault occurs a fourth of the line-length away from the generator on one line. The radius is calculated from measurements on the healthy line. The faulted line is cleared at different times producing both stable and unstable swings. The simulations were done in "Power System Blockset" in MATLAB, SIMULINK. Simulation is done in phase quantities.

Small oscillation

The fault is cleared by opening the faulted line at 0.5 s resulting in a small oscillation.

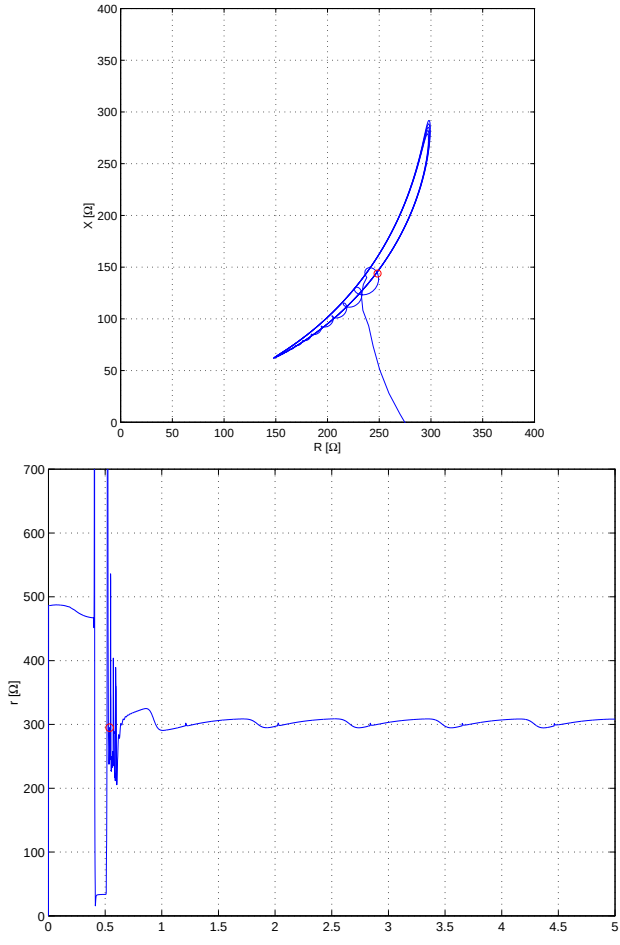

Figure 2.14: Impedance loci seen from R (top) and estimated radius (bottom). Fault at 0.4 s, fault cleared at 0.5 s. The mark in the upper diagram is at 0.54 s

Large oscillation

The fault is cleared by opening the faulted line at 1.2 s resulting in a very large but stable swing.

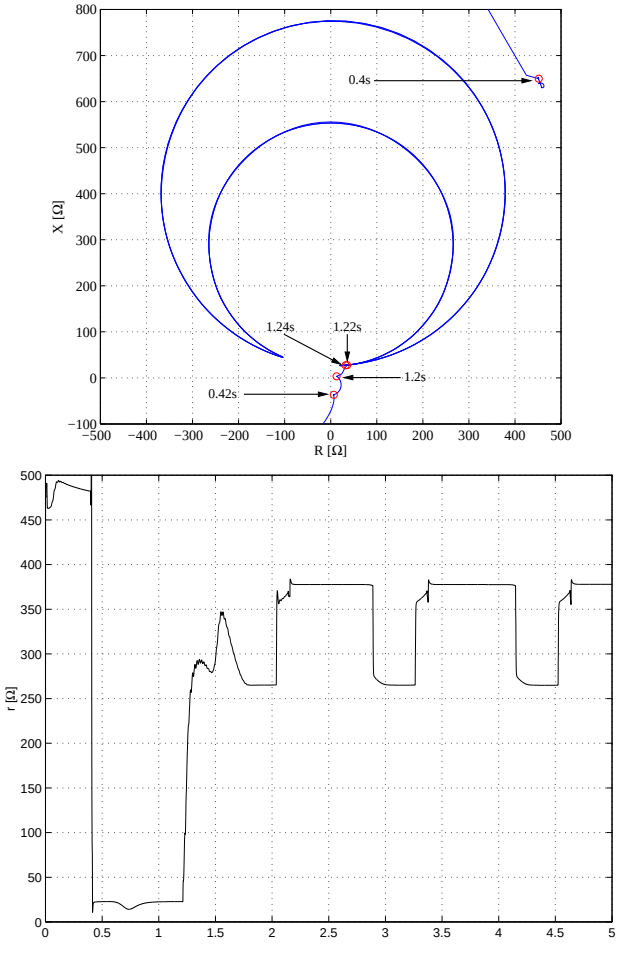

Figure 2.15: Impedance loci seen from R (top) and estimated radius (bottom). Fault at 0.4 s, fault cleared at 1.2 s.

Reclosing

The faulted line is opened at 0.7 s reclosed on th the fault again at 1.2 s and finally opened at 1.5 s.

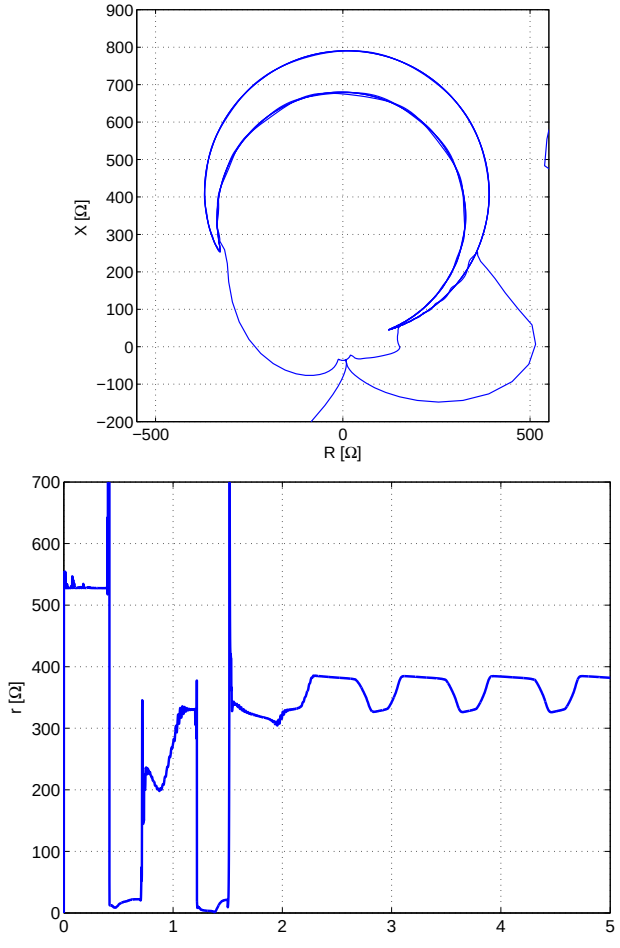

Figure 2.16: Impedance loci seen from R (top) and estimated radius (bottom).

Poleslip

The fault is cleared by opening the faulted line at 1.0 s but this is too late to save the system from poleslipping. To demonstrate the usefulness of restricting the centre to an area instead of a line, the lower part of Figure 2.17 is obtained by restricting the centre to the imaginary axis. The peaks in the estimated radius

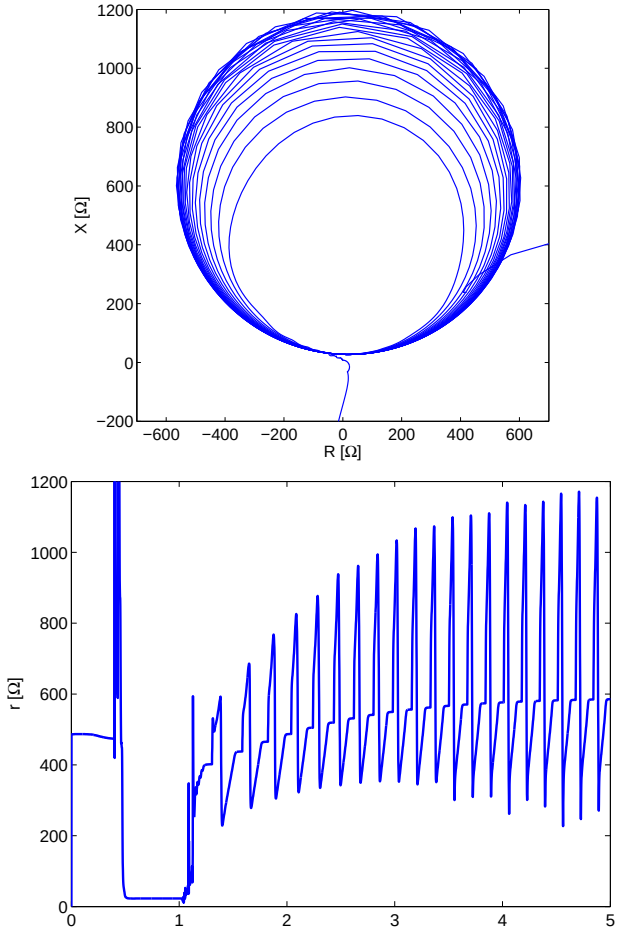

Figure 2.17: Impedance loci seen from R (top) and estimated radius (bottom).

are due the measured impedance not forming perfect circles with the centre on the imaginary axis. Allowing X_0, R_0 to be in a specified area such as in Figure 2.12 improves the result drastically. as seen in Figure 2.18.

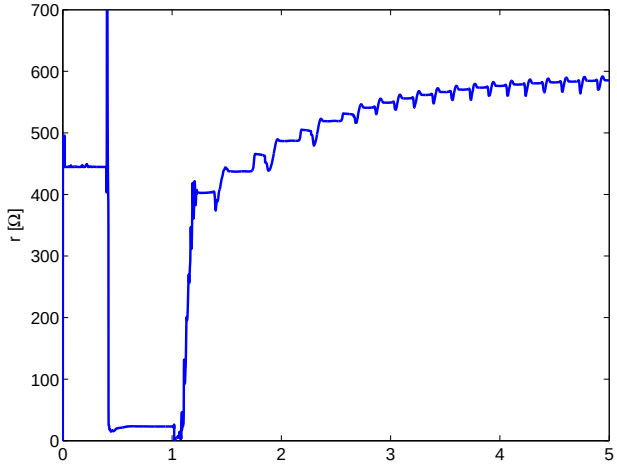

Figure 2.18: Estimated radius when both R_0, X_0 are free.

Comments

The simulation results seems a bit strange as there should only be one circle instead of two. This is probably because the used generator model is not a true representation of the classical model. Most probably it incorporates both synchronous and transient reactances although it claims not to do so.

2.4 Concluding remarks

Power swing detection can often be replaced by fault detection in distance protection of transmission lines. The idea is to detect fault or non-fault instead of a power swing. This has the advantage that fault detection is faster than swing detection because power swings are a slow phenomena compared to faults. In this context, a power swing is regarded as normal, although undesirable opera-

tion. A method suggested in the literature is to use the fault transient as a fault indicator. If the apparent impedance enters the protected zones within a specified time after a transient, then the system is believed to be in a faulted state and the relays are tripped. Possible problems with this setup is to tune the timer and how to distinguish a fault transient from the disconnection of the fault or disconnection/reconnection of a line.

A new fault-detection method, based on the physical behaviour of a two machine system is proposed. The method works by finding a new coordinate system in which it is easier to distinguish faults from non-faults. The new coordinate system uses the fact that the apparent impedance seen in a two machine system moves on a circle. The proposed method does not rely on timers or transients and needs virtually no tuning. When evaluated on a number of case studies with parallel lines, all faults were detected as faults and all power swings were detected as non-faults.

Chapter 3

Damping estimation

In this chapter different methods to determine frequency and damping of electromechanical oscillations in a power system will be discussed. There are two approaches to this, (1) ring-down analysis and (2) normal operation analysis. In ring-down analysis, signals measured after a large disturbance are used to calculate the eigenvalues of the monitored system. The disturbance can be a line switching, fault, probing by HVDC or anything else that have a large impact on the system. These disturbances are typically pulse or step disturbances. As the large disturbances occur infrequently it can be assumed that the observed ring-down is due to only one disturbance and hence the observed behaviour can be regarded as a step or pulse response of a system with unknown initial conditions. To cover for the nonlinear dynamics, a high-order linear model is fitted to the observed ring-down. Different methods can be used but the one that seems to most common in the power systems area is Prony's method see for example Hauer et al. (1990); Pierre et al. (1992). A comparison between three different methods has been performed in Sanchez-Gasca and Chow (1999).

In normal operation identification, the system is only excited by ambient data, this was probably first exploited in Pierre et al. (1997). In that paper the electromechanical dynamics of the WSCC system was identified from an hour long measurement of active power on a major transmission line. Identification from ambient excited systems serves two purposes:

- In a long timescale, the obtained information can be used to calibrate models. It can also aid in generation planning in that infeasible regions will be detected.

- In a short timescale, it is possible to track time varying dynamics. In case an infeasible region is entered operators can be alarmed or special protection schemes can be enabled automatically. The tracking capability has been investigated in Hauer et al. (1998) where it was found that proper determination of the damping was a major obstacle. The estimates turned out to have a large standard deviation compared to the frequency estimates.

Estimation of time varying dynamics often requires the use of recursive algorithms. It can be argued that any algorithm that operates on a batch of data can be used for estimation of varying parameters by performing the estimation on the last N samples. This, however, is often computationally expensive and also introduce dependency on old data that is not valid after, for example, a line disconnection.

The rest of this chapter will discuss choice of suitable measurement signals and a review of some methods that can be used to identify t power system dynamics. Attention is paid to the case where the system is excited only by ambient noise.

3.1 Input signals

Determination of frequency and damping of electro-mechanical modes in a power system is an output-only identification problem. Proper determination of damping from spectral estimates requires, according to Bendat and Piersol (1980), that four conditions are fulfilled: (1) The auto-spectrum of the excitation, $G_{xx}(f)$, must be reasonably uniform over the frequency of the mode; (2) the relative damping ζ_i must be small; (3) the analysis resolution bandwidth B_e must be much smaller than the half-power point bandwidth B_i of the mode, and (4) the mode must not overlap heavily with neighbouring modes. These requirements can formally be expressed as:

1. $G_{xx}(f) \approx$ constant for $f_i - 3B_i \leq f \leq f_i + 3B_i$.

2. $\zeta_i < 0.05$
3. $B_e < 0.2B_i$
4. $(f_i - f_{i-1}) > 2(B_i + B_{i-1})$

Where the relative damping ζ for a pair of eigenvalues at $\sigma \pm j\omega$ is defined as:

$$\zeta = \frac{-\sigma}{\sqrt{\sigma^2 + \omega^2}} \tag{3.1}$$

For power systems, some of these conditions are not always met or are unknown at the time of estimation. Condition 1 is unknown during normal operation and results from Johansson and Martinsson (1986); Ledwich and Palmer (2000) indicate that the excitation has a low-pass characteristic. Condition 2 can be viewed as the wanted result and is thus not an issue. Condition 3 depends on the method in use and the data available and is not considered here. Finally, condition 4 is also unknown.

It is suggested that cross-spectrum estimates should be preferred over auto-spectrum estimates. Cross-spectral estimates together with the coherence function will then aid in determining if a peak in the spectral estimate is due to a peak in the exciting signal or to a mode in the system. As focus here is on damping estimation from local measurements, cross-spectrum estimates are not available unless cross-spectrum with mixed units are considered.

Choice of measurement signal

Active power on a transmission line is the signal that seems to be the most common in use for determination of electro-mechanical (EM) mode parameters (frequency and damping). From a systems view this choice is sensible in that an oscillation is due to a power imbalance at the swinging generators. The missing/exceeding power thus have to be transferred to/from the generators on the transmission lines. From an estimation point of view it means that the measured variable is closely connected to the phenomenon that is to be estimated, which is good. Among the drawbacks are that many estimation techniques require the signal to have a mean value of zero. Furthermore, the mean level of the power can make large jumps. Both these inconveniences can be taken care

of by proper pre-filtering of the signal. Due to the non-linear dynamics of a power system, large oscillations will be accompanied with harmonics, which makes estimation more difficult. For power this becomes apparent when the angle between swinging machines approaches and exceeds 90°. With the frequency range of interest spanning about a decade there is not much that can be done about this but increasing the model order or changing the estimation signal.

The angle between swinging machines is a signal that is perhaps even more tightly connected to the oscillation phenomena. Until recently it has, however, been impossible to measure. An angle difference measurement is obviously not a local measurement and thus requires a viable communication structure. The properties of angle difference are similar to those of active power. For large oscillations, angle difference is not as nonlinear as active power, thereby reducing the amount of harmonics.

If mode estimation is performed at the distribution level, which could be the case for damping controllers, then information on transmission line power is unavailable. Signals at this level that contain system wide information are frequency and voltage. Voltage share many of the properties of power but the connection to the swing phenomena is weaker. The influence on voltage caused by electro-mechanical oscillations can be expected to be small because of the voltage control on the generators. Modern voltage control is typically much faster than the electro-mechanical oscillations.

Local frequency share most of the properties with angle difference. An advantage with frequency is that the jumps visible in power, angle difference and voltage measurements are removed by the integral relation between frequency and angle. Depending on system, however, frequency measurements might have a substantial low frequency (up to 0.05 Hz) behaviour which is not present in the other measurements. This comes from the rigid body motion caused by frequency control.

A closer look at frequency and voltage

Assuming a single machine infinite bus system, what can be expected to be seen in frequency/voltage measurements? For simplicity, only the case with a purely

reactive transmission-line and the classical generator model is studied.

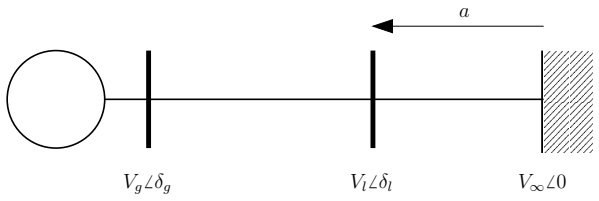

Figure 3.1: Single machine infinite bus system, where a is the relative distance from the infinite bus to the generator.

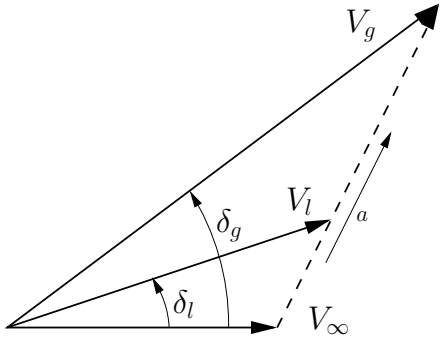

Figure 3.2: Voltage vectors for the infinite bus system in Figure 3.1.

The angle of the voltage vector at a distance a from the infinite bus is given by:

$$\delta_l = \arctan\left(\frac{aV_g\sin(\delta_g)}{(1-a)\,V_\infty + aV_g\cos(\delta_g)}\right) \tag{3.2}$$

Taking the derivative of this with respect to the angle of the voltage vector at the generator gives

$$\frac{d\delta_l}{d\delta_g} = \frac{aV_\infty V_g\cos(\delta_g)(1-a) + a^2V_g^2}{2aV_\infty V_g\cos(\delta_g)(1-a) + (1-a)^2V_\infty^2 + a^2V_g^2} \tag{3.3}$$

which always have a value in $[0, 1]$ (Figure 3.3) for $0 \leq \delta_g \leq \pi/2$, with equality for $a = 0$ and $a = 1$. The quantity $\frac{d\delta_l}{d\delta_g}$ can be seen as an observation gain,

that is how much does our observation change when the generator oscillates. An oscillation in this system is thus best observed as close as possible to the swinging generator ($a = 1 \rightarrow \frac{d\delta_l}{d\delta_g} = 1$). Assuming a sinusoidal oscillation,

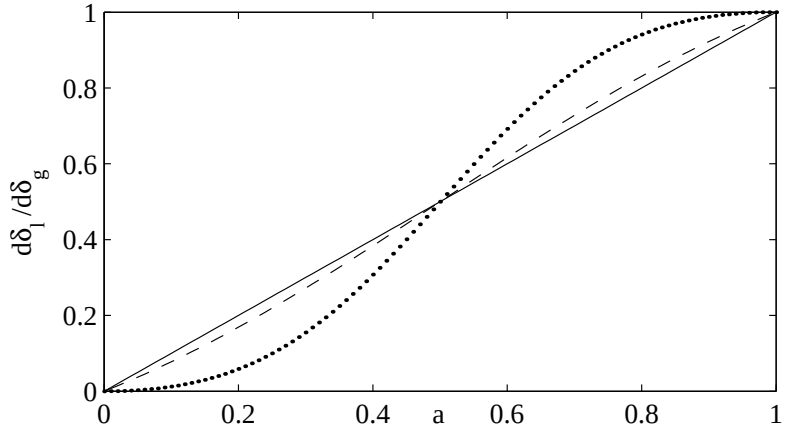

Figure 3.3: $\frac{d\delta_l}{d\delta_g}$ as function of a for $V_g = V_\infty = 1$ and $\delta_g = 0$ (solid), $\pi/4$ (dashed) and $\pi/2$ (dotted).

the instantaneous voltage somewhere along the line can be described as a phase modulated signal with amplitude $\hat{V}$:

$$V(t) = \hat{V}\sin(\underbrace{\omega t + \Delta_0 + \Delta_g \sin(\omega_{osc} t)}_{\theta(t)}) \tag{3.4}$$

Taking the time derivative of the phase angle $\theta(t)$ gives the instantaneous frequency

$$\frac{d\theta}{dt} = \omega + \Delta_g \omega_{osc} \cos(\omega_{osc} t) \tag{3.5}$$

With $\omega = 100\pi$, $\Delta_g = 1^\circ$ and $\omega_{osc} = \pi$, this gives a maximal change in frequency of $\pm 9mHz$ which corresponds to a change in cycle-time of $\pm 3.5\mu s$ which is less than $1‰$ of the cycle-time of the fundamental.

Performing the same kind of analysis on the measured voltage gives the voltage

magnitude

$$V_l = \sqrt{a^2 V_g^2 + (1-a)^2 V_\infty^2 + 2a(1-a)V_\infty V_g \cos(\delta_g)} \tag{3.6}$$

and the change in voltage due to generator swing

$$\frac{dV_l}{d\delta_g} = \frac{-a(1-a)V_\infty V_g \sin(\delta_g)}{V_l} \tag{3.7}$$

This result is however not as easy to interpret as the result for frequency measurement. With sensible values on V_g and V_∞, the result from equation 3.7 will most certainly be small but the result depends heavily on V_g and V_∞ as seen in Figure 3.4. When using change in voltage it thus best to look some-

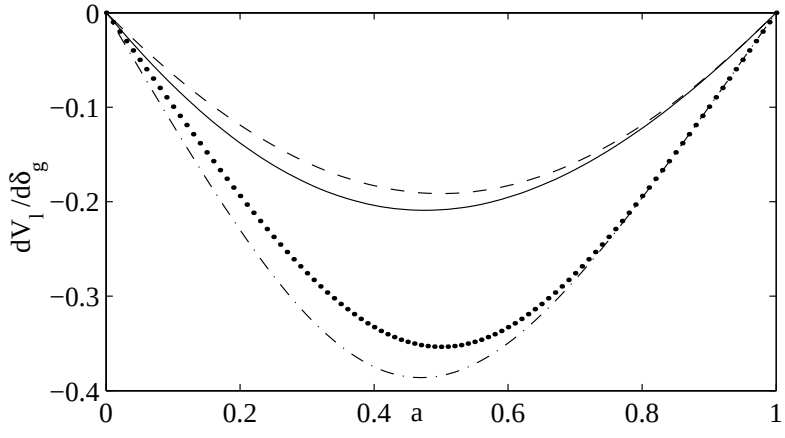

Figure 3.4: $\frac{dV_l}{d\delta_g}$ as function of a for $V_g = V_\infty = 1$ and $\delta_g = \pi/4$ (dashed) and $\pi/2$ (dotted) and for $V_g = 1.2$, $V_\infty = 1$ and $\delta_g = \pi/4$ (solid) and $\pi/2$ (dash-dotted).

where between the swinging parts as the oscillation will be unobservable at the endpoints.

Effects of filtering

Filter design is usually performed with pure oscillations even though the filters are intended to be used with signals that contain a lot of information that is not

in the form of sustained oscillations.

It has been very difficult to find anything in the published literature about how a filter distorts the damping of a signal, since normal analysis only give amplitude and phase information. The damping of a signal is closely related to the peak-width when looking at the signal in the frequency domain. For damped signals it is thus crucial to know how the peak-width is changed by the filter.

As the EM modes are within a known frequency range we will band-pass filter the signals before performing the mode estimation. Traditional filters such as Butterworth and Chebyshev tend to be like more or less well-tuned resonance circuits. Thus, a filter with a narrow passband may oscillate with almost no damping and by this indicating that the system we look at seems closer to instability than it really is.

Finite Impulse Response (FIR) filters are filters which output only depends on the input signal, not on the filtered output. Because of this FIR filters do not have an oscillatory behaviour. For steep and narrow passbands they often tend to need many samples from the input signal and because of this, the time delay from input to output can be substantial (several seconds). Many design techniques for FIR filters also give filters with ripple in the passband. This is not limited to FIR filters; Chebyshev type I filters also have this property Claesson et al. (1990).

EXAMPLE
Consider a band-pass filter with ripple in the passband and a signal coming from a system with poor damping (Figure 3.5). The spectrum of the filtered output as seen in Figure 3.5 is now distorted by the filter in such a way that both the frequency and the damping, determined by the width of the peak, of the input signal is wrong.

Looking at the poles and zeros of the filter and the oscillatory system, Figure 3.6, we can also see that there is almost a pole-zero cancellation. This means that if the damping becomes worse, the signal generated from the oscillatory system might be close to or completely cancelled by the filter and thus invisible in the output.

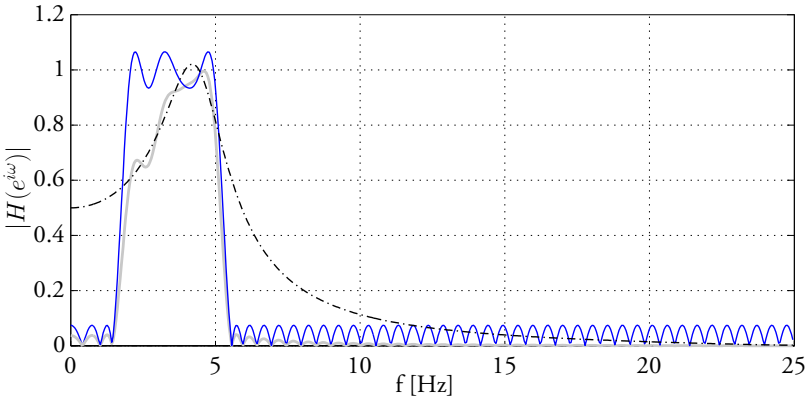

Figure 3.5: Spectrum of input signal (dash-dotted), amplitude function for band-pass filter (solid) and spectrum of the filtered output (solid grey). Notice that the peek has moved and that the shape has changed so much that damping estimated from peak-width is wrong.

Conclusions

As a consequence of the results shown earlier, all filters used in this report have a flat characteristic in the passband. The filters used are mostly first order filters. When a higher roll-off is needed several cascaded first order filters have been applied. The cascaded filters do not have to have the same cut–off frequency.

3.2 Loads and their behaviour

Loads in power system are typically represented as a mixture of constant power, constant impedance and constant current sources. In recent years, dynamic models such as Karlsson and Hill (1994) have been introduced. Common for all these models are that the power they consume is constant unless something happens with the voltage. In our case, we are interested in the random load variations in the timescale of seconds, as these variations make the power system oscillate during normal operation. In Johansson and Martinsson (1986) it is shown that the random load variations have low-pass characteristics and that the standard deviation of the load variation is always less than 2%. The largest

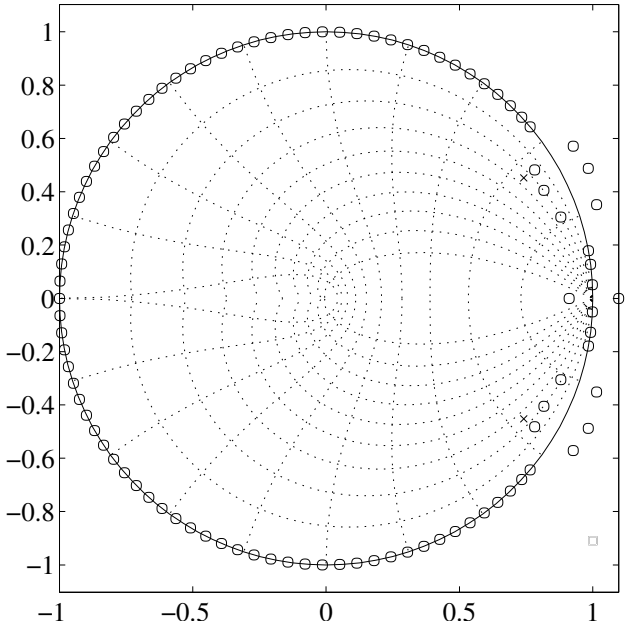

Figure 3.6: Poles of oscillatory system `'x'` and zeros of bandpass-filter `'o'`. It is seen that the pole is difficult to see behind the zero when moving along the unit circle.

deviation from the mean value that has been observed is less than 5% of the mean value itself. These results are based on one hour measurements under several different load conditions.

In Johansson and Martinsson (1986) it is also shown that the statistical properties of the load changes with the load/time of day, that is the load is not stationary in a stochastic sense. The consequences of this are hard to tell but the change in load behaviour is probably smaller than the change in power system dynamics with changing load and time of day.

3.3 Batch estimation

When doing batch estimation, a model is fit to a number of consecutive measurements. This requires that the data has the same stochastic properties for the whole measurement period. Power systems are, as discussed earlier, not stationary in the stochastic sense. If, however we limit our data to for example one hour, then it is probable that the stochastic properties can be considered stationary during this hour. This means that we can derive a model for this specific hour [1].

Linear prediction error methods

The idea behind prediction error methods is to predict future values of a sampled signal, $y(0), y(1), \ldots, y(n)$, by a linear combination of the previous samples. The simplest and most well-known of this class of systems is the autoregressive (AR) model,

$$y(n) = \sum_{k=1}^{p} a_k \, y(n-k) + e(n) \tag{3.8}$$

where $e(n)$ is white noise.

We would now like to determine the coefficients a_k such that the prediction error

$$\epsilon(k) = y(k) - \hat{y}(k|k-1) \tag{3.9}$$

is minimized. $\hat{y}(k|k-1)$ denotes the predicted output at time k given data up to time $k-1$. Minimization of all $\epsilon(k)$ with respect to the parameters a_k in some norm

$$J = \min_{a_k} \sum_{i=p+1}^{m} ||y(i) - \hat{y}(i|i-1)|| \tag{3.10}$$

[1] An hour is probably too long time during the load increase/decrease during morning/afternoon. In this case we might need to use a shorter time interval.

gives the characteristic polynomial of the model

$$A(q) = q^p - a_1\, q^{p-1} + \cdots - a_{p-1}\, q - a_p \tag{3.11}$$

Solving 3.11 now gives us the frequency and damping of the identified modes. It should be noted that equation 3.8 also can be used in the backward direction, that is calculating $y(n)$ from $y(n+1), y(n+2), \ldots, y(n+p)$.

Several different methods exist to solve this problem in an efficient way. Well-known methods are the Yule-Walker and Burg methods (Proakis and Manolakis, 1988, pp 821-831) which can be efficiently solved via the Levinson-Durbin algorithm. These methods were originally developed for spectral estimation and use the auto-covariance of the signal rather than the signal itself. The Levinson-Durbin algorithm however makes these methods useless for this application because the resulting models will always be stable. The Burg algorithm furthermore exhibits spectral line splitting at high signal-to-noise ratios and introduces spurious peaks at high model orders.

If we give up the Levinson-Durbin algorithm we get the unconstrained Burg algorithm which does not have the above mentioned disadvantages. The price we pay is that it is computationally more expensive. Instead of working with the autocovariance the description of this method will follow the lines of Kumaresan and Tufts (1982) where we work directly with the data.

Equation 3.8 can be rewritten into matrix form as

$$\begin{bmatrix} y(0) & y(1) & \ldots & y(p-1) \\ y(1) & y(2) & \ldots & y(p) \\ \vdots & \vdots & \ldots & \vdots \\ y(n-p) & y(n-p+1) & \ldots & y(n-1) \end{bmatrix} \begin{bmatrix} a_p \\ a_{p-1} \\ \vdots \\ a_1 \end{bmatrix} = \begin{bmatrix} y(p) \\ y(p+1) \\ \vdots \\ y(n) \end{bmatrix} \tag{3.12}$$

or shorter

$$\mathcal{Y} = \Phi\theta \tag{3.13}$$

Performing singular-value-decomposition (SVD) on Φ $(n-p+1 \times p)$ we get

$$\Phi = U\Sigma V^H \tag{3.14}$$

where U $(n-p+1 \times n-p+1)$, V $(p \times p)$ are unitary matrices [2] and Σ $(n-p+1 \times p)$ is a diagonal matrix with positive values $[\sigma_1, \sigma_2, \ldots, \sigma_p]$ (assuming $n-p+1 > p$) on the diagonal. From this we now get

$$\theta = V\Sigma^{+}U^{H}\mathcal{Y} \tag{3.15}$$

where Σ^{+} is a diagonal $(n \times m - p + 1)$ matrix with values $[1/\sigma_1, 1/\sigma_2, \ldots, 1/\sigma_p]$ on the diagonal. The solution given by this method minimizes equation 3.10 in 2-norm.

Model order selection

So far we have only dealt with $AR(p)$ models. Our power system is most certainly not an $AR(p)$ system but can be approximated as such a one if we make the model large enough. What size to choose is difficult but generally we get a better fit and a smaller J in equation 3.10 when the model order p is increased. The better fit does not imply that we get a more accurate model with respect to the physical system. Most likely we will get what is called overfitting, that is we also model the noise in the system. Methods such as Akaikes information criterion (AIC) Akaike (1974) and Rissanens minimum description length (MDL) Rissanen (1978) are methods to help us choose a model order that is not too large. Still, the models given by one of these criteria will contain a lot of unwanted information. The problem now becomes to find the interesting information in the model.

Using the method in equation 3.15 it is often possible to see a jump in the singular-values (σ_k), Figure 3.8. This jump can indicate that this is where the useful information ends, with the remaining singular values corresponding to noise/overfitting. By setting the singular values after the jump to zero we emphasize what we think is the important dynamics Kumaresan and Tufts (1982). However, doing this introduces radial bias, which in the discrete frequency domain corresponds to bias in the real part in the continuous frequency domain, that is, bias in the estimated damping. This bias is smaller the larger the model is. It can also be compensated for by manipulating the remaining singular values. This method was also suggested in Kumaresan and Tufts (1982) but un-

[2] A unitary matrix (U) has the property that $U^H = U^{-1}$ and where ^{H} denotes complex conjugate and transposition.

fortunately the instructions are not very clear so this special bias compensation has not been very successful. In Rao (1988) it is shown that the sensitivity of the roots of the prediction polynomial with respect to the filter coefficients decreases with increasing filter-length. This is only true when the signals are pure sinusoids and is of course only valid for the roots belonging to the sinusoids.

The drawback with a model of very high order is that finding the roots of a large polynomial is numerically difficult.

EXAMPLE
Consider the signal (see Figure 3.7)

$$y = e^{-0.01t}\sin(\pi t) + e^{0.0012t}\cos(1.3\pi t) + 0.5\,e(t)$$

for $t \in [0, 100]$, where $e(t)$ is zero mean Gaussian noise with standard deviation 1. Bandpass filtering the signal with a fourth order filter and trying different model orders, AIC and MDL gives us the model orders 198 and 35. Using equation 3.15 with a model order of 200 we get the singular values in

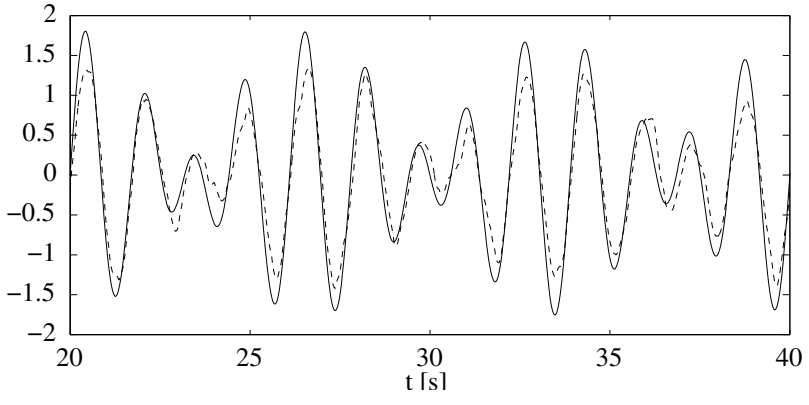

Figure 3.7: Signal without noise (solid) and bandpass-filtered noisy signal (dashed).

Figure 3.8. Clearly there is a jump between the fourth and fifth singular value, indicating that there are four interesting poles. In Figure 3.9 the results are shown for models of order 4, 200 and 200 where $\sigma_5, \ldots, \sigma_{200}$ are set to zero. The fourth order model is obviously poor as there is only one pole(pair) in the

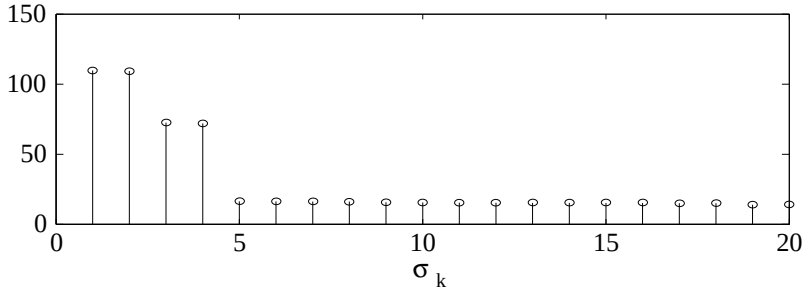

Figure 3.8: Magnitude of singular values.

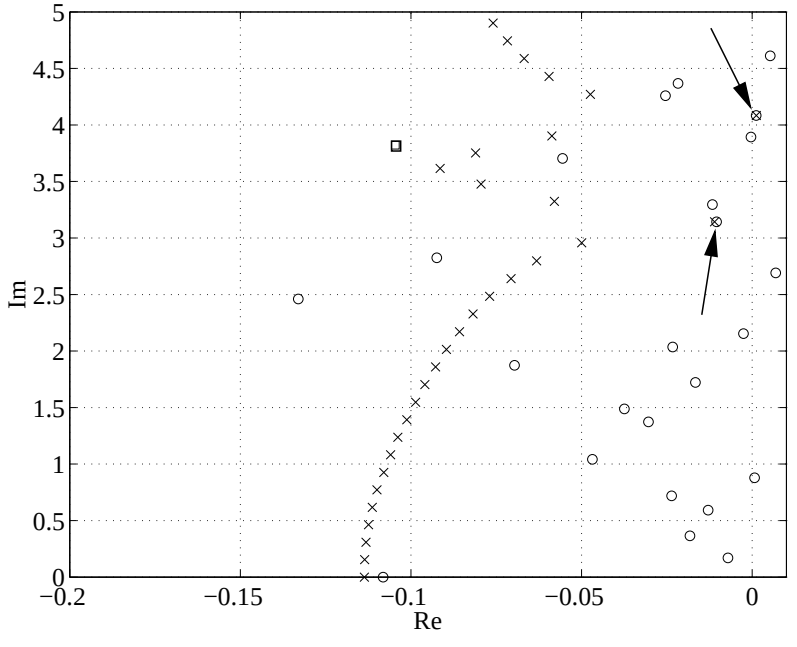

Figure 3.9: Pole locations for models of order, 4 '□', 200 '○' and 200 where $\sigma_5, \ldots, \sigma_{200}$ are set to zero '×'. The arrows indicate where the true poles are located.

region, with the other polepair having a large negative real value. The model of order 200 has poles in the correct locations but also a lot of other poles that correspond to noise/overfitting. How to find the true poles among the other ones is non-trivial. For the model of order 200 with 4 "dominant"poles we can see that there are poles at the correct locations and that the rest of the poles are separated from these four poles, making it easier to find the interesting dynamics. The "dominant" poles for this model are $-0.01105 \pm i3.1429$ and $0.001195 \pm i4.0842$ which are very close to the correct values $-0.01 \pm i3.1415$ and $0.0012 \pm i4.0841$

Other parametrisations

The identification has been performed using the shift operator q, which shifts discrete-time data one step forward. This is just one choice of operator. Another common operator is the δ operator Middleton and Goodwin (1990). Higher order operators such as the Kautz operator Wahlberg (1991); Kautz (1951) might sometimes be better.

Damping estimation from spectral estimates

Note: The angular frequency (ω) used in this section is the *discrete time* angular frequency, that is $\omega = \omega_c/\omega_s$ where subscript c indicates continuous time frequency and subscript s denotes sampling frequency. In order for the Nyqvist sampling theorem to hold, it must be assured that $\omega_c < 2\,\omega_s$.

An alternative to the time domain methods is to determine frequency and damping from spectral estimates. Provided that the conditions on page 42 are fulfilled, the relative damping can be estimated as:

$$\zeta_i = \frac{B_i}{2f_i} \tag{3.16}$$

Calculating the absolute damping σ from 3.1 requires the knowledge of ω which is *different* from the peak frequency value. For low damping, the difference is small and the frequency peak value can be used instead of ω.

The spectral estimate can be computed in a number of ways. It should be noted

that the polynomial identified in the prediction error methods (equation 3.11) can be used to compute the power spectrum as

$$P_{LP}(\omega) = \frac{P_e}{|A(e^{j\omega})|^2} \tag{3.17}$$

where P_e is the variance of the prediction error and subscript LP is used to denote linear prediction error method. This approach can be useful for high order models where it is computationally expensive to find the roots with high accuracy. The interpretation of the poles or pattern of poles might also be easier to do in the frequency plane.

Fourier transforms

The fast way to compute a spectral estimate is to use the Fast-Fourier-Transform which is a special version of the Discrete-Fourier-Transform. Direct usage of these transforms produce, however, poor result on data typical for power-systems. The poor behaviour is probably due to the signals not containing pure sinusoids but rather damped sinusoids with varying phase. The estimates are drastically improved when data is windowed and several estimates are averaged, that is by using Welch's method. Still, choice of segment length, number of segments, window and size of window is an elaborate work.

Capon

The Capon spectral estimator is an estimator that provides a minimum variance unbiased estimate of the spectral components in a signal. It is known that the linear prediction (LP) method exhibits sharp peaks, thus having high spectral resolution. The spectral envelope is however often poorly modelled which has been noticed in, among other fields, speech processing see Murthi and Rao (2000) for a discussion about this. The Capon method, which is a minimum variance (MV) method, produces a better estimate of the envelope and might thus be a suitable candidate for a spectral estimator that is usable for damping estimation where the shape of the envelope is important. The theoretical foundations of the method can be found in Lacoss (1971) and are not discussed here.

The Mth order Capon spectral estimate is given by:

$$P_{MV}^{(M)}(\omega) = \frac{1}{\mathbf{v}^H(\omega)\mathbf{R}_{M+1}^{-1}\mathbf{v}(\omega)} \tag{3.18}$$

where $\mathbf{v}(\omega) = [1, e^{j\omega}, e^{j2\omega}, \dots, e^{jM\omega}]^T$ and where $\mathbf{R}_{M+1}$ is the $(M+1) \times (M+1)$ Toeplitz autocorrelation matrix of the input signal. The autocorrelation r_{yy} of a signal $y(k)$ can be estimated by:

$$r_{yy}(k) = \begin{cases} \frac{1}{N}\sum_{l=1}^{N-k} y(l)\, y(l+k) & k = 0, \dots, N-1 \\ r(-k) & k = -N+1, \dots, -1 \\ 0 & |k| \geq N \end{cases} \tag{3.19}$$

Alternatively, the spectrum can be parametrically written as

$$P_{MV}^{(M)}(\omega) = \frac{1}{\sum_{k=-M}^{M} \mu(k) e^{-j\omega k}} = \frac{1}{|B(e^{j\omega k})|^2} \tag{3.20}$$

The parameters $\mu(k)$ and the spectrum in general can be obtained from the LP coefficients a_k (3.11) and prediction error variance P_e.

$$\mu(k) = \begin{cases} \frac{1}{P_e}\sum_{l=0}^{M-k}(M+1-k-2l) a_l a_{l+k}^* & \text{for } k = 0, \dots, M \\ \mu(-k) & \text{for } k = -M, \dots, -1 \end{cases} \tag{3.21}$$

Multiple window methods

A multiple window method for spectrum estimation is a method which uses several orthogonal windows to estimate the spectrum. The idea behind this Thomson (1982) is that if we have some prior knowledge about what the spectrum looks like, we can the get a better estimate of that part of the spectrum Hansson and Salomonsson (1997). The main problem with this method for damping estimation is that a spectral estimate does not tell if the input signal is stable or unstable. This method is thus not capable of providing all the information we need.

Chirp z-transform

The idea behind using the chirp z-transform (CZT) is to modify the discrete Fourier transform (DFT) to look for growing/decaying oscillations instead of pure sinusoids. A plot of the DFT of three different test signals is shown in Figure 3.10. It can here be seen that the spectral estimate of the signal becomes flatter the quicker the signal grows.

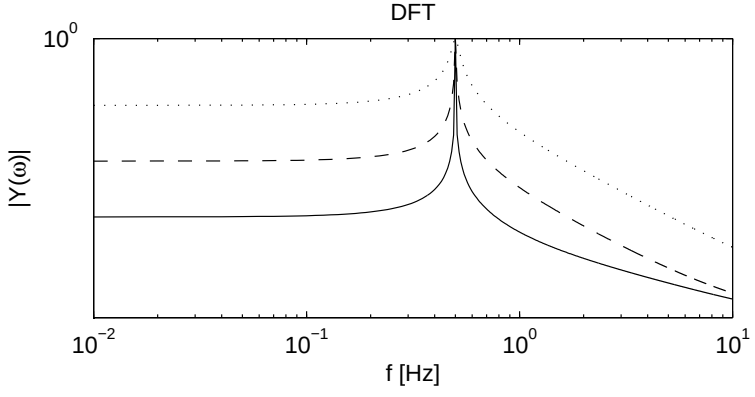

Figure 3.10: DFT of $e^{0.001t}\sin(\pi t)$ (solid), $e^{0.01t}\sin(\pi t)$ (dashed) and $e^{0.1t}\sin(\pi t)$ (dotted).

The DFT of a time signal $y(0), y(1), \ldots, y(N-1)$ is given by:

$$Y(\omega_k) = \sum_{n=0}^{N-1} y(n) e^{-j\omega_k n} \tag{3.22}$$

$$\omega_k = 2\pi k/N \tag{3.23}$$

with $0 \leq k < N$. We notice that the factor $e^{-j\omega_k n}$ is a point that is located on the unit circle, which is where poles to a system with undamped oscillations will appear. If we now modify this factor so that we get points on a circle with radius r_0 we get a transform that is well suited to detect systems that have poles at a distance r_0 from the origin.

$$Y(\omega_k) = \sum_{n=0}^{N-1} y(n)\, r_0\, e^{-j\omega_k n} \tag{3.24}$$

By varying r_0 we can now search for signals with different damping (Figure 3.11). This is a special case of the CZT; in the full CZT we allow $r = r_0\, r_\delta^n$, where r_δ is a complex constant.

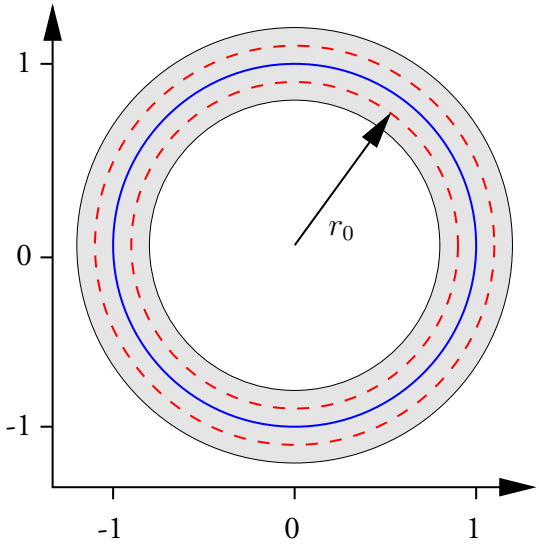

Figure 3.11: Search region for the CZT.

Given that a number of CZTs are performed there are two ways to determine the damping. The first one is to look at the phase of the signal, which was suggested in Bounou et al. (1992). When r_0 is changed, it can happen that a pole that was previously inside the circle moves to being outside of the circle. This will show up in the phase as a phase jump of 360 degrees. In the lower part of Figure 3.12 it can be seen that there is a phase shift of 180 degrees at 0.5 Hz for three of the CZTs, with the fourth one having a phase shift of *minus* 180 degrees. This indicates that the true damping is somewhere in the interval between the dotted line and the dash-dotted line, that is $r_0 \in [1.0002, 1.0004]$. When the signal is noisy this method cease to work because noise in the input signal will show up as phase noise in the CZT, which makes it impossible to see any difference between phase jumps caused by noise or by the real signal.

The second method is to look at the width of the peak at the resonance fre-

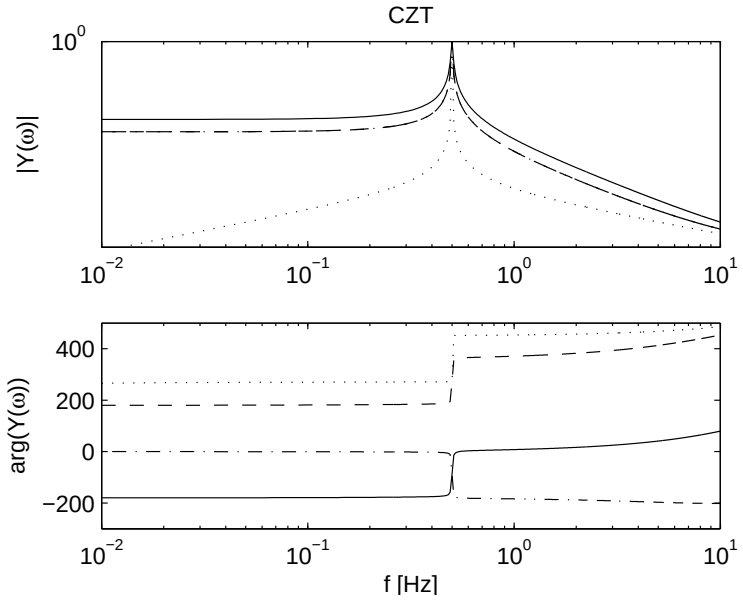

Figure 3.12: CZT for $e^{0.01t}\sin(\pi t)$ with r_0 0.9998 (solid), 1 (dashed), 1.0002 (dotted) and 1.0004 (dash-dotted). r_0 corresponding to $e^{0.01t}$ is in this case 1.00020002

quency. This method is much more robust to noise (see Figure 3.13) but problems arise when there are several peaks in the spectra. Now each peak has to be analysed separately, which needs segmentation of the spectra into interesting parts and then individual normalization for each peak.

The main drawback with this method is that when the studied system has a damped oscillation that is excited several times during the measurement period, the CZT does not recognize this as a damped oscillation. This is correct, because there are several damped oscillations. It now becomes difficult to determine r_0 and r_0 is usually found at the upper bound. The chance of false alarm is thus not negligible, which makes this method difficult to use for identification during normal operation. This drawback might be compensated for by using a shorter measurement period but this also affects the spectral resolution. If the oscillation frequency is known it is possible to get better resolution around that frequency but if this compensates fully for the shorter measurement time is hard

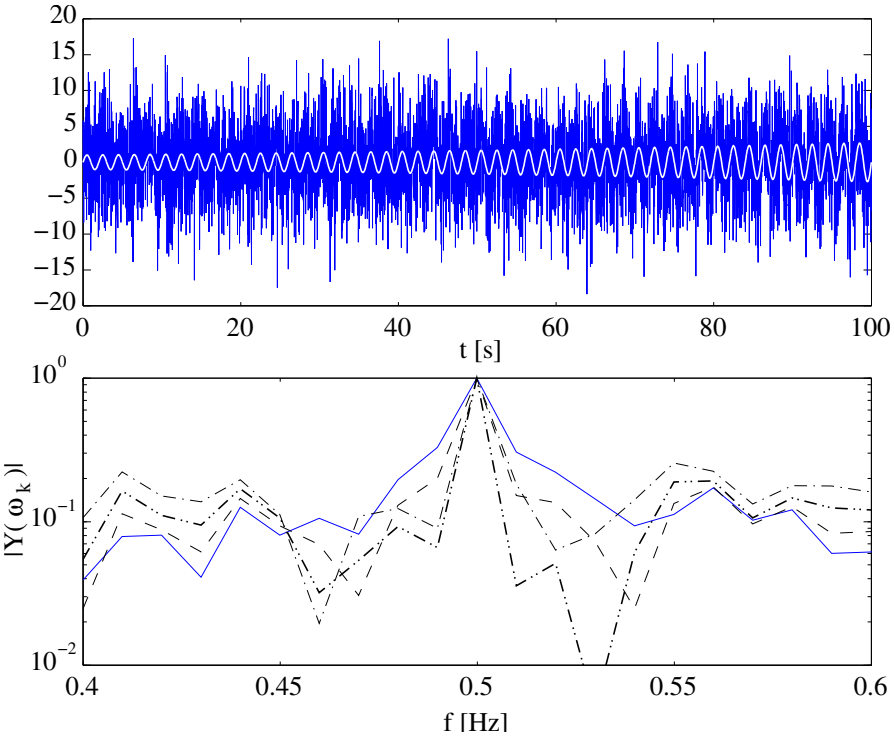

Figure 3.13: Noisy data and true signal (top), CZTs for noisy data (bottom). r_0 0.9998 (solid), 1 (dashed), 1.0002 (dash-dot-dotted) and 1.0004 (dash-dotted). The true value of r_0 is 1.00020002.

to tell.

Sliding window

The idea of calculating the Fourier transform of a window that slides over a signal and then determine the damping from the different spectral estimates was first presented in Lee and Poon (1988). It has since been modified to better cope with multi-mode systems in Lee and Poon (1990); O'Shea (2000, 2002).

For a single mode system it can be described as:

$$y(k) = A\, e^{(j\omega_c+\sigma)k} + e(k) \tag{3.25}$$

with e being white Gaussian noise. Assuming rectangular observation windows the first window is applied from $k = 0$ to $k = T_w$, and the second from $k = T_g$ to $k = T_g + T_w$, the estimate of the damping is

$$\hat{\sigma} = \frac{1}{T_g} \log \frac{F_{T_g}(\hat{\omega}_c)}{F_0(\hat{\omega}_c)} \tag{3.26}$$

For same reasons as for the chirp-z transform this method requires clean ring-down signals to work.

3.4 Recursive identification

Recursive identification is useful when we want to use the estimated mode-parameters for control or alarm. Doing recursive estimation means that the complete model is computed/updated at each sampling interval, which means that it is possible to track varying parameters. This implies that the model order is in some way dependent on the sampling interval as there now is a time limit on each update. Recursive identification techniques furthermore require that the parameters in the model vary much slower than the dynamics of the system being identified. If this is not the case it becomes impossible to distinguish between system dynamics and parameter dynamics. Slower does not mean that it is impossible to have jumps in the parameters. A line switching for example will cause a jump in the parameters but the parameters will then stay at the new value until another event occurs. The recursive identification algorithm will not be able to track the change in parameters instantaneously, it will take some time depending on the choice of algorithm and tuning parameters. But as long the time between events is long enough, the algorithm will adjust to the new operating conditions.

Recursive least squares

The recursive least-squares method solves the same problem as equation 3.10 when using the 2-norm. In the case where the parameters (θ) are time-varying

there is the problem that all information about the past is saved although it may be increasingly irrelevant. To be able to track varying parameters better, forgetting is introduced, that is less attention is paid to old data. An alternative is to restart the estimator if for example some change detection algorithm alarms.

The recursive least squares method can be derived in the following way. First define regressors and parameter estimate:

$$\begin{aligned} \varphi_k &= \begin{bmatrix} y(k-p) & y(k-p+1) & \dots & y(k-1) \end{bmatrix}^T \\ y_k &= y(k) \quad \theta = \begin{bmatrix} a_p & a_{p-1} & \dots & a_1 \end{bmatrix}^T \end{aligned}$$

at time k the data is organised as

$$\Phi_k = \begin{bmatrix} \varphi_1^T \\ \vdots \\ \varphi_k^T \end{bmatrix} \quad Y_k = \begin{bmatrix} y_1 \\ \vdots \\ y_k \end{bmatrix}$$

which is equivalent to equations (3.12, 3.13). The solution to equation 3.10 at time k can then be written as:

$$\hat{\theta}_k = (\Phi_k^T \Phi_k)^{-1} \Phi_k^T Y_k$$

Introduce

$$\mathbf{P}_k = (\Phi_k^T \Phi_k)^{-1} = \left(\sum_{i=1}^{k} \varphi_i \varphi_i^T \right)^{-1} \tag{3.27}$$

after some manipulation the solution can now be expressed as

$$\mathbf{P}_k^{-1} = \mathbf{P}_{k-1}^{-1} + \varphi_k \varphi_k^T \tag{3.28}$$

$$\hat{\theta}_k = \hat{\theta}_{k-1} + \mathbf{P}_k \varphi_k (y_k - \varphi_k^T \hat{\theta}_{k-1}) \tag{3.29}$$

This formulae is not usually used because of requirement to calculate the inverse of $\mathbf{P}_k$ in each iteration. Instead equation 3.28 is rewritten using the matrix inversion lemma so that $\mathbf{P}_k$ is updated instead of $\mathbf{P}_k^{-1}$

Modifying the loss-function (equation 3.10) to forget old samples it now becomes

$$J(k) = \sum_{i=1}^{k} \lambda^{k-i}(y(i) - \hat{y}(i|i-1))^2 \tag{3.30}$$

where $\hat{y}(i|i-1) = \varphi_k^T \hat{\theta}_k$ and $\lambda \in [0, 1]$ is our forgetting factor. Performing the same steps as above the algorithm can now be written as:

$$\epsilon_k = y_k - \varphi_k^T \hat{\theta}_k \tag{3.31}$$

$$\hat{\theta}_k = \hat{\theta}_{k-1} + \mathbf{P}_k \varphi_k \epsilon_k \tag{3.32}$$

$$\mathbf{P}_k = \frac{1}{\lambda}\left(\mathbf{P}_{k-1} - \frac{\mathbf{P}_{k-1}\varphi_k\varphi_k^T\mathbf{P}_{k-1}}{\lambda + \varphi_k^T\mathbf{P}_{k-1}\varphi_k}\right) \tag{3.33}$$

where again $\hat{\theta}_k$ is the parameter estimates at time k and φ_k^T is $[y(k-p), y(k-p+1), \ldots, y(k-1)]$ for a model of order p. $\mathbf{P}(0)$ is an initial estimate of the covariance of the parameters θ. It is commonly chosen as a diagonal matrix with large positive values on the diagonal. $K(k)$ is a time-varying gain vector. Basic theory of recursive identification can be found in Ljung and Söderström (1983).

Directional forgetting methods

Estimator windup is a common phenomenon in recursive identification with forgetting. The new information arriving does not update the parameter estimates because the prediction error is small. At the same time old information is constantly forgotten although this information is still valid. After some time everything about the past is forgotten and the output from the estimator is highly unreliable even if the prediction error is small. There are several alternatives to circumvent this problem. One is to stop the updating when no new usable information is collected. This requires us to in some way specify a criterion for when the data is usable or not which is non-trivial. Another alternative is to only forget old information in the same direction as the new data is collected; this is called directional forgetting.

Two different methods for directional forgetting have been tried, one from Cao and Schwartz (2000) and one from Parkum (1992). *Note:* due to the more

complicated update of the $\mathbf{P}$ matrix in these methods, the notation is expressed in pseudo-code which is indicated by the use of the assignment ($:=$) operator rather than the equivalence ($=$) operator. The order in which the calculations are performed is therefore most important.

The algorithm from Parkum (1992) is expressed as:

$$K := \mathbf{P}\varphi_k \left[I + \varphi_k^T \mathbf{P}\varphi_k\right]^{-1} \tag{3.34}$$

$$\hat{\theta} := \hat{\theta} + K\left(y_k - \varphi_k^T \hat{\theta}\right) \tag{3.35}$$

$$\mathbf{P} := \frac{\alpha_1 - \alpha_0}{\alpha_1}\mathbf{P} + \alpha_0 I \tag{3.36}$$

$$\mathbf{P} := \left(I - K\varphi_k^T\right)\mathbf{P} \tag{3.37}$$

where $0 < \alpha_0 < \alpha_1 < \infty$, which limits the eigenvalues of $\mathbf{P}$ between α_0 and α_1. The upper limit prevents estimator windup and the lower limit guarantees that the estimator is always alert to some extent.

The algorithm from Cao and Schwartz (2000) has only one parameter, $\lambda \in [0, 1]$ which is the forgetting factor.

$$\mathbf{P} := \begin{cases} \mathbf{P} & \text{if } |\varphi_k| < \epsilon \\ \mathbf{P} + \frac{1-\lambda}{\lambda}\frac{\varphi_k \varphi_k^T}{\varphi_k^T \mathbf{P}^{-1} \varphi_k} & \text{otherwise} \end{cases} \tag{3.38}$$

(3.39)

$$\mathbf{P} := \mathbf{P} - \frac{\mathbf{P}\varphi_k \varphi_k^T \mathbf{P}}{1 + \varphi_k^T \mathbf{P}\varphi_k} \tag{3.40}$$

$$\hat{\theta} := \hat{\theta} + \mathbf{P}\varphi_k\left(y_k - \varphi_k^T \hat{\theta}\right) \tag{3.41}$$

This algorithm also has the property that it works as a least-squares estimator without forgetting when $|\varphi_k| < \epsilon$.

Extended Kalman filter

The models described in the previous sections have all been linear in their parameters. This facilitates the construction of the estimator but to find the modes of the model we have to find the roots of a polynomial. Furthermore, it is

difficult to incorporate prior knowledge about modes into this kind of model because the information will be spread out on all coefficients in the polynomial in a nontrivial way. If we want to identify the actual mode parameters we have to use a non-linear estimator. The most well-known non-linear estimator is probably the Extended Kalman filter (EKF). The EKF has been successfully used for estimation of sinusoids in noise Scala et al. (1996); Scala and Bitmead (1996); Nishiyama (1997) some of these ideas have been used for determination of frequency and voltage-amplitude in a power system Dash et al. (2000).

It is known that the EKF can have poor convergence properties. The convergence properties can be very dependent on the parametrisation of the model. For systems that are highly nonlinear there seems to be some interesting results in Julier (1997). In this method the Jacobian of the system is not needed. Instead noise is processed through the system model to find out the distribution one step ahead.

Because of these factors a number of different models were tried. Describing either the system as an $AR(p)$ model or the output as a sum of exponentially growing/decaying sinusoids. As there exist several implementations of EKFs with different properties Chui and Chen (1999), a number of different algorithms were tested. Unfortunately the achieved results were disappointing. On synthetic data the methods work well but are still very sensitive to unmodelled dynamics. On measured data, however, the methods have failed completely. This is not necessarily due to the methods, it might be a poor parametrisation of the model. Because no usable results have been achieved with EKFs, no models are presented here.

Recursive spectral estimates

As pointed out earlier it might sometimes be easier to get an understanding of the system under identification by looking at a spectral estimate rather than eigenvalues. It is worth to notice that $\mathbf{P}_k$ as defined in equation 3.27 is actually an estimate of $\mathbf{R}^{-1}$ used in the Capon method (equation 3.18). This enables us to easily track the spectral estimate over time.

$$P^{MV}(\omega) = \frac{1}{\mathbf{v}^H(\omega)\mathbf{P}_k\mathbf{v}(\omega)} \tag{3.42}$$

If more detailed information is needed it is then possible to solve for the eigenvalues. It should be noted that using forgetting in the updates of $\mathbf{P}_k$ as in (3.31) makes $\mathbf{P}_k$ a biased estimate of $\mathbf{R}^{-1}$. Using the directional forgetting methods the interpretation of $\mathbf{P}_k$ becomes even more difficult as now only parts of $\mathbf{P}_k$ are updated. Tests have, however, indicated that the spectral estimates obtained with these update techniques work.

3.5 Conclusions

A number of different methods for estimation of eigenvalues of a dynamic system have been investigated. The CZT and FFT sliding window method are unsuitable when working with direct analysis of ambient measurements. Used on derived quantities, such as the auto-covariance of the data they should be usable. This has, however, not been investigated.

The envelope of a spectral estimate is the key variable when determining the damping from spectral estimates. Many methods developed for spectral estimation focus on the spectral resolution, giving sharp peaks for frequencies present in the signal. While relevant in many cases it is a major drawback in damping estimation. Among the studied methods, the Capon method often gives a smooth estimate which seems usable for determination of the damping. If used to track time varying dynamics all spectral estimators have the drawback that they are unable to distinguish decaying signals from increasing signals. For signals that are close to pure sinusoids they need to be complemented with another detection mechanism to tell if the system is stable or not.

The LP methods works well in many cases but it can be observed that increasing the model order move the poles closer to the imaginary axis. One way to avoid high model order can be to use another system model. In many cases a low order $ARMA(p, q)$ model

$$y(k) = a_1 y(k-1) + \ldots + a_p y(k-p) + c_0 e(k) + \ldots + c_q e(k-q)$$

performs much better than a high order $AR(p)$ model. The solution to the $ARMA$ model is, however, much more complicated than the solution to the AR model. When using $ARMA$ models on test signals the difference in performance compared to AR models was small. This, however, need not be the

case for all systems. Depending on system the more expensive use of $ARMA$ models might be justified.

The EKF seems interesting and should probably be studied in more detail. In particular it could be beneficial to combine a low order EKF together with a high resolution spectral estimation algorithm. The spectral estimator would then feed the EKF with the imaginary parts of the eigenvalues hopefully making it easier to determine the damping of of a few selected poles.

Presentation of system damping to an operator is an elaborate task. For linear systems it can be expressed either as eigenvalues or by a spectrum. It seems that a spectrum is easier to interpret for an operator than the location of eigenvalues. This is especially true for high order models.

Chapter 4

Damping estimation – Case studies

In this chapter the algorithms from the previous chapter are tested on four different cases. One case is a simulation where the power system becomes unstable after increasing the transfer on a line. Three cases are based on measurements. Two of these cases represent the NORDEL system which is represented in normal operation and operation with a weakened connection between Sweden and Zealand (Denmark). The last case is the event on August 10, 1996 in the WSCC system described on page 2 in the introduction.

Wall-outlet measurements of voltage and frequency were performed at the technical university of Denmark in Copenhagen. Despite the small variations in frequency it was possible to identify two modes; one at 0.3 Hz and the other one at 0.5 Hz. The damping was so high that it could not be determined to more than satisfactory.

A simulation of the NORDEL power system was performed in the ARISTO simulator. Transfer on a critical line was increased until the system became unstable. The unstable mode was identified from different "measurements". Using a recursive estimator with a low order model it was possible to automatically detect instability before an operator could have done it.

Phasor measurement units were located in a substation close to a large generator in Zealand and in the substation in Sweden where the tie-lines to Zealand originate. Upon disconnection of the two 400kV lines between Sweden and Zealand (leaving only two 130kV lines for the interconnection) an oscillation with a frequency of 0.5 Hz was visible. The damping of this oscillation was determined within 3 s using a low order recursive algorithm.

The WSCC system was highly stressed on the afternoon of August 10, 1996. Due to a number of events the system approached small signal instability, which eventually was reached, resulting in separation of the network into four islands. It will be shown that usage of the described methods would have detected low damping at least 5 min before the separation.

4.1 Wall outlet

Voltage (rms) and frequency were measured in a 230V wall-outlet at the Technical University of Denmark (DTU). There are three measurement series: The first one consists of 10 minutes long measurements from each hour starting at lunch and continuing until midnight. The second one is an entire day (24 h) with small gaps at each hour, needed to save data to disk. The third measurement series is a one hour long measurement with each sample time-stamped, with the time coming from a GPS clock. The measurement equipment gives one sample per period of the measured frequency, thus giving a sequence with a varying sampling rate. Analysis was performed on raw data and on data that had been interpolated into fixed sampling rate but no significant differences were observed. Based on this, all subsequent analysis were performed assuming constant sampling rate. This is an adequate assumption considering that the variation in sampling frequency is less than 1‰ of the fundamental.

A number of measurement series were discarded because of large peaks in the frequency and voltage measurements. These peaks are due to a laser printer connected to the same outlet as the measurement equipment (Figure 4.1).

Looking closer at frequency (Figure 4.2) and remembering the results from equation 3.5 we notice that it is probably going to be quite difficult to estimate the damping from these measurements. In order to get any result, data

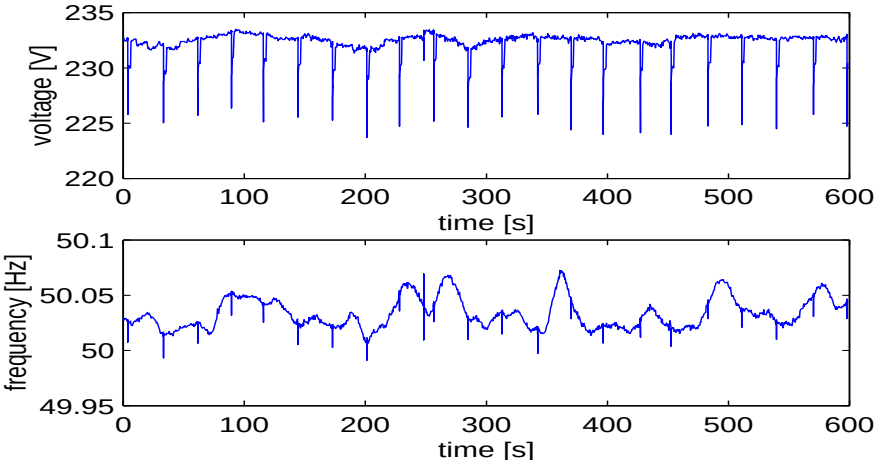

Figure 4.1: Voltage and frequency in a wall outlet, the peaks are due to a laser printer warming up the drum.

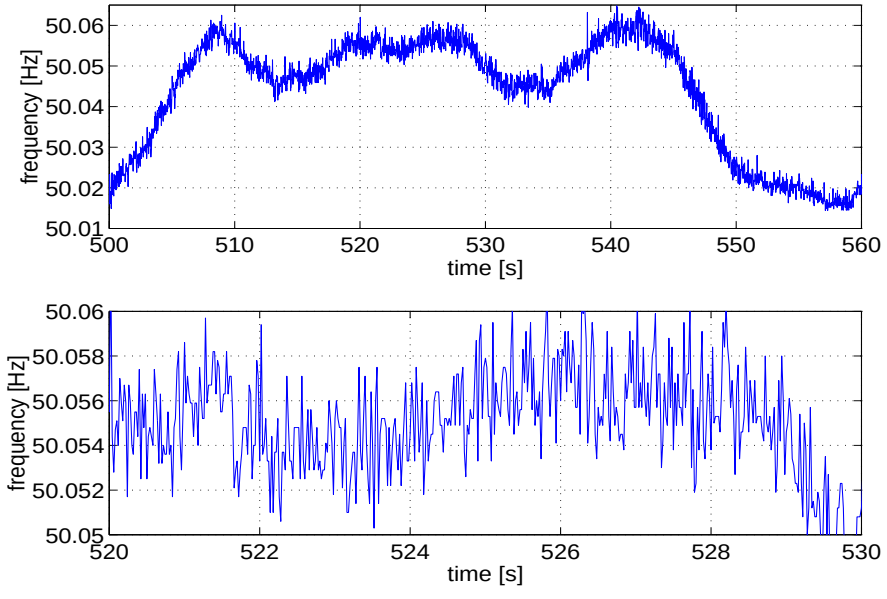

Figure 4.2: Close-up of frequency variation.

were bandpass filtered with two first-order high-pass filters (cut-off frequency $\omega_c = 0.6$) and then low-pass filtered with two first order low-pass filters (cut-off frequency $\omega_c = 6.3$). Some of the measurement series also contained peaks at $[1, 2, \ldots, 25]$ Hz. In order to eliminate these peaks a notch filter tuned to $[1, 2, 3, 4, 5]$ Hz was used. Data were then downsampled by a factor of 20, corresponding to a sampling frequency of 2.5 Hz. [1]

Analysis

To get an idea of what to look for, spectral analysis using Welch's method, Proakis and Manolakis (1988), was performed on a one-hour measurement that had been bandpass filtered but not decimated (Figure 4.3). In this figure we can see that there is a peak at about 0.3 Hz, another peak at about 0.5 Hz and depending on window length maybe one peak near ≈ 0.6 Hz. After this the data was lowpass-filtered and downsampled to 2.5 Hz.

As the damping seems to be quite high we will probably need all available data and thus batch estimation was performed on the one hour data series, and both the normal and the SVD-method were used. The chosen predictor-lengths were [2,4,6,8,10,20,100] delays corresponding to [0.8, 1.6, 2.4, 3.2, 4.0, 8.0, 40] seconds. The total filter-length for the SVD method was chosen to 100 making the two longest filters equal. The singular values for the SVD method are seen in Figure 4.4. In contrast to Figure 3.8 there is no obvious jump in the magnitude of the singular values, making it more difficult to estimate the needed model order.

The pole location for the different models can be seen in Figure 4.5, where the poles in the upper figure are estimated using normal least-squares technique and the SVD method is used for the bottom figure. For both methods it can be seen that the higher th model order is, the lower the damping of the modes becomes. There is also a significant difference between the pole locations for the different methods. The poles obtained with the SVD method have much lower damping than poles obtained using the normal method. We can also see that the damping for the pole with imaginary part ≈ 2 (corresponding to

[1] Downsampling is done because it will prevent an unnecessarily long model as there seems to be no useful information above 1 Hz.

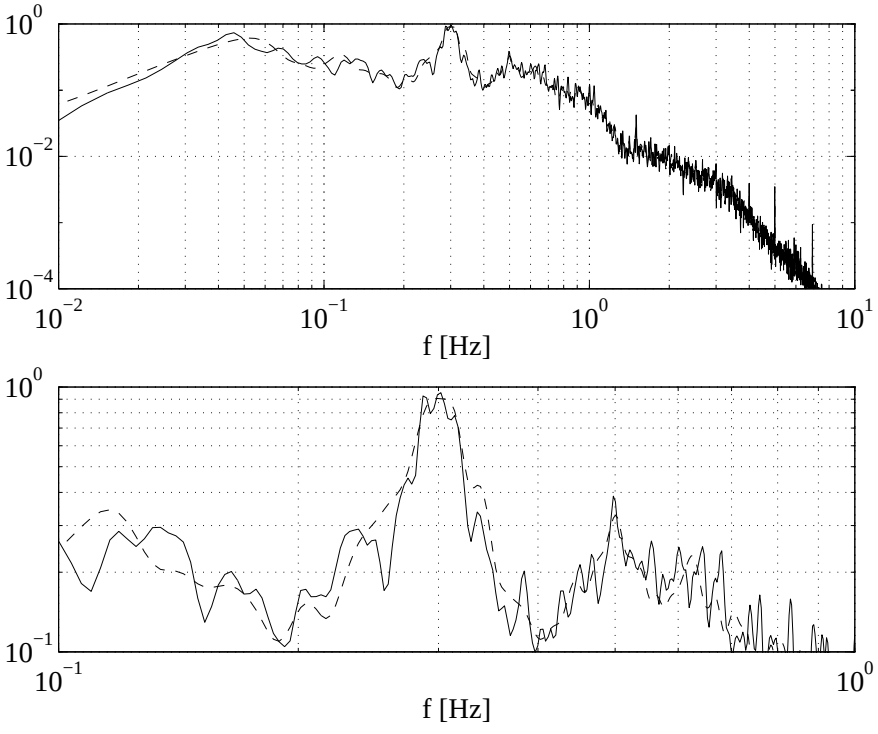

Figure 4.3: Spectral estimate of line-frequency 2001-02-21 (top) and details of upper figure (bottom). Data is bandpass filtered, spectrum is estimated with Welch's method, sampling frequency 50 Hz, FFT length 16384, Hanning window with length 8192 (solid) and 4096 (dashed).

0.3 Hz) changes its location drastically for the normal algorithm with the real part varying between -1.3 (second order system but imaginary part wrong) up to -0.05 for 100th order system. For the SVD method the change in real part for this mode is not that large, -0.06 up to -0.045, but as mentioned earlier the difference between pole location for the two methods is large.

Choosing the appropriate method and model order from the pole location is not obvious. One way to compare different models is to calculate their spectra and compare with the estimated spectrum in Figure 4.3 which is done in Figures 4.6

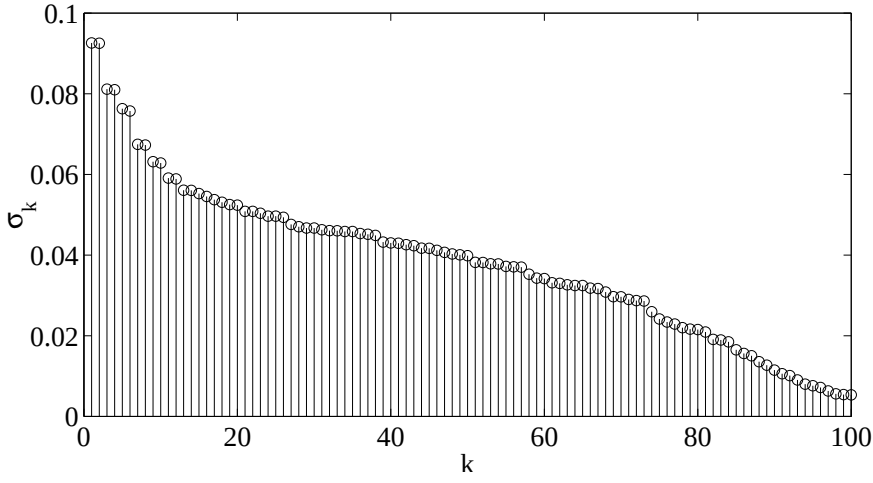

Figure 4.4: Singular values (σ_k) for a 100th order model, notice that there is no sharp jump like in Figure 3.8.

and 4.7. We can now see quite a large difference between the model spectrum for the low order model and the estimated spectrum. The difference decreases with increasing model order and is quite small at 0.3 Hz for the 100th order model (Figure 4.7)

Another way to compare models is to look at the prediction error, or even easier, at the auto-covariance function of the prediction error. If the predictor is good, the prediction errors should be white noise. In Figure 4.8 we can see that the 20th order model indeed gives a white prediction error whereas a 20th order SVD model still have some dependency between the prediction errors. For the second order model we can again see that the normal method performs better than the SVD method even though the estimated frequency (Figure 4.6 top) is not correct!

Results

Various model orders and structures have been tried on a one hour measurement series. Sufficient model order seems to be about 20. The damping for the mode

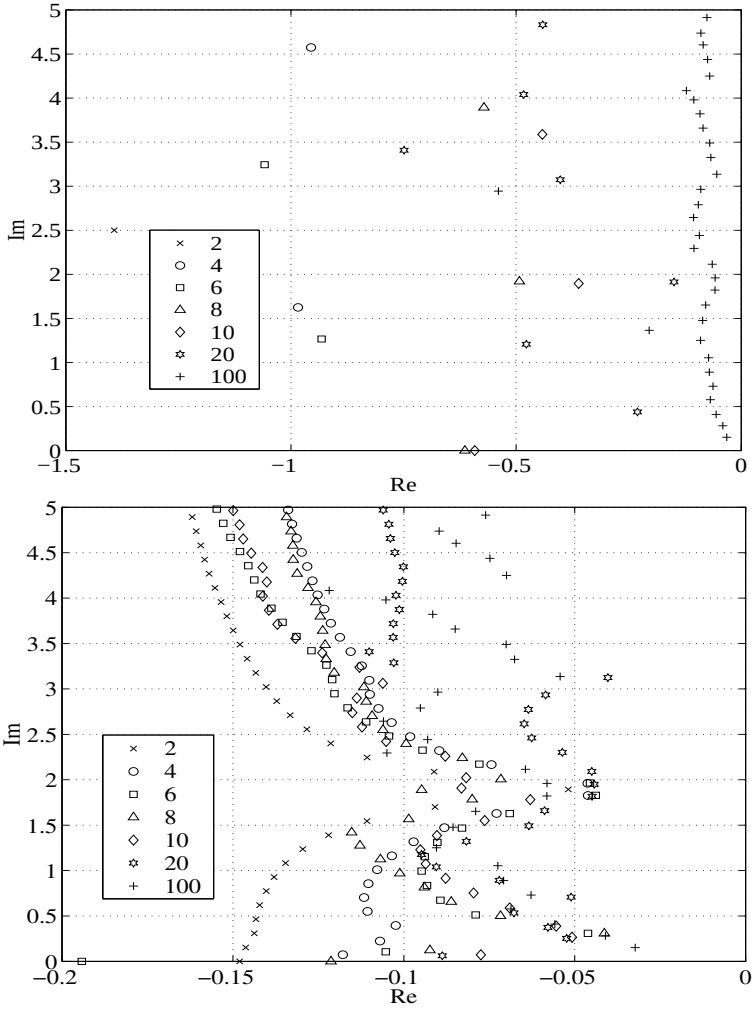

Figure 4.5: Poles from normal prediction error method (top) and poles from SVD method with predictor length 100. Notice the different scales for the real axes. The 100th order model '+' are equal in both figures. Using the SVD method the peaks are easier to find from pole locations. The damping, however, is to low to be realistic. For both methods it can be observed that increasing the model order will move the poles closer to the imaginary axis.

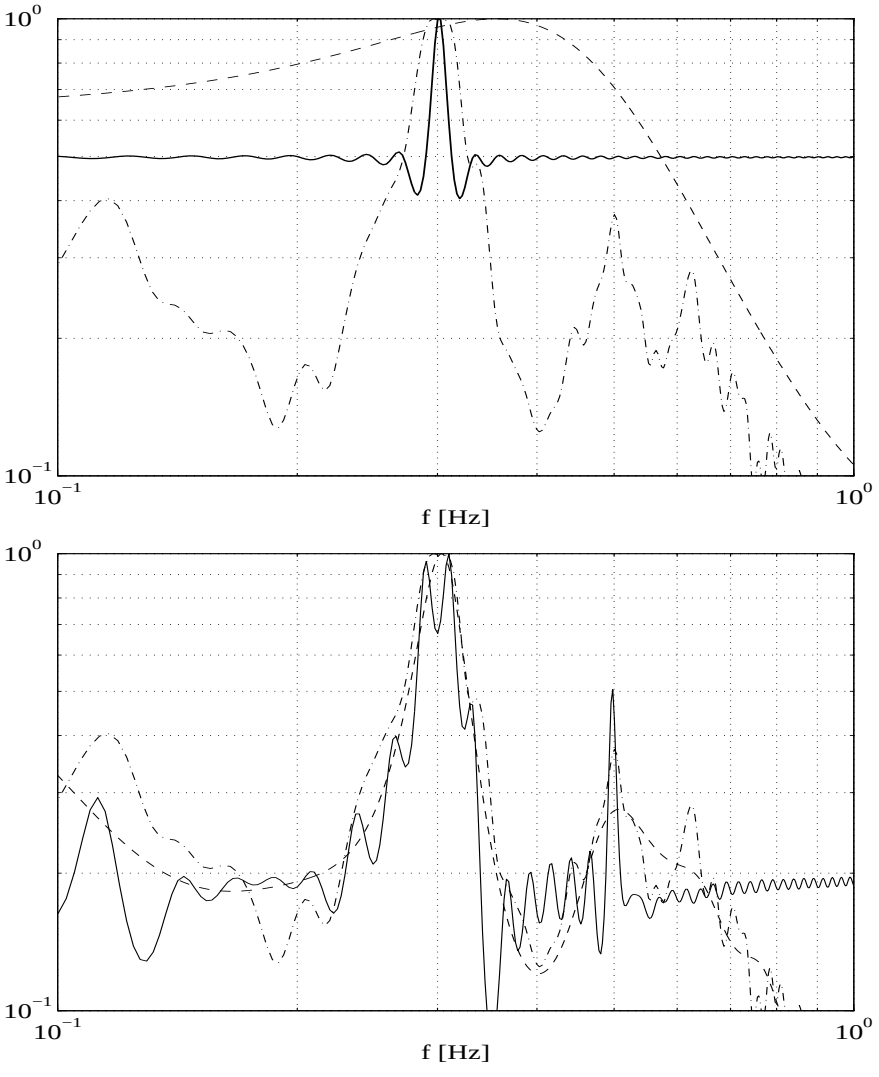

Figure 4.6: Spectral estimates obtained with Welch's method of line-frequency (dashed-dotted) and spectrum for second order model (dashed) and 100th order model (solid) with 2 dominant poles (top). Spectral estimates of line-frequency (dashed-dotted) and spectrum for 20th order model (dashed) and 100th order model (solid) with 20 dominant poles (bottom).

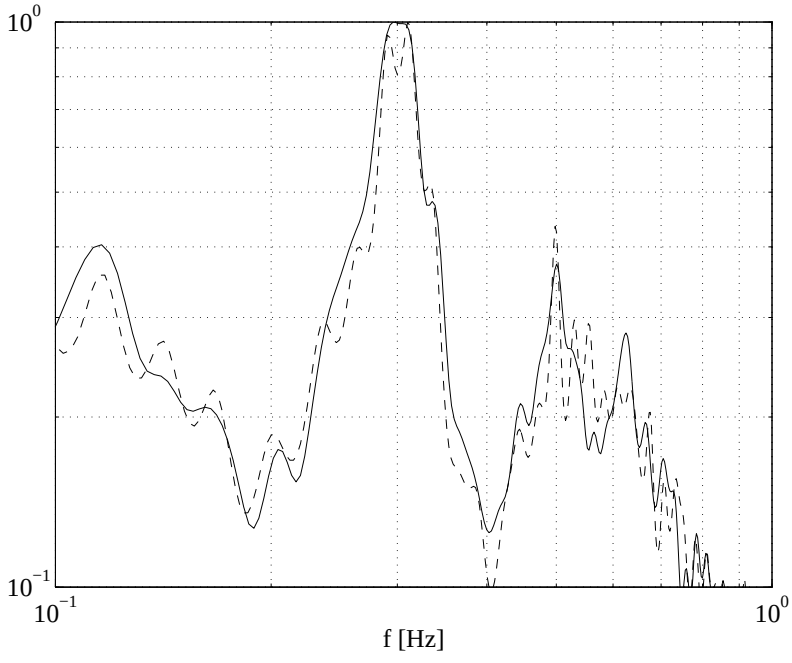

Figure 4.7: Spectral estimate of line-frequency obtained with Welch's method (solid) and spectrum from 100 order model (dashed).

at 0.3 Hz is approximately in the interval -0.18 to -0.12 which is sufficiently high. The modes at higher frequencies have even higher damping and are thus not interesting. The uncertainty in the damping for these modes is also too large.

Conclusions

Prediction error methods are good at what they are constructed for, predicting the next value. For the used data they are not very good at predicting anything more than the next sample. Using the same model for predicting M steps ahead results in large prediction errors. This is perhaps more due to the data having too large damping than to the method itself. Estimating an M-step predictor (Ledwich and Palmer (2000)) instead of a one step predictor does not

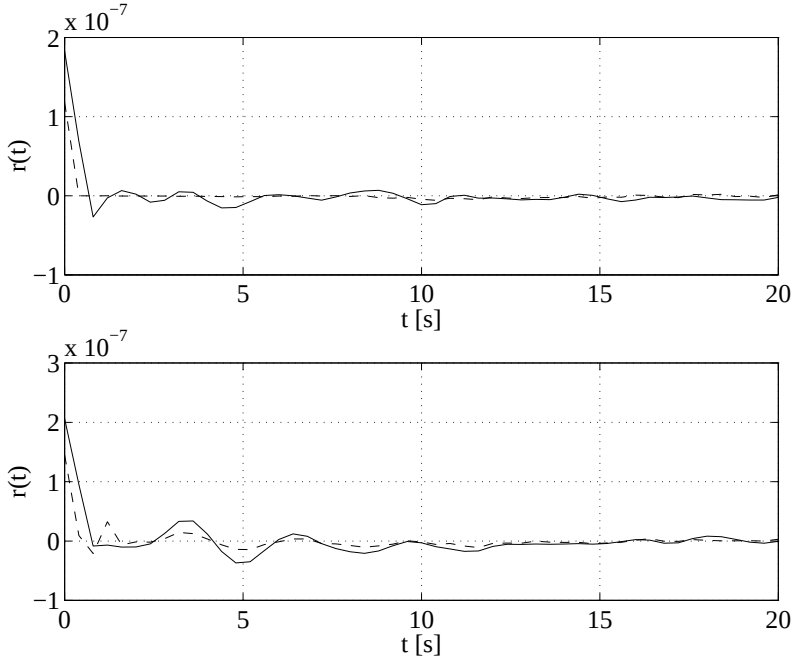

Figure 4.8: Covariance of the prediction-error for 20th order models (top) and second order models (bottom). Dashed lines are from normal prediction error methods, solid lines from SVD method with predictor length 100.

improve the results. For the estimated models it is hard (impossible) to draw any conclusions about the dynamics of the actual system by looking at the roots of the models. Two models that make almost identical prediction errors can have vastly different roots. Again this is probably due to the data having a low signal-to-noise ratio.

The following behaviour has been observed :

- The higher order of the model, the lower is the damping of all the poles. Whether this is true or if it depends on the fact that the roots of a high order polynomial have to be found is unknown. But it is known that it is difficult to get high accuracy for roots of high order polynomials.

- A short measurement series seems to give models with lower damping.
- A model that is estimated using only a few singular values gives large prediction errors and a spectrum that looks strange. However, the important poles are easy to identify.

4.2 Simulated data from Aristo

The damping in the NORDEL system is in normal cases high enough to not cause any problems. This makes it hard to verify the ability to make early warnings in case of poor damping as we may have to wait a long time before we can get measurements from a situation with poor damping. Because of this the measured signals were completed with simulated data to benchmark the methods. The simulations were performed in ARISTO which is a simulation tool developed by Svenska Kraftnät [2] for operator training. The choice of ARISTO as simulation tool was simple because it is the only simulator having random load-variations.

The simulation was performed on a detailed model of the transmission and subtransmission network in NORDEL. Frequency data obtained from these simulations is thus not directly comparable with the measurements because the lowest voltage level in the model is 70 kV.

In the simulation we start in a situation with low damping and one important line disconnected. The damping is decreased even more by ramping up generation in one part of the system and ramping down generation in another part until the stability is lost. To prevent separation, the disconnected line is again taken into operation.

Analysis

For the analysis we now use the recursive methods because the system is not stationary (generator ramping). Before identification the data were bandpass filtered and downsampled to a sampling rate of 2.5 Hz.

[2] the Swedish National Power Grid operator

First, the normal RLS method (equation 3.31) was tried. The estimates obtained with this method were noisy and it was believed that this was due to poor excitation. In order to make the estimates somewhat less noisy two direction-forgetting methods were tried. The results here are obtained with the method in Cao and Schwartz (2000) (equation 3.38-3.41). This method was chosen because it was easy to tune to the different signals.

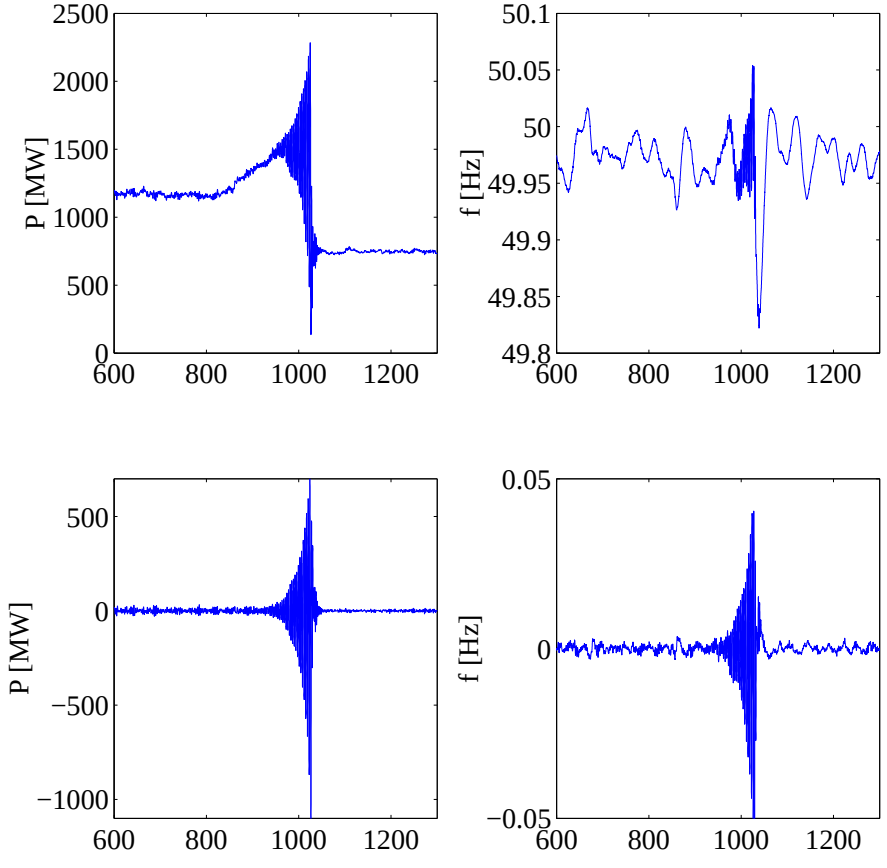

Figure 4.9: Power and frequency signals (top), bandpass filtered signals (bottom). Notice the slow dynamics in the unfiltered frequency signal.

In Figure 4.9 we see two signals from the simulation (top) and the bandpass-

filtered signals used for identification (bottom). A close-up of these signal is depicted in Figure 4.10 where oscillations are readily observed. We also notice that the oscillations are easier to see in the filtered power signal than in the filtered frequency signal. This is not surprising as frequency is a secondary effect of oscillations in power. It can also be that a mode is better seen in some signals than in other signals, Samuelsson (1997).

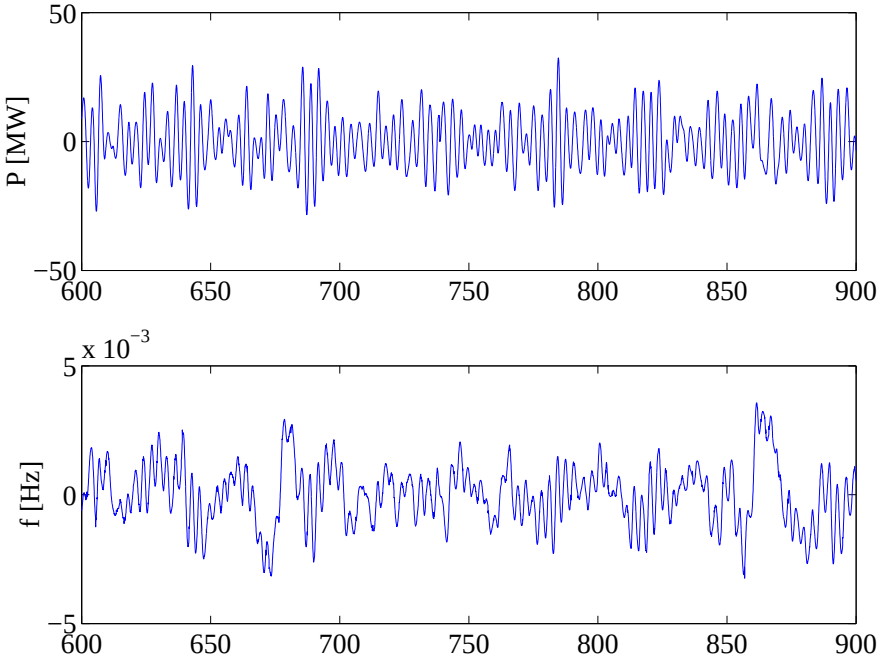

Figure 4.10: Close up of the bandpass filtered signals in Figure 4.9.

Results

Results from identification around the time when instability occurs is seen in Figure 4.11, where we once again have power but this time between Sweden and Finland while the frequency is recorded in Lund. The reason that power between Sweden and Finland is used instead of power between Sweden and

Norway as in Figure 4.9 is that the power between Sweden and Finland was the best signal that was available to determine instability. These results were obtained with a fifth order model and forgetting factor of $\lambda = 0.98$.

In Figure 4.11 we can see that the power signal is superior to the frequency signal for detection of instability. The shaded areas indicate where one would consider the system unstable. We can also see that as the damping (σ) decreases so does the oscillation frequency (ω) of this mode which is reasonable as the synchronizing power becomes weaker when the angular difference between the involved machines increases.

All frequency signals have approximately the same behaviour. If instead frequency difference is used we get a result that is close to that obtained with power as input signal. The frequency difference should be taken between distant places in order to obtain a good result. Looking closer to the figure we see that both the real and imaginary values for the different signals are different at $t = 900$ and $t = 1050$. This is probably due to the fact that in the beginning the estimators have locked on different modes, with the estimator for the power signal already locked on the mode that goes unstable. The estimator used on the frequency signal has, however, locked on another mode that in the beginning is more visible in this signal. As the other mode becomes more dominant the estimator finds this new mode as more dominant and tracks its behaviour.

Conclusions

It has been shown that it is possible to track changing dynamics with a low-order model. The SNR must however be sufficiently large. This is the case when the system is unstable or close to instability. For a well damped system however, the results obtained are not any better than for batch estimation.

All used frequency signals have approximately the same behaviour. In comparison with the best signals in this simulation they are very slow at indicating instability. If instead frequency difference is considered, the result becomes comparable with the best single-point measurements.

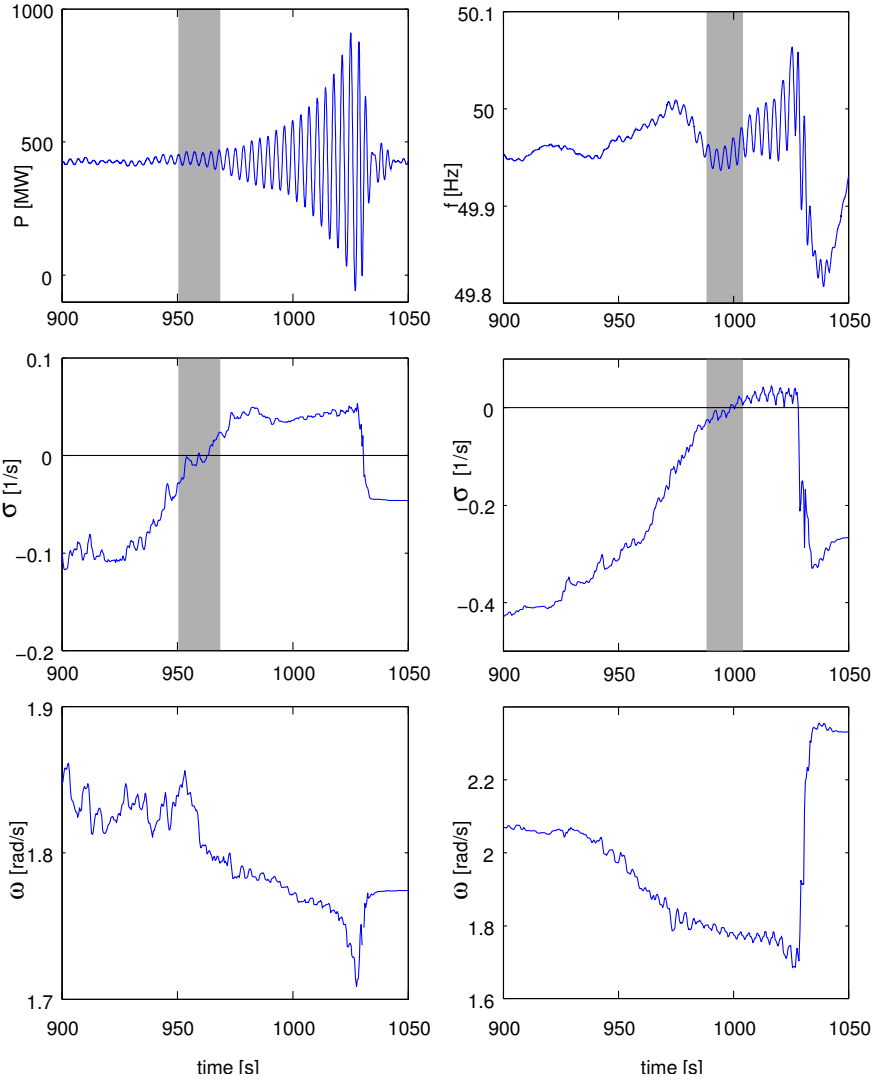

Figure 4.11: Frequency in Lund (top,right) and power transfer to Finland (top,left). Estimated real (σ) (middle) and imaginary part (ω) (bottom) of the mode with lowest damping. Grey areas indicate where an operator first can suspect instability. Notice the different scales for σ and ω belonging to different signals.

4.3 PMU-measurements

In April 2002, the two 400kV cables connecting Sweden and Zealand (Denmark) were taken out of service for two weeks due to construction work on the Danish side. During this time connection between the countries were maintained with two 130kV cables. The disconnection of the 400kV cables raised the interest from ABB to test their newly developed phasor measurement units (PMU), RES 521-PMU. This because the previous time the 400kV cables were disconnected the two systems separated within minutes.

To acquire measurements, one PMU was placed in the substation closest to Asnesværket, a large generating unit on Zealand. The other PMU was located at the substation in Söderåsen from where the cables to Zealand originate. The PMUs measured frequency, 130kV and 400kV voltage phasors and current phasors for the lines to the powerplant and towards Zealand. For the analysis, the angle difference between the 400kV phasors is used together with local frequency and frequency difference. The accuracy of the measurements are quoted to be:

- Frequency accuracy: ± 0.005 Hz
- Synchronization accuracy [GPS]: ± 0.5 ms
- Angle value accuracy: $\pm 0.1^\circ$

Analysis

From the analysis of the wall-outlet measurements we know that two modes, one at 0.3 Hz and the other at 0.5 Hz can be expected. Using frequency- or angle-difference as the input to the estimation algorithms, modes that are coherent in both areas will be cancelled. Having two modes present we can hope that one of them will vanish when using difference signals and thus leaving a single mode system to be estimated.

Before being used in the algorithms, the signals were first bandpass filtered and then downsampled to 5 Hz sampling rate.

Estimation of a fifth order model with the directional forgetting algorithm in Cao and Schwartz (2000) and with angle difference as input gave the result shown in Figure 4.12. The Figure shows the disconnection of the 400kV

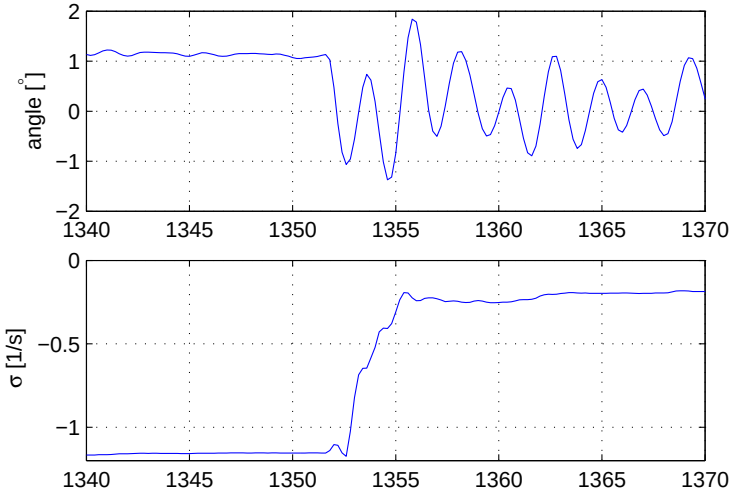

Figure 4.12: Results from the disconnection of the 400kV lines. Angle difference between Denmark–Sweden and estimated real-part of the eigenvalue with lowest damping.

lines. It can be observed that the damping estimates move from a well damped system (real part of eigenvalue ≈ -1) and settles on a new poorly damped value (real part of eigenvalue ≈ -0.1) after about 3s or 1.5 cycles of the oscillation. The mode found by the algorithm is the 0,5 Hz mode, suggesting that the 0.3 Hz mode is coherent in the two areas.

Applying the same method on data from the reconnection of the lines gave a substantially poorer result. Here the change in the damping estimates were hardly visible. Indeed, this is the desired behaviour of the algorithm! The directional forgetting algorithm will forget data in the same direction as the new data arrives. Connection of the 400kV lines significantly reduces the input signal to the estimator (Figure 4.13). Consequently, this can be seen as loss of estimator excitation, that is, the estimator is not updated with the new data and hence the old results will linger. A solution to this can be to monitor the variance of the input signal and force a restart of the estimator when the variance

of the input signal changes.

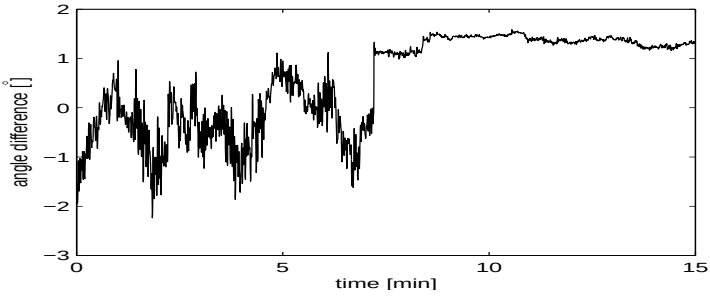

Figure 4.13: Angular difference at 400kV level between Denmark–Sweden at the reconnection of the 400kV lines.

From the previous result it is obvious that the recursive estimator needs to complemented with something that indicates the uncertainty in the estimated eigenvalues. A common feature of the recursive estimators is the so called P matrix. The output from the recursive estimators is an estimate of the characteristic polynomial for the identified system. Solving this polynomial gives the eigenvalues of the observed system. The P matrix is an estimate of the covariance matrix for the coefficients in the characteristic polynomial. Large values on the diagonal would then indicate that the coefficients in the polynomial are uncertain. However, the propagation of uncertainty in the coefficients to uncertainty in the eigenvalues is nontrivial.

An alternative approach is to continuously update the spectral estimate of the input signal. The area under the curve will give an estimate of the power in the signal. Results obtained when the signal energy is large will then be more trustworthy than results obtained with low signal energy. This is based on the assumption that there are no pure oscillations in the signal. A pure sinusoid will show up as a peak whenever the energy in the sinusoid is comparable to the background noise. In Figure 4.14 and 4.15 we see the result for the disconnection and reconnection of the 400kV lines. In these figures the peak value has been normalized in order to provide a better overview of what is happening. It is apparent that the increased signal energy at the disconnection gives a mode estimate that is much more reliable than before the disconnection. The energy level is, however, individual to each signal and need to be determined individu-

ally. This can be seen by comparing Figure 4.14 with Figures 4.16 and 4.17. The two last figure shows the spectral estimates obtained from the local frequency measurements in Asnesværket and Söderåsen. We can especially note that the energy level at Söderåsen (Figure 4.16) is substantially higher before the disconnection than the energy level of the difference signal (Figure 4.14). This is however not reflected in a better mode estimate.

Conclusions

It has been shown that monitoring a single mode system in real-time is viable. Signal energy is used as an indicator of estimation quality. Proper removal of signal components increases the reliability of the estimates of the remaining signals.

4.4 August 10 1996

The root cause to this event where the system became small signal unstable was a series of different events, each weakening the system. Due to improper modelling of the loads and the pacific DC intertie the continued operation of the system was not classified as insecure. For a more in depth analysis of this event see Kosterev et al. (1999).

Analysis

The signal used in the analysis is active power on one of the lines comprised in the pacific AC intertie. The original signal is rather noisy and spectral estimate of the complete event show that there is a substantial amount of power located around 2.5 Hz. The cause of this peak in the spectral estimate is unknown. Before damping estimation is performed, the signal is bandpass filtered and downsampled to 5 Hz sampling frequency. Spectral estimates covering the time of interest are depicted in Figure 4.18. There it can be seen that the damping is low from 400 s and onwards. At about 550 s there is a spontaneous growing oscillation which is duely reflected in the spectral estimates. The event at 730 s which is the initializing event for the instability has, however, a transient beha-

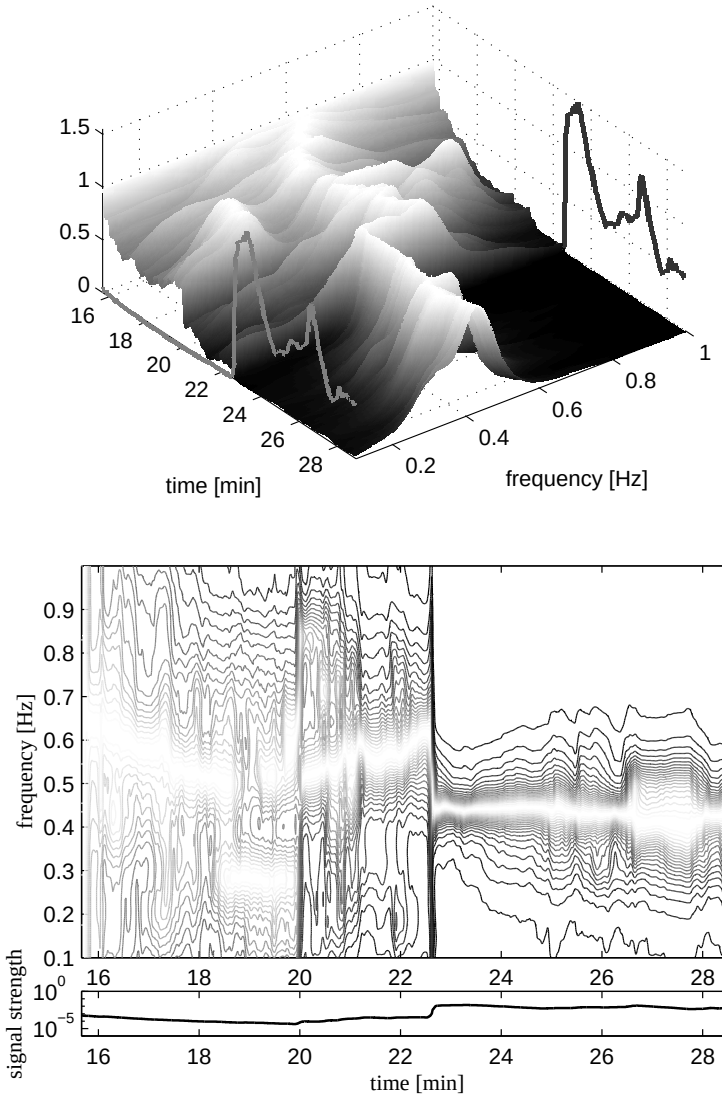

Figure 4.14: Spectral estimates of frequency difference between Denmark–Sweden as function of time when the 400kV lines between Sweden and Zealand are disconnected. 3d view (top) and level curves (bottom). The lines at 0.1 and 1 Hz in the upper plot indicate signal strength.

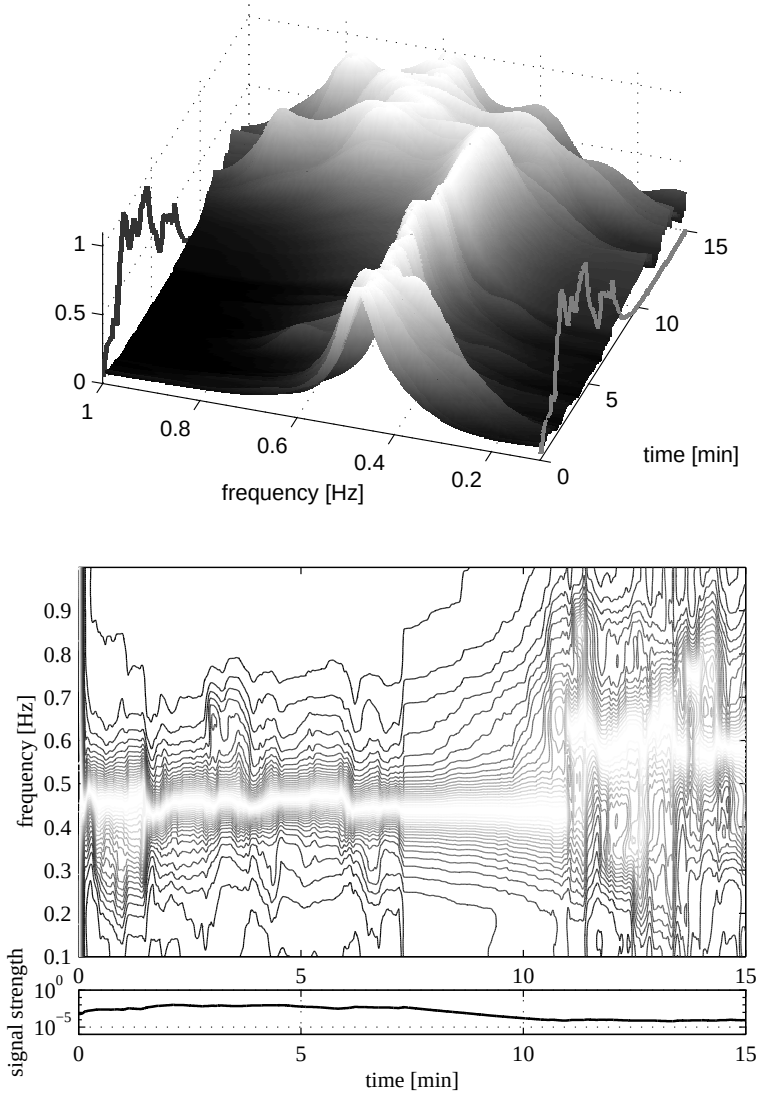

Figure 4.15: Spectral estimates of frequency difference between Denmark–Sweden as function of time when the 400kV lines between Sweden and Zealand are reconnected. 3d view (top) and level curves (bottom). The lines at 0.1 and 1 Hz in the upper plot indicate signal strength.

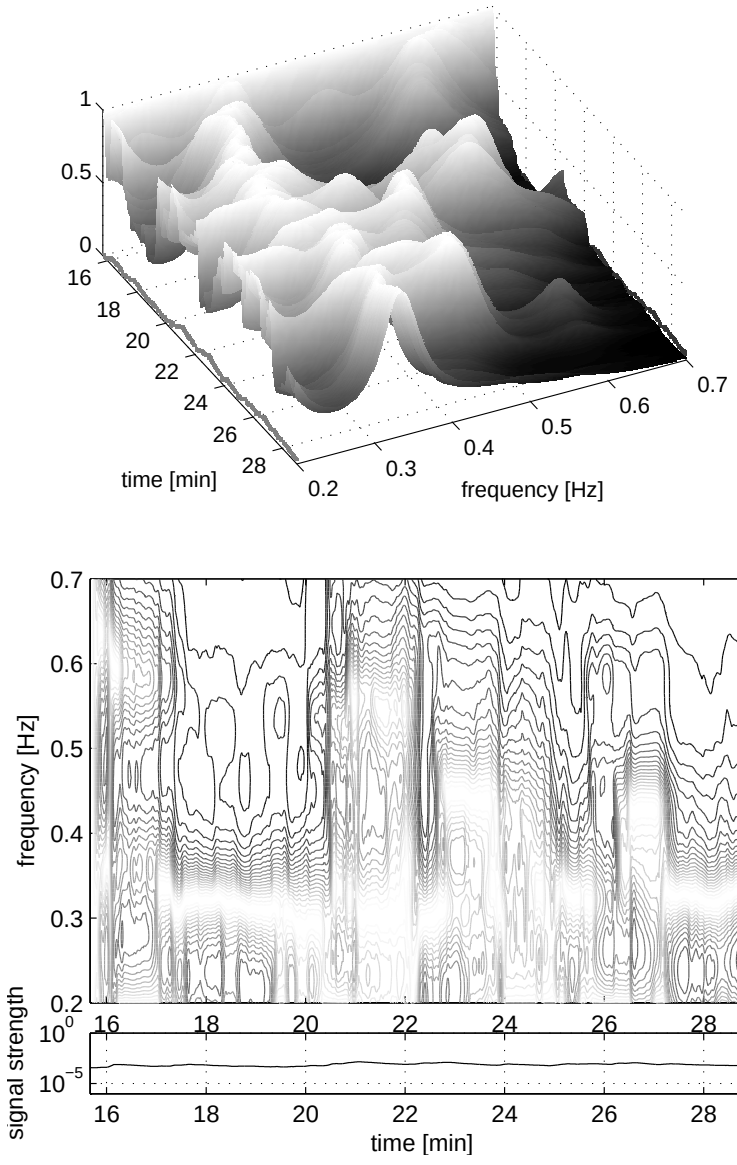

Figure 4.16: Spectral estimates of frequency deviation at Söderåsen as function of time when the 400kV lines between Sweden and Zealand are disconnected. 3d view (top) and level curves (bottom). The lines at 0.2 and 0.7 Hz in the upper plot indicate signal strength.

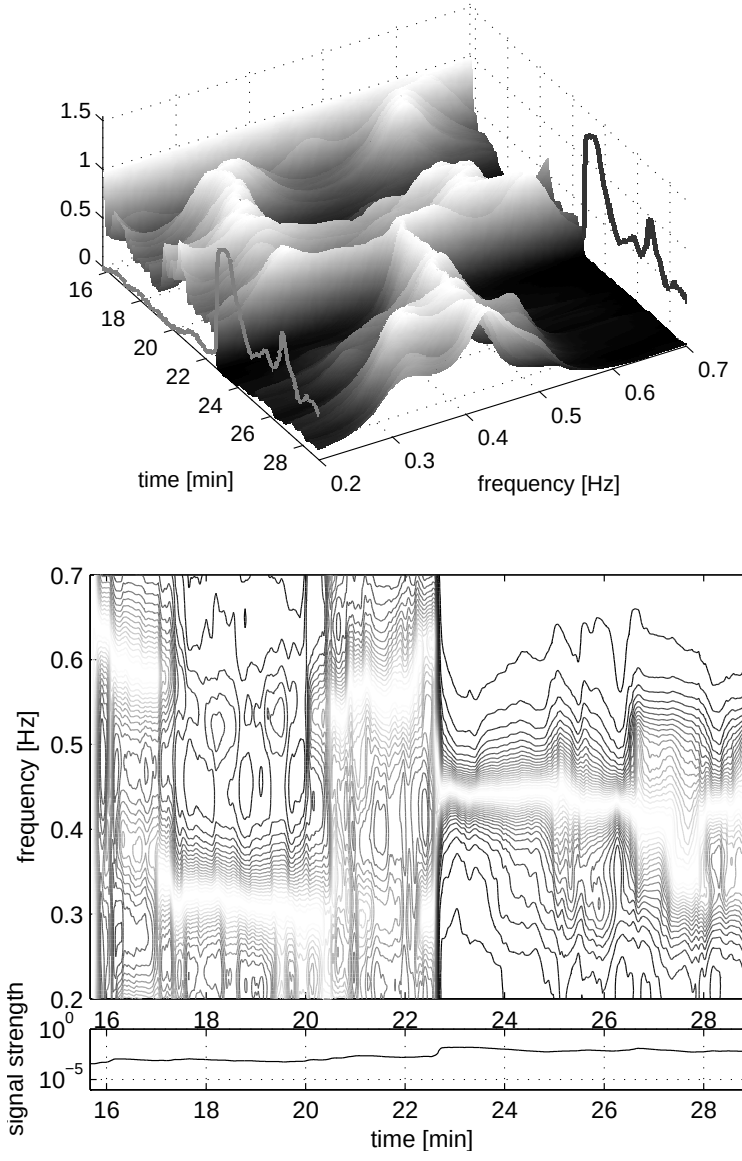

Figure 4.17: Spectral estimates of frequency deviation at Asnesværket as function of time when the 400kV lines between Sweden and Zealand are disconnected. 3d view (top) and level curves (bottom). The lines at 0.2 and 0.7 Hz in the upper plot indicate signal strength.

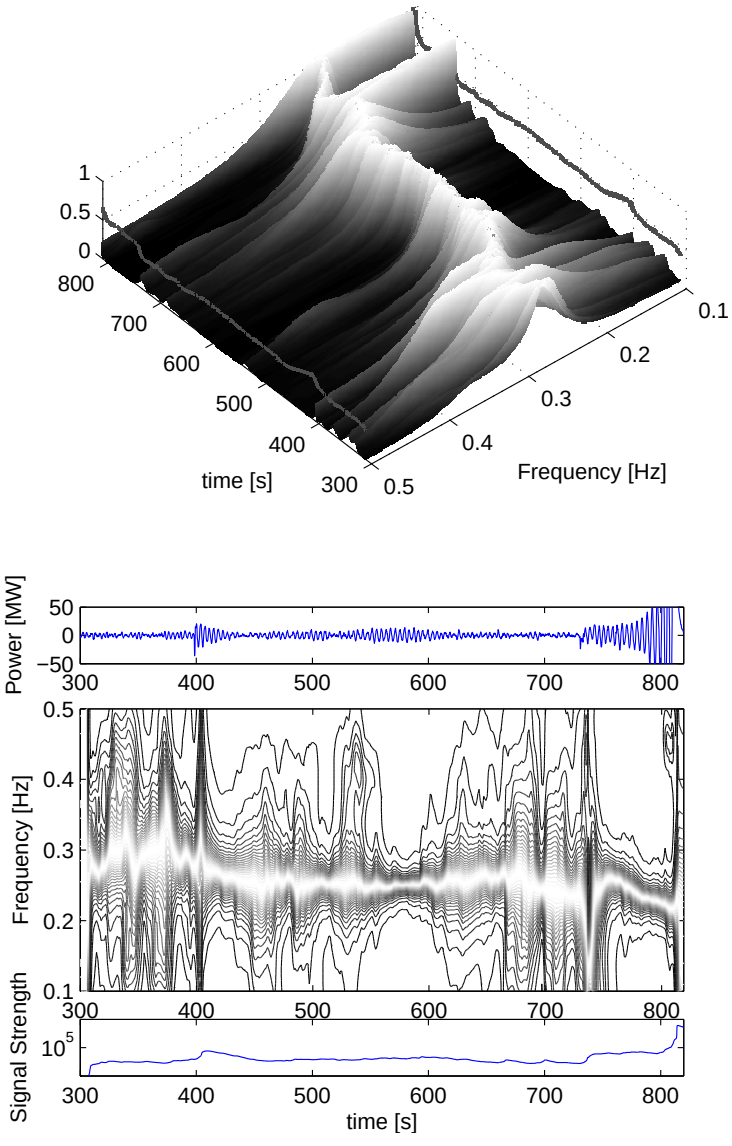

Figure 4.18: Spectral estimates of power transfer on one line of the pacific AC intertie. 3d view (top) and level curves (bottom). The lines at 0.1 and 0.75 Hz in the upper plot indicate signal strength.

viour that is difficult to interpret. The decrease in oscillation frequency after the event can, however, be regarded as a typical sign of increasing oscillations. When combined with the increase in signal power it can be assumed that there is a growing oscillation. The detection is, however, too late in time to be useful.

Using an AR model to determine the damping proved to be difficult. When comparing the results with those in Figure 4.19, the damping obtained with the AR models was always to large. Changing model structure to an $ARMA$ model did not improve the result until the MA part contained as many delays that a whole period of the oscillation could be covered. The estimator is reset

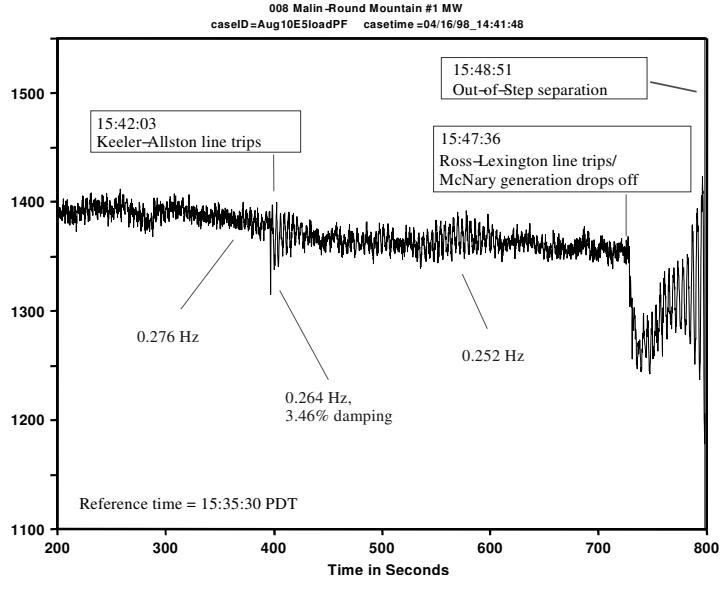

Figure 4.19: Analysis of the event on August 10 1996, from discussion in Kosterev et al. (1999).

when the prediction error is to large. Following a reset operation the estimator is blocked for new reset operations until the number of data used for estimation is larger than the number of parameters to estimate.

The result with a sufficiently long MA part is depicted in Figure 4.20. The behaviour between 300 s and 400 s is due to the estimator not being sufficiently excited and hence having trouble to produce accurate estimates. Following the

reset operation at 400 s it takes approximately 10 s before the estimates settle. This is explained by the need to estimate 40 parameters, which at a sampling rate of 5 Hz takes at least 8 s. The spontaneous oscillation at 550 s is detected

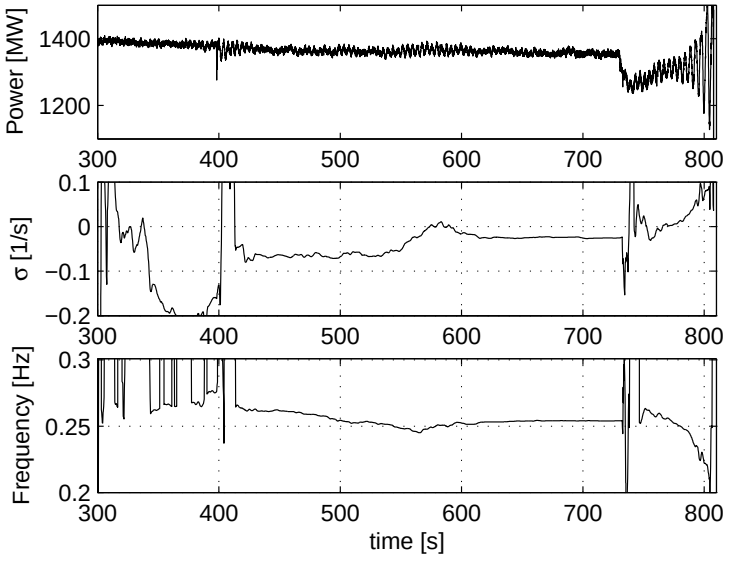

Figure 4.20: Power on transmission line (top), estimated real part of the eigenvalue with lowest damping (middle) and estimated oscillation frequency (bottom).

and so is the instability after the disturbance at 730 s. Settling of the estimator after the event at 730 s is somewhat slow depending on the number of parameters to estimate being large and the input signal to the estimator containing a lot of other dynamics than the electro-mechanical mode information sought here. In this case however, it is not a major drawback as an operator ought to be alarmed already at 400 s when the estimator indicate that the real part of the eigenvalues being larger than -0.1 and at 600 s it is obvious that the system is close to instability.

The improved behaviour when using an $ARMA$ model means that there is a need to model coloured noise. Two possible reasons for this are (1) The random load switching that drives the system can not be approximated with

white noise. If this is the case it is a major difference between the WSCC and the NORDEL network as the assumption of white noise seems to work well in the NORDEL system. What is even more remarkable is that the simulations of the NORDEL system are driven by the coloured noise models developed in Johansson and Martinsson (1986). Still, the assumptions on the noise being white in the frequency range of interest is sufficient to obtain good estimates. (2) According to Kosterev et al. (1999), the phase angle between the north and the south part of WSCC increased from 59° to 69° following the outage of the Keeler-Alston line (at 400 s in Figure 4.19). For angle differences of this size, the oscillations might well exhibit nonlinear phenomena. A possible explanation to the superior performance of the $ARMA$ model may thus be that the MA part helps in capturing the nonlinear phenomena.

Estimation of ARMA models

An $ARMA$ model is described as

$$y(k) = a_1 y_{k-1} + \ldots + a_p y_{k-p} + e_k + c_1 e_{k-1} + \ldots + c_q e_{k-q} \tag{4.1}$$

or more conveniently as

$$\begin{cases} y_k &= \varphi_k^T \theta + e_k \\ \theta &= [a_1 \ldots a_p \;\; c_1 \ldots c_q]^T \end{cases} \tag{4.2}$$

A natural choice of regression vector would be

$$\varphi_k = [y_{k-1} \ldots y_{k-p} \;\; e_{k-1} \ldots e_{k-q}]^T \tag{4.3}$$

which is impossible to implement as the disturbance sequence e_k is unavailable for measurement. To be able to use the recursive techniques described in 3.4 it is common to replace the sequence e_k with the prediction error

$$\epsilon_k = y_k - \varphi_k^T \hat{\theta}_{k-1} \tag{4.4}$$

the modified regression vector is then

$$\varphi_k = [y_{k-1} \ldots y_{k-p} \;\; \epsilon_{k-1} \ldots \epsilon_{k-q}]^T \tag{4.5}$$

This method is often referred to as *pseudolinear regression* or *recursive maximum likelihood method*. For more in depth treatment of parameter estimation in $ARMA$ models see for example Johansson (1993) and Ljung and Söderström (1983).

4.5 Concluding remarks

Several methods have been used to try to determine the damping in an electric power system using measurements both from normal operation (well-damped) and from cases with poor damping.

For normal operation spectral and prediction error methods were used. Both methods are successful for determination of the frequency of the modes. The damping is substantially harder to determine in the case of low signal-to-noise ratio (SNR) and neither method is well suited to determine the damping. This is most easily seen in the spectral methods where the peaks for the electromechanical modes are small compared to the rest of the spectrum. When using a prediction error method it might not be as easy to tell when the result is uncertain whereas this is easy to tell by visual inspection for the spectral methods.

For the cases with poor damping, recursive least squares methods with directional forgetting were used. This to minimize problems with estimator windup. For the NORDEL system it was sufficient with a fifth order model to achieve good results. In this case the estimator will show that the system is close to instability or unstable when it is still difficult to tell this from visual inspection of the signals. The ability to track changing dynamics is heavily dependent on which signals that are used as input to the estimator. System wide signals such as frequency or angle difference between distant locations or active power on important lines seems to contain much more information than voltage or frequency at one location.

In the WSCC case detection of instability is somewhat slow due to the need of a high order model. Regardless of this, the estimate of the damping shows that the system is close to instability several minutes before the system goes unstable.

Given that the (SNR) is high enough it is possible to determine the electromechanical mode-parameters from frequency measurements. In the NORDEL

system the SNR is usually too low which means that it is hard to estimate the damping during normal situations. For a poorly damped system the methods work better but frequency is not the best signal to use. Active power on an important line or frequency difference between distant locations are to be preferred.

Chapter 5

Reactive covariation

In this chapter it will be studied how the power injected into a distribution network changes when the power consumed at the load buses is changed. When disconnecting an active load in a distribution network, both the active and reactive power supplied to the distribution network will change. The size of the active and reactive variations depend both on network topology and the voltage sensitivity of the loads.

When doing active-power modulation at the load buses for enhancing damping of the electro-mechanical swing modes it is essential to know how the feeding power changes. This is due to the fact that the desired action, caused by switching active load, is to some extent counteracted by the inevitable change in reactive power caused by switching active power. For voltage stability issues the problem can be reformulated to how to disconnect as small amount as possible of active power to get a desired change in reactive power consumption at the feeding bus. This problem is thus vastly different from the much studied problem of describing how an aggregated load, such as a distribution network with loads, reacts to feeding voltage variations. The latter problem has been studied in for example Hill (1993); Karlsson and Hill (1994); Romero Navarro (2002); Dous (1999). For a survey of load models see; on Load Representation for Dynamic Performance (1993, 1995). For admittance type loads, it is shown that the voltage angle between the load and the feeding point is a good indicator of the amount of covariation of reactive power. The result is also ap-

plicable to constant power type loads as long as the reactive consumption at the load bus is moderate.

5.1 Problem statement

The basis for the analysis is a general passive network fed from one ideal voltage source (Figure 5.1). This ideal voltage source typically represents the connection between the transmission and distribution network and the voltage is typically 130 kV or higher. We would now like to know how the feeding power is affected by changes of the power at the load buses.

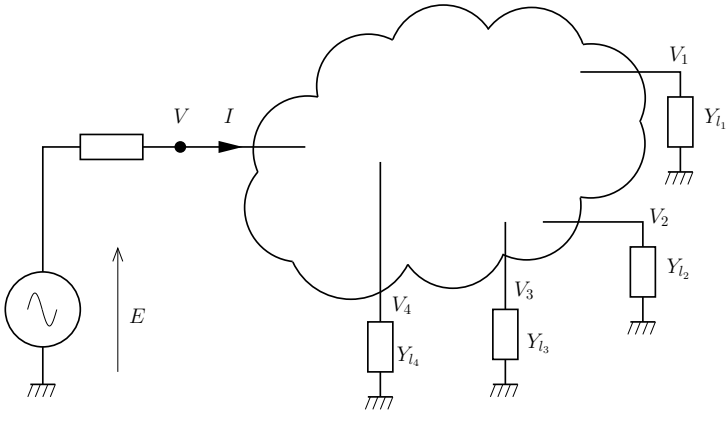

Figure 5.1: Idealised distribution network

The conventional way to solve this problem is by repeated load-flow calculations. Drawbacks with this approach are:

- Requires a complete model of the system as well as knowledge about the loads at all buses. This makes it difficult to use if we want to decentralize the control of the loads to the loads themselves.
- Computationally expensive as we need to solve the load flow for a change in power at each of the load buses.

- Provides no insight to why the system responds in a certain way when load is switched at a specified bus.

The tap-changing control on transformers is neglected because the timescale of electro-mechanical dynamics is much faster than that of the tap-changer control. Furthermore, according to Welfonder et al. (1994, 1989); Romero Navarro (2002) we might safely assume that the loads have a constant impedance characteristic in the electro-mechanical dynamics timescale.

The system can thus be desired by:

$$\mathbf{Y}V = I \tag{5.1}$$

Where $\mathbf{Y}$ is the bus admittance matrix, V is a vector of bus voltages and I is a vector of externally injected currents. Having only one feeding point, this means that the vector I only has one element that is non-zero.

Network-simplification

A network such as the one described above can be simplified to only contain certain buses while keeping the behaviour of the full network.

First the system is partitioned into the buses that are to be kept (subscript $_1$) and the buses to eliminate (subscript $_2$). The bus admittance matrix can now be partitioned into:[1]

$$\mathbf{Y} = \begin{bmatrix} \mathbf{Y}_{11} & \mathbf{Y}_{12} \\ \mathbf{Y}_{21} & \mathbf{Y}_{22} \end{bmatrix} \qquad V = \begin{bmatrix} V_1 \\ V_2 \end{bmatrix} \qquad I = \begin{bmatrix} I_1 \\ 0 \end{bmatrix} \tag{5.2}$$

Solving for V_2 we get:

$$\mathbf{Y}_r V_1 = I_1 \tag{5.3}$$

$$\mathbf{Y}_r = \mathbf{Y}_{11} - \mathbf{Y}_{12}\mathbf{Y}_{22}^{-1}\mathbf{Y}_{21} \tag{5.4}$$

that is the new bus-admittance matrix is the original bus-admittance matrix for the part of the system that should be kept plus an extra admittance matrix

[1] Having the buses to be kept as the first p buses of the system implies no loss of generality as the number of the buses can be arbitrarily chosen.

which makes up for the reduced buses. The reduction thus removes the physical interpretation of the component values. This is perhaps most noticeable for the loads where it is easy to believe that a load in the reduced system is the same load as in the original system. The reduction only preserves the behaviour of the system in such a way that if an extra load is connected to the reduced system, the load bus voltage and the total current fed to the network will be the same as for the original network.

5.2 Small disturbance analysis

π-link

The simplest structure that preserves some structure when reducing a network is the π-link (Figure 5.2), where the two buses correspond to the feeding bus and a load bus.

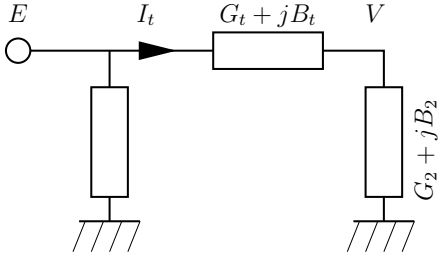

Figure 5.2: π-link

It can be noticed that the admittance at the load bus, $Y_2 = G_2 + jB_2$ in Figure 5.2 is not the same admittance as the load admittance at the specified bus in the original system. Adding load to the load bus produces however the same result for both networks.

Straightforward calculations on the π-link gives:

$$V = E\frac{G_t + jB_t}{G_t + G_2 + j(B_t + B_2)} \tag{5.5}$$

$$I_t = E\frac{(G_t + jB_t)(G_2 + jB_2)}{G_t + G_2 + j(B_t + B_2)} \tag{5.6}$$

The reason for calculating I_t instead of the total current is that the change in total current is the same as the change in I_t.

Adding a load by connecting a conductance between the load bus and the reference is equal to change G_2 with the same amount. Changing G_2 is thus equal to adding/removing load. For small load changes, the change in current can estimated by using the derivative of I_t with respect to G_2.

$$\frac{dI_t}{dG_2} = E\left(\frac{G_t + jB_t}{G_t + G_2 + j(B_t + B_2)}\right)^2 = \frac{V^2}{E} \tag{5.7}$$

The last equality in equation 5.7 is interesting because it shows that the only information needed to predict the change in current are the bus voltages. These voltages can be obtained either by phasor measurements or by load-flow calculations.

Inspired by this we also note that the change in current due to reactive load variations is given by

$$\frac{dI_t}{dB_2} = jE\left(\frac{(G_t + jB_t}{G_t + G_2 + j(B_t + B_2)}\right)^2 = j\frac{V^2}{E} \tag{5.8}$$

An estimate ($\Delta\hat{I}_t$) of the real change in I_t (ΔI_t) is thus given by:

$$\Delta\hat{I}_t = \frac{V^2}{E}(\Delta G_2 + j\Delta B_2) \tag{5.9}$$

Assuming a small disturbance, we can consider the voltage V constant and thus replace the change in conductance, ΔG_2, and susceptance, ΔB_2, by the change in active and reactive-power $\Delta P, \Delta Q$

In order to get an accurate prediction it is essential to how much active and reactive power that is switched. For small voltage angles, the amount of switched

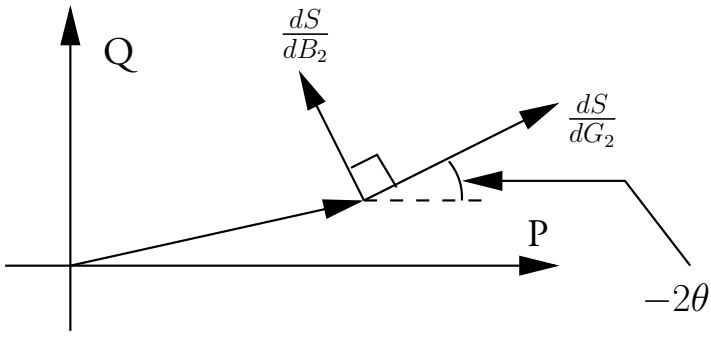

Figure 5.3: Change in feeding power due to change in load power. θ is the angle between E and V.

reactive power influences mainly the direction of the feeding power whereas the active power mainly influences the gain. This is easily understood when looking at Figure 5.3. There it can be seen that the change caused by reactive power will affect the angle of the feeding power much more than a change in active power, at least when the feeding power is mainly active power.

EXAMPLE Consider the simple distribution network depicted in Figure 5.4. This network is symmetric in the sense that all equipment on one voltage level

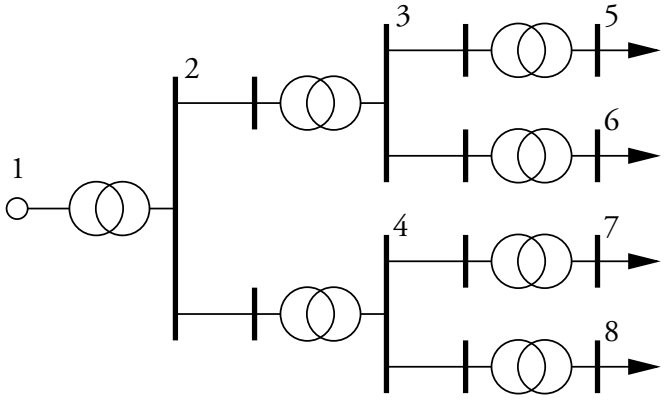

Figure 5.4: Simple distribution network.

are equal (transformer ratings and line length). The only thing that differs are the active loads, where the conductance varies by a factor of three at most.

	$\Delta B = -0.1$	
bus nr	ΔI	$\Delta I/\Delta\hat{I}$
5	$0.0476\angle -11.51$	$0.9999\angle -0.50$
6	$0.0320\angle -6.63$	$1.0004\angle -0.33$
7	$0.0927\angle -24.15$	$0.9975\angle -0.96$
8	$0.0470\angle -15.17$	$0.9998\angle -0.49$

	$\Delta B = 0$	
bus nr	ΔI	$\Delta I/\Delta\hat{I}$
5	$0.0473\angle -17.22$	$0.9991\angle -0.49$
6	$0.0316\angle -15.16$	$0.9995\angle -0.33$
7	$0.0925\angle -27.00$	$0.9967\angle -0.95$
8	$0.0467\angle -20.87$	$0.9990\angle -0.49$

	$\Delta B = 0.1$	
bus nr	ΔI	$\Delta I/\Delta\hat{I}$
5	$0.0475\angle -22.92$	$0.9982\angle -0.48$
6	$0.0319\angle -23.69$	$0.9987\angle -0.32$
7	$0.0925\angle -29.86$	$0.9959\angle -0.94$
8	$0.0469\angle -26.57$	$0.9981\angle -0.48$

Table 5.1: Change in current when load susceptance is changed by $-10\%, 0\%, 10\%$ and conductance is increased by 10 % at each bus, all angles in degrees. ΔI is the actual change in current, $\Delta I/\Delta\hat{I}$ indicates the relative estimation error.

As seen in table 5.1 the results obtained with this simple prediction are quite encouraging, provided that the size of the switched load is as intended.

Multiple loads

If multiple loads are considered a π-link is not enough. With n loads we now get a network with $n+1$ buses where all buses are connected to each-other (Figure 5.5). To get the cross-coupling between load buses from measurements is nontrivial. A first start might be to neglect the cross-couplings when calculating

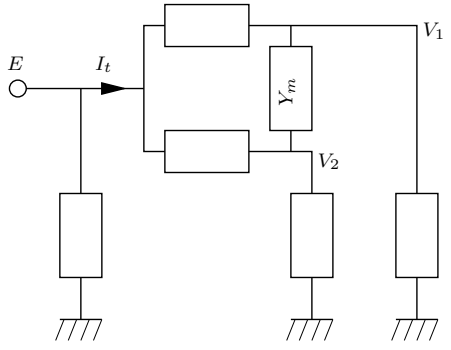

Figure 5.5: Network simplified to two load buses.

the change in current. Neglecting the cross-couplings we get

$$\Delta\hat{I} = \sum_{k \in loadbuses} \frac{V_k^2}{E}(\Delta P + j\Delta Q) \tag{5.10}$$

EXAMPLE Again the system in Figure 5.4 is used but this time all load buses are kept. As seen in table 5.2 the results are acceptable.

This result is probably due to that a distribution network is designed in such a way that the coupling between load buses is small. This seems reasonable because we would not like our lamps to flicker just because someone starts a vacuum-cleaner in the next block.

5.3 Large example

Here the derived algorithms are tested on a larger system, the Österlen test system Larsson (2001). This system uses constant power loads and also features

	ΔI	$\Delta I/\Delta\hat{I}$
$\Delta B = -0.1$	$0.2174\angle -17.31$	$0.9973\angle -1.04$
$\Delta B = 0$	$0.2169\angle -22.22$	$0.9960\angle -1.02$
$\Delta B = 0.1$	$0.2180\angle -27.11$	$0.9947\angle -1.01$

Table 5.2: Change in current when load susceptance is changed by $-10\%, 0\%, 10\%$ and conductance is increased by 10 % at all buses. ΔI is the actual change in current, $\Delta I/\Delta\hat{I}$ is the relative estimation error.

on-load tap-changing control. The previously derived result is applied to this

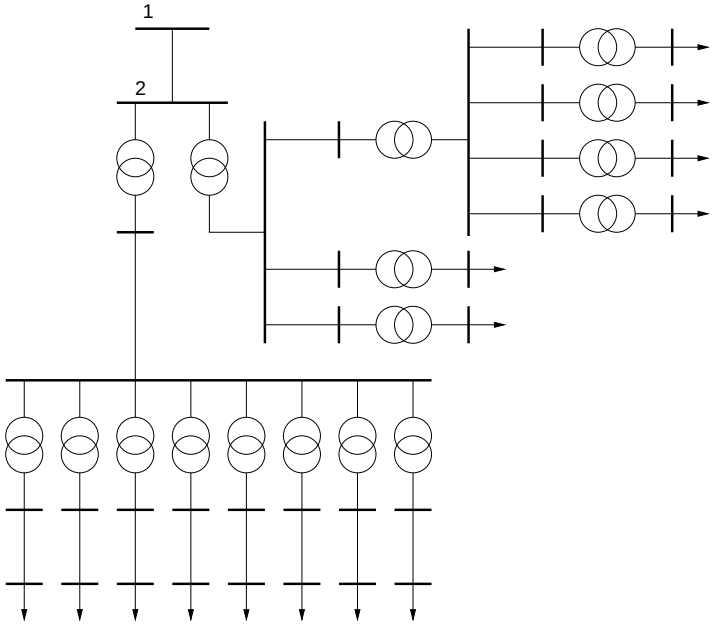

Figure 5.6: The Österlen test system.

network and for bus 1 we get the result in tables 5.3,5.4

As seen in tables 5.3 and 5.4 the direction of the change is within 1° (table 5.4 bus 11) of the correct value whereas the size differs with up tp 20% (table 5.4

	$\Delta S/\Delta\hat{S}$		
bus nr	$\Delta Q = -0.1$	$\Delta Q = 0$	$\Delta Q = 0.1$
3	$1.0059\angle 0.17$	$0.9894\angle 0.25$	$0.9739\angle -0.09$
4	$1.1081\angle -0.10$	$1.0617\angle 0.42$	$1.0163\angle -0.38$
5	$1.1060\angle -0.17$	$1.0549\angle 0.44$	$1.0061\angle -0.66$
6	$1.1144\angle -0.18$	$1.0631\angle 0.45$	$1.0134\angle -0.55$
7	$1.1175\angle -0.26$	$1.0616\angle 0.47$	$1.0082\angle -0.79$
8	$1.1432\angle -0.46$	$1.0773\angle 0.56$	$1.0110\angle -0.54$
9	$1.1110\angle -0.20$	$1.0584\angle 0.45$	$1.0080\angle -0.68$
10	$1.1114\angle -0.25$	$1.0561\angle 0.46$	$1.0039\angle -0.84$
11	$1.1495\angle -0.56$	$1.0763\angle 0.62$	$1.0040\angle -0.89$
12	$1.0862\angle -0.15$	$1.0483\angle 0.38$	$1.0103\angle -0.21$
14	$1.0914\angle -0.21$	$1.0440\angle 0.44$	$0.9985\angle -0.58$
15	$1.1319\angle -0.45$	$1.0716\angle 0.41$	$1.0129\angle -0.81$
16	$1.1134\angle -0.20$	$1.0677\angle 0.36$	$1.0220\angle -0.24$
17	$1.0889\angle -0.19$	$1.0425\angle 0.44$	$0.9979\angle -0.55$
all	$1.0955\angle -0.30$	$1.0484\angle 0.24$	$1.0033\angle -0.78$

Table 5.3: Large example during low-load $\Delta P = -0.1$

bus 11). This error in size is probably due to the fact that the loads are constant-power type loads whereas the calculations are derived assuming admittance-type loads. Scaling the prediction so that the active part of the prediction equals the active power that is switched makes the size prediction much better. This is equivalent to assuming a lossless line.

The combination that gives the best prediction is thus quite strange. The angle is given by assuming constant admittance type load and network with losses. Whereas the size is given by the amount of switched active load assuming lossless lines. The success of this scheme is most likely highly dependent on the operating region and the changes in active/reactive power. One obvious case where it will fail is when only reactive power is switched.

	$\Delta S/\Delta\hat{S}$		
bus nr	$\Delta Q = -0.1$	$\Delta Q = 0$	$\Delta Q = 0.1$
3	$1.0443\angle 0.30$	$1.0167\angle 0.46$	$0.9906\angle -0.08$
4	$1.1856\angle -0.36$	$1.1071\angle 0.78$	$1.0278\angle -0.39$
5	$1.1789\angle -0.28$	$1.1055\angle 0.75$	$1.0310\angle -0.23$
6	$1.1784\angle -0.30$	$1.1032\angle 0.76$	$1.0272\angle -0.32$
7	$1.1497\angle -0.04$	$1.0878\angle 0.71$	$1.0257\angle -0.06$
8	$1.2100\angle -0.91$	$1.1128\angle 0.90$	$1.0104\angle -0.23$
9	$1.1763\angle -0.24$	$1.1052\angle 0.74$	$1.0331\angle -0.16$
10	$1.1792\angle -0.40$	$1.0980\angle 0.80$	$1.0171\angle -0.61$
11	$1.2293\angle -1.01$	$1.1283\angle 0.91$	$1.0209\angle -0.18$
12	$1.1267\angle -0.14$	$1.0802\angle 0.56$	$1.0319\angle 0.27$
14	$1.1294\angle -0.15$	$1.0697\angle 0.71$	$1.0093\angle -0.07$
15	$1.1913\angle -0.68$	$1.1126\angle 0.61$	$1.0312\angle -0.31$
16	$1.1929\angle -0.65$	$1.1167\angle 0.58$	$1.0375\angle -0.19$
17	$1.1106\angle 0.15$	$1.0648\angle 0.70$	$1.0184\angle 0.29$
all	$1.1518\angle -0.52$	$1.0854\angle 0.40$	$1.0184\angle -0.58$

Table 5.4: Large example during high-load $\Delta P = -0.1$

Analysis

The good agreement between when using constant impedence results for constant power type loads raises the question. Is this always true?

To try to answer this, a single load infinite bus system with a purely reactive line is studied, Figure 5.7. This is a system commonly used in voltage stability analysis see, Cutsem and Vournas (1998) and Taylor (1994).

In the following subscript $_r$ will be used for the receiving end and subscript $_s$ for the sending end.

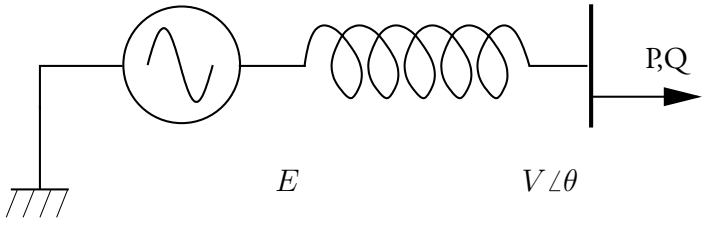

Figure 5.7: Single load infinite bus system.

The consumed active and reactive power is given by:

$$P_r = -E\,V\,Y\sin(\theta) \tag{5.11}$$
$$Q_r = E\,V\,Y\cos(\theta) - V^2\,Y \tag{5.12}$$

Solving this we get (assumes consumption of both active and reactive power)

$$V = \sqrt{\frac{Y\,E^2 - 2\,Q_r + \sqrt{Y^2\,E^4 - 4\,Q_r\,Y\,E^2 - 4\,{P_r}^2}}{2\,Y}} \tag{5.13}$$
$$\tan(\theta) = -\frac{P_r}{\frac{1}{2}\,Y\,E^2 + \frac{1}{2}\sqrt{Y^2\,E^4 - 4\,Q_r\,Y\,E^2 - 4\,{P_r}^2}} \tag{5.14}$$

Substituting this back into equations 5.11, 5.12 we get

$$P_s = P_r \tag{5.15}$$
$$Q_s = \frac{1}{2}\,Y\,E^2 - \frac{1}{2}\sqrt{Y^2\,E^4 - 4\,Q_r\,Y\,E^2 - 4\,{P_r}^2} \tag{5.16}$$

As the transmission is purely reactive we have $\frac{dP_s}{dP_r} = 1$ and $\frac{dP_s}{dQ_r} = 0$. The expressions for the reactive variation are now given by

$$\frac{dQ_s}{dP_r} = \frac{2\,P_r}{\sqrt{Y^2\,E^4 - 4\,Q_r\,Y\,E^2 - 4\,{P_r}^2}} \tag{5.17}$$
$$\frac{dQ_s}{dQ_r} = \frac{Y\,E^2}{\sqrt{Y^2\,E^4 - 4\,Q_r\,Y\,E^2 - 4\,{P_r}^2}} \tag{5.18}$$

The direction of the change in feeding power (ΔS_s) is then given by

$$\tan(\arg(\Delta S_s)) = \frac{\frac{dQ_s}{dP_r}}{\frac{dP_s}{dP_r}} = \frac{dQ_s}{dP_r} \tag{5.19}$$

comparing this with equation 5.14 it is noticed that if $Y^2\,E^4 \gg 4\,Q_r\,Y\,E^2 + 4\,{P_r}^2$ then $\tan(\arg(\Delta S_s)) \approx 2\tan(\theta)$ which for small θ gives $\arg(\Delta S_s) \approx 2\,\theta$.

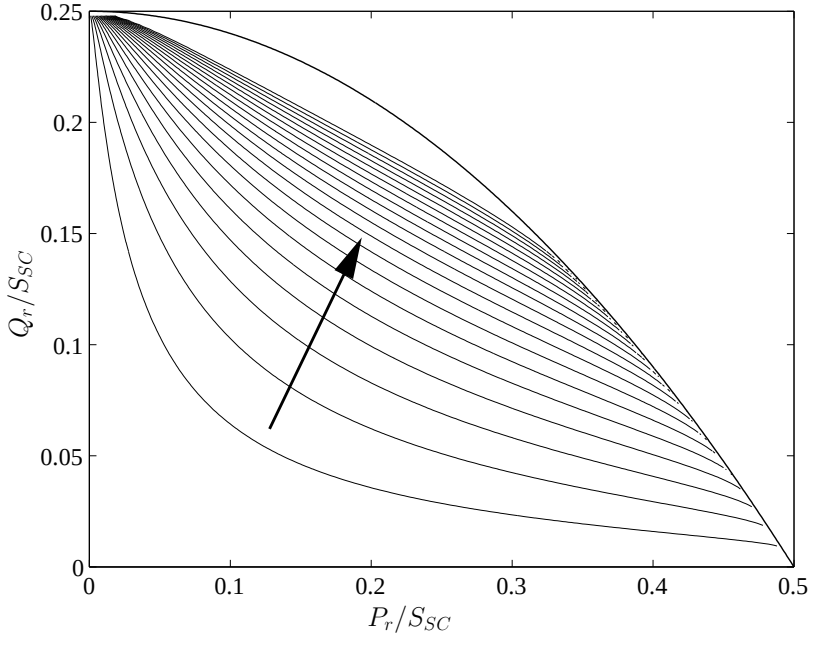

Figure 5.8: Level curves of the angular error obtained when using the approximation -2θ rather than $\arg(\frac{dS_s}{dP_r})$ to calculate the direction of the change in feeding power (ΔS_s) when changing active load (P_r) as a function of P_r, Q_r. The spacing between the curves is 1°, the thick line indicates the admissible operating region and the arrow indicates the direction in which the error increases.

A better view of the correctness of the estimate is seen in Figure 5.8 where the difference between the correct angle of ΔS_s and the estimated angle is plotted for a change in consumed active power, ΔP_r. As seen in this figure the approximation is good when the consumed reactive power is small compared to the consumed active power.

5.4 Non-infinite bus

All the previous analysis has only concerned a distribution network connected to an infinite bus. If instead the infinite bus is replaced by a Thévenin equivalent of the feeding system, then the system in Figure 5.9 is obtained. For this circuit

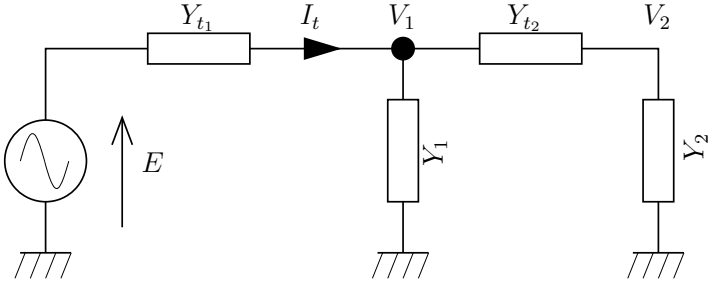

Figure 5.9: Thévenin source and π-link.

we have:

$$\frac{dI_t}{dY_2} = \frac{V_2^2}{E} \tag{5.20}$$

$$\frac{dV_1}{dY_2} = -\frac{dI_t}{dY_2}\frac{1}{Y_{t_1}} = -\frac{V_2^2}{E\,Y_{t_1}} \tag{5.21}$$

where we notice that the expression for change in current is the same as derived in section 5.2, the difference is that it now is the Thévenin source that is the reference. The circuit in Figure 5.9 can easily be transformed to a π-link by a $Y-\Delta$ transform of Y_{t_1}, Y_1, Y_{t_2}. The change in feeding voltage is just calculated as the voltage drop across the internal impedance in the Thévenin equivalent.

The power injected into the π-link from the Thévenin equivalent is

$$S_1 = V_1\, I_t^* \tag{5.22}$$

where * denotes complex conjugate. Differentiating the above expression and simplifying we get:

$$\frac{dS_1}{dY_2} = V_1\frac{d}{dY_2}I_t^* + \frac{dV_1}{dY_2}I_t^* = V_1\left(\frac{V_2^2}{E}\right)^* - \frac{V_2^2}{E\,Y_{t_1}}\frac{S_1}{V_1} \tag{5.23}$$

Inserting $E = V_1 + I_t\, Z_{t_1} = V_1 + \left(\frac{S_1}{V_1}\right)^* Z_{t_1}$ in the above equation we get

$$\frac{dS_1}{dY_2} = V_1 \left(\frac{V_2^2}{V_1 + \left(\frac{S_1}{V_1}\right)^* \frac{1}{Y_{t_1}}} \right)^* - \frac{V_2^2}{V_1\, Y_{t_1} + \left(\frac{S_1}{V_1}\right)^*} \frac{S_1}{V_1} \tag{5.24}$$

Where the first term corresponds to a π-link connected to an infinite bus and the second term can be seen as a correction for the voltage drop in the Thévenin equivalent. With the same assumptions as earlier, the change in feeding power at V_1 is now given as

$$\Delta\, S_1 = \frac{dS_1}{dY_2} \left(\Delta P + j\Delta Q\right) \tag{5.25}$$

For constant power type loads in a reactive network, it is, as described in section 5.3, normalize the real part of $\frac{dS_1}{dY_2}$ or the real part of $\frac{dI_t}{dY_2}$ to achieve better results. For the studied cases, the difference between the two normalizations is insignificant.

An alternate way to calculate the change in feeding power is to use

$$\Delta\, S_1 = \left(V_1 + \Delta V_1\right) \left(I_t + \Delta I_t\right)^* - S_1 \tag{5.26}$$

Again, the difference in the results between this formulae and equation (5.25) is minimal.

When these results are applied to the system in Figure 5.6, then for bus 2 we get the results in tables 5.5 and 5.6

	$\Delta S/\Delta\hat{S}$		
bus nr	$\Delta Q = -0.1$	$\Delta Q = 0$	$\Delta Q = 0.1$
3	$1.0362\angle 0.31$	$1.0304\angle 0.27$	$1.0255\angle 0.09$
4	$1.0844\angle 0.20$	$1.0511\angle 0.44$	$1.0198\angle -0.28$
5	$1.0841\angle 0.20$	$1.0479\angle 0.46$	$1.0153\angle -0.49$
6	$1.0878\angle 0.18$	$1.0509\angle 0.46$	$1.0169\angle -0.42$
7	$1.0898\angle 0.15$	$1.0497\angle 0.49$	$1.0138\angle -0.60$
8	$1.1193\angle -0.04$	$1.0674\angle 0.58$	$1.0172\angle -0.48$
9	$1.0865\angle 0.18$	$1.0490\angle 0.47$	$1.0151\angle -0.51$
10	$1.0871\angle 0.17$	$1.0478\angle 0.48$	$1.0132\angle -0.63$
11	$1.1230\angle -0.07$	$1.0656\angle 0.64$	$1.0116\angle -0.76$
12	$1.0756\angle 0.11$	$1.0504\angle 0.39$	$1.0259\angle -0.08$
14	$1.0784\angle 0.15$	$1.0462\angle 0.45$	$1.0170\angle -0.38$
15	$1.0976\angle -0.04$	$1.0530\angle 0.41$	$1.0118\angle -0.68$
16	$1.0878\angle 0.07$	$1.0539\angle 0.36$	$1.0210\angle -0.22$
17	$1.0772\angle 0.17$	$1.0459\angle 0.45$	$1.0174\angle -0.35$
all	$1.0828\angle 0.08$	$1.0490\angle 0.33$	$1.0182\angle -0.51$

Table 5.5: Large example during low-load $\Delta P = -0.1$

	$\Delta S/\Delta\hat{S}$		
bus nr	$\Delta Q = -0.1$	$\Delta Q = 0$	$\Delta Q = 0.1$
3	$1.0320\angle 0.59$	$1.0222\angle 0.50$	$1.0140\angle 0.17$
4	$1.1151\angle 0.31$	$1.0594\angle 0.82$	$1.0067\angle -0.37$
5	$1.1116\angle 0.34$	$1.0595\angle 0.79$	$1.0097\angle -0.24$
6	$1.1116\angle 0.34$	$1.0584\angle 0.80$	$1.0079\angle -0.31$
7	$1.0971\angle 0.47$	$1.0541\angle 0.74$	$1.0131\angle -0.07$
8	$1.1625\angle -0.12$	$1.0860\angle 0.95$	$1.0097\angle -0.37$
9	$1.1101\angle 0.35$	$1.0597\angle 0.78$	$1.0113\angle -0.18$
10	$1.1128\angle 0.33$	$1.0557\angle 0.83$	$1.0028\angle -0.54$
11	$1.1714\angle -0.21$	$1.0915\angle 0.96$	$1.0111\angle -0.34$
12	$1.0893\angle 0.23$	$1.0586\angle 0.58$	$1.0275\angle 0.25$
14	$1.0908\angle 0.37$	$1.0507\angle 0.73$	$1.0123\angle -0.03$
15	$1.1197\angle -0.04$	$1.0629\angle 0.63$	$1.0072\angle -0.38$
16	$1.1201\angle -0.05$	$1.0646\angle 0.60$	$1.0098\angle -0.29$
17	$1.0807\angle 0.51$	$1.0503\angle 0.71$	$1.0205\angle 0.27$
all	$1.1035\angle 0.17$	$1.0564\angle 0.58$	$1.0115\angle -0.39$

Table 5.6: Large example during high-load $\Delta P = -0.1$

5.5 Large disturbance analysis

The previous analysis has only been concerned about small disturbances. In this section we try to answer the question if it is possible to predict the behaviour for large disturbances without solving the complete load-flow problem. We keep the assumption made earlier, that is, only one feeding voltage and admittance type loads.

First, recall equation 5.3 for the reduced system.

$$V_1 = \begin{bmatrix} V_f \\ \tilde{V} \end{bmatrix} \qquad I_1 = \begin{bmatrix} I_f \\ 0 \end{bmatrix} \qquad \mathbf{Y}_r V_1 = I_1 \tag{5.27}$$

Modifying the above equation into standard shape we get

$$\tilde{\mathbf{Y}} \begin{bmatrix} I_f \\ \tilde{V} \end{bmatrix} = \begin{bmatrix} V_f \\ 0 \end{bmatrix} \tag{5.28}$$

Solving for the feeding current and substituting it back into equation (5.28) we obtain

$$I_f = \tilde{\mathbf{Y}}_{11}^{-1} \left(V_f - \tilde{\mathbf{Y}}_{12} \tilde{V} \right) \tag{5.29}$$

$$\underbrace{\tilde{\mathbf{Y}}_{21} \tilde{\mathbf{Y}}_{11}^{-1} V_f}_{b} = \underbrace{\left(\tilde{\mathbf{Y}}_{21} \tilde{\mathbf{Y}}_{11}^{-1} \tilde{\mathbf{Y}}_{12} - \tilde{\mathbf{Y}}_{22} \right)}_{A} \tilde{V} \tag{5.30}$$

This substitution transforms the circuit to only contain load buses. The feeding voltage is replaced with current injections at all buses. We would now like to know how the solution ($\tilde{V}$) changes when the modified admittance matrix is changed, that is

$$b = (A + \delta A)(\tilde{V} + \delta \tilde{V}) \tag{5.31}$$

and where b represents the feeding voltage. A whole class of disturbances can now be applied to the modified admittance matrix, disturbances that have a limited norm, $||\delta A|| < C$. This can be interpreted as a number of disturbances that all have absolute value smaller than C. If the load-admittance varies much between the load buses it makes sense to scale the equations. The only way

of scaling that has been tried is to make the real part of the diagonal elements equal, for example 1. With $0 < C < 1$ this can now be seen as a relative disturbance. Using norms for the disturbance means that there is no control on where non-zero elements show up is the disturbance of the admittance matrix. This means that there can be non-physical disturbances such as the admittance of a line being different in different directions. It is thus a very coarse and general description of the potential disturbances.

Applying the following inequality on the disturbed system (equation 5.31), where $\kappa(A)$ denotes the condition number of A,

$$\frac{\left|\left|\delta\tilde{V}\right|\right|}{\left|\left|\tilde{V}\right|\right|} \leq \frac{1}{1-\kappa(A)\frac{||\delta A||}{||A||}}\kappa(A)\frac{||\delta A||}{||A||} \tag{5.32}$$

it is now possible to use the result backwards and calculate the norm of the maximal change in current.

$$\delta I_f = -\tilde{\mathbf{Y}}_{11}^{-1}\tilde{\mathbf{Y}}_{12}\delta\tilde{V} \tag{5.33}$$

$$||\delta I_f|| \leq \left|\left|\tilde{\mathbf{Y}}_{11}^{-1}\tilde{\mathbf{Y}}_{12}\right|\right| \left|\left|\delta\tilde{V}\right|\right| \tag{5.34}$$

As it is only possible to calculate the norm of the change, there is no way to tell which direction the change will have. The answer is an upper bound on the change in feeding current/power.

5.6 Conclusions

It has been shown that the ability to predict the change in feeding power (active and reactive) to a distribution network when a small load is switched further down is closely related to the angular difference of the voltages at the load bus and the feeding bus. For admittance type loads the size of the change is given by the voltage levels at the load bus and the feeding bus. The main advantage with the method is that no network model is needed if phasor measurements are available. If phasor measurements are lacking, a load-flow combined with the outlined method will give the same result as with phasor measurements but with a computational cost that is much lower than repeated load-flow calculations.

The theory is developed for constant admittance type loads but works well on constant power type loads provided that consumed active power is much larger than consumed reactive power and that we are operating far from transmission limits.

Given that the coupling between loads is small the results can also be used when several loads are switched, although the result is not as accurate as for a single load.

When large loads are switched it is possible to determine the size of the change in feeding power but not the direction. Furthermore a detailed network model is needed. The cost of the computations needed to get the result might be much higher than the cost of a number of load-flows.

At present only networks fed from a single source are treated. It is possible to extend the results for multi-source networks. This will, however, require more knowledge about the network.

Chapter 6

Distributed load control for damping enhancement

The goal of this chapter is to illustrate how the results from the previous chapters can be used to achieve damping enhancement by distributed control of active load. In Samuelsson and Eliasson (1997); Samuelsson (1997) it was shown that control of active power at the transmission network level enhances the damping of the electro-mechanical modes. In this chapter, the behaviour when using the load in the distribution network as actuators will be investigated. The chapter starts with a section about load control and ends with case studies of the three machine system in Anderson and Fouad (1993) and a 16-machine model of the NORDEL power system, Akke (1989).

6.1 Active load control

In this section different control strategies and ways to implement load-control is described. Furthermore, characteristics for loads suitable for load-control are discussed. Finally the size of a distributed actuator is discussed.

Loads

As few loads, suitable for load control, are connected directly to the transmission network there is a need to decentralize the loads as control elements. A load suitable for load control should typically consume little or no reactive power and have a dynamics that is much slower than the electro-mechanical dynamics. It is also advantageous if the load have a "constant energy" type behaviour. The motivation for the first requirement is that the reactive variation when loads are switched on or off should be small. For a purely active load the only contribution to reactive variation will then be the contribution from the distribution network. The second requirement is motivated by the acceptance to loss of power. With load dynamics much slower than the electro-mechanical dynamics, a short disconnection of an operating load will be almost unnoticeable. The argument for the third requirement is that it simplifies pricing of the damping service. If a load consumes the same amount of energy, no matter if it is used for damping or not, then the producing companies need not be compensated for loss of production.

A load category that fulfils all the requirements are resistive heating loads such as residential water heaters, coffee machines, electric heating, electric cookers and resistive furnaces. Also electric district heating boilers can be considered but they are rare and not always in operation. Other plausible loads are power-electronically controlled loads that can be allowed to change their setpoint. This can include pump and fan drives as well as battery chargers. Loads unsuitable for load control are for example refrigerators that have a motor which is directly connected to the grid.

Control strategies

Load control is usually a quantized type of control, that is the control signal is changed in steps rather than continuously. This together with the fact that it is *energy* that should be removed/added to the generators implies that as much power as possible should be used in order to give a high control authority. In the rest of this section we will therefore assume on-off control.

Control systems can be divided into feedback and feed-forward/precomputed

control.

In feedback control measurement or quantities estimated from measurements are used as inputs to a controller. Advantages with this type of control are that the system is continuously monitored and that the effects of the control action is directly visible to the controller. A power system is conveniently described by a differential algebraic (DAE) system. The algebraic part implies that there are direct connections between controlled and observed quantities. Here, there will be a direct connection between load and phase-angle. Using local frequency, which is the time derivative of the phase-angle, as controller input implies that the frequency measurement must be done with care in order to avoid large disturbances in the measurements.

One way to avoid this is to use a precomputed control signal. With this approach, once the sequence is started there is no need to calculate estimates as the estimates will not influence the control. The control signal can easily be extracted from the outputs of a damping estimator by making a square wave control action with the same frequency as the mode that should be damped. The frequency and damping are given by the estimator. The sequence is then started a zero crossing of the measured signal. The main advantage with this approach is simplicity. Drawbacks are that only single mode systems are this easy to handle. With on-off control it is only the signal of the observed quantity that is of interest. A multi mode oscillation will not have only one frequency and to synthesize a control signal from several observed modes is impossible as there is no information about the phase and amplitude of the different modes. Furthermore, applying control will not change the frequency of the oscillation but rather its phase. If a long control signal is pre-computed it might end with that the control signal and the actual monitored signal are out of phase, leading to excitation rather than damping of the system.

Centralized – Decentralized control

Load control for damping enhancement as performed in Samuelsson (1997) suggests the following quantities as suitable feedback signals:

- local bus frequency

- frequency of the closest machine
- estimated mode frequency

For a centralized damping controller, which is a controller that has access to transmission level measurements, all the suggested quantities can be used. This approach will probably achieve the highest performance but the requirements on communication bandwidth is high. The communication requirements can be summarized as:

- System measurements need to be brought to the controller.
- Loads need to send their status, telling the controller how much damping power they have available.
- Control actions need to be communicated to the loads.

One issue with a centralized controller is the time delay introduced by the communication. To get high performance this delay should be kept small or considered in the control design. It can be argued that todays fast communication like the internet should be fast enough. Looking at the capacity of a communication link this is generally true. The capacity is, however, the capacity during ideal circumstances. This often means that there are few hosts on the network and that the data is sent in large packets. In a control system, the data is typically one measurement sent at an fixed interval. This means that the data packets are small giving a large overhead for the protocol part of the transmission. Also, the number of hosts will be large, at least one for each load and one for each measurement site.

In a decentralized system, measurements and control action are performed at the same place, locally. While removing the need of communication there is now an increase in the number of required measurement units (one for each load). Also, the number of quantities suitable as feedback signals are reduced to local frequency. With a decentralized system there is also the possibility of the different control loops counteracting each other as only local data are available. The effect of counteraction be minimized by proper selection of control parameters but this is against the whole idea with a decentralized system. One case where this is clearly visible is tap changer control in distribution networks.

In Larsson (2001) it was shown that the number of tap-changing operations in a radial network could be reduced by 45% while maintaining a better voltage profile when introducing a centralized controller.

A mixture of the two extremes could prove useful in that the requirements on communication capacity is relieved while maintaining some coordination and keeping the number of measurement units down. A possible scenario is to locate the measurement and control equipment in a substation. Control signals are then sent on the power lines to the loads. In case of on-off control this is particularly convenient as only two different kind of messages (on or off) need to be sent. Advantages with this solution are

- Simple interface to actuators
- Limits counteraction
- Limits sensitivity to communication/hardware problems compared to centralized system.
- Number of measurement units small and hopefully of better quality compared to decentralized system.

Actuator sizing

Given that an area is equipped with controllable loads, what is the size of the compound actuator and what is the size affected by? The maximal capacity of the actuator is given by the total amount of load with control equipment installed. The possibility to use the maximal rating is heavily dependent on the types of loads and how they are allowed to operate. Comparing load-control with load-shedding we conclude that it is always allowed to disconnect operating loads and then reconnect them again. The reverse, to engage a load that initially is off is more dependent on the type of load. Residential water heaters for example, can probably be turned on although the water is sufficiently hot. Electric cookers on the other side, should probably not be turned on except for parts that happens to be in use at the moment.

The size of the actuator can thus vary considerably depending on load composition, allowed switching and initial state of the individual loads.

Another question that needs to be answered is how much of the available power should be used for damping purposes. If damping power is free, then everything that can be used to achieve a high damping can be used. The reactive covariation will counteract the desired action caused by the active load. However, as long as the reactive covariation is small compared to the active variation, a higher damping is achieved with larger control-power. The bottom part of Figure 6.6 illustrates the influence of reactive covariation.

When there is a cost associated with damping power there will be a trade-off between the cost of additional damping versus the usefulness of the increased damping. In such a scenario, the price of damping power will be determined by the need of damping power versus the availability and quality of damping power, where high quality power has low reactive covariation.

Who can supply the damping power? Technically, the damping power is supplied by the end user. From a market perspective the damping power can be supplied either by the end user, the transmission system operator or a distribution company. In all cases it is the person/organization that makes the investments in equipment for load control that should be seen as the seller of damping power.

For a truly decentralized system without communications the damping power provider is probably the end consumer or the transmission system operator. The high accuracy requirement on the damping detector will make the detector expensive. This will probably limit control installations to large loads. To get a high penetration of control equipment on smaller loads the damping detector will need to be cheap or subsidized. Even with cheap detectors it will take long time before the penetration of controlled loads is high as the cost in upgrading the equipment will be substantial.

When having a system that relies on communication between the loads and a central controller, the distribution companies can enter the damping market. In this case the distribution company typically has communications for remote metering and possibly also for broadband connections. The idea now is to connect suitable loads such as heating loads to outlets that can be controlled by the distribution company. The distribution company can now sell controllable load to the transmission system operator. The end customer can be compensated by a lower tariff or energy price.

In all cases, it is hard to estimate the amount of power available for control. For a centralized system one can envision a system where the loads send their respective state to the controller. The central controller will then act not only as a controller but also as a load-dispatcher that can select a suitable amount of load to use.

6.2 Case studies

The on-off control strategy is evaluated on two test cases, the three-machine system in Anderson and Fouad (1993) and a 16-machine system of the NORDEL network. The main goal with these studies is to study the impact the reactive covariation has when using load-modulation for damping enhancement. Reactive covariation comes from the distribution network. These networks are, however, not modelled in detail in the simulations. Instead, the results from the previous chapter is used to mimic the behaviour of load-modulation in a distribution network.

The controllers use local bus frequency as their input signal. Thus no estimation of the damping or oscillation frequency is performed.

Three-machine system

A three machine system has two oscillatory electro-mechanical modes and thus forms the first step towards a general multi-machine system. The nine bus system of Anderson and Fouad (1993), also known as the WSCC 9 system, is selected for having the generic meshed network with one mesh, Figure 6.1. The generators are modelled by third order models without damper windings and the magnetization is controlled by a proportional AVR measuring terminal voltage. The mechanical input power is kept constant. The loads are equipped with load control using local frequency as input.

For the studied load case the system has two modes, one at 1.3 Hz and one at 1.8 Hz. In the 1.3 Hz mode the generators at buses 2 and 3 swing against the generator at bus 1. In the 1.8 Hz mode the generator at bus 2 swings against the generator at bus 3.

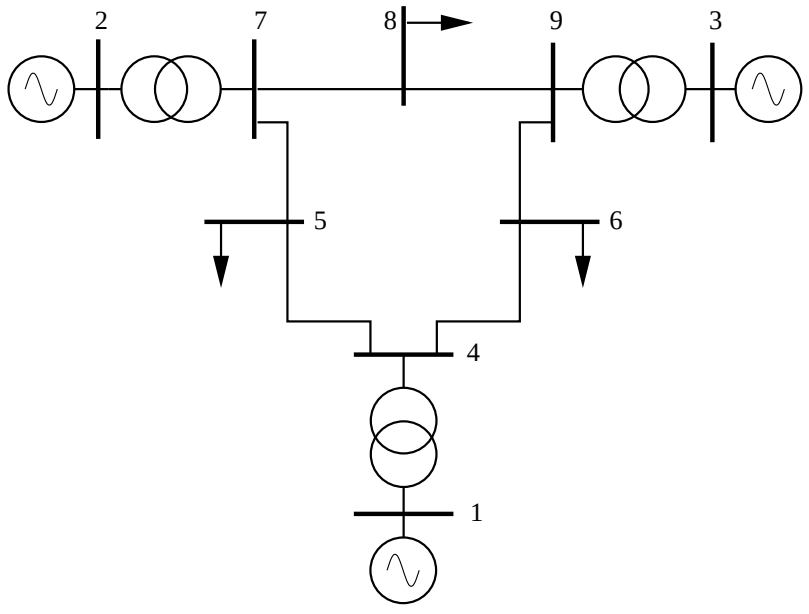

Figure 6.1: The Andersson-Fouad test system

With the loads located approximately halfway between the generators we can expect both mode observability (from frequency) and mode controllability to be small.

At 5s the system is excited by a fault at bus 8 which is removed after 0.1s. In Figure 6.2 the frequency deviations at the loads are seen.

Introducing damping by means of load control at all load busses increases the damping significantly as seen in Figure 6.3. In this case the active modulation was 5% of the load at each bus and no reactive covariation. Although the frequency deviation decays it settles with a peak value of at most 0.1 Hz. This large value can be explained by looking at the frequency deviation at the load busses (Figure 6.4). There it is seen that the frequency deviation at the load busses is small making the remaining oscillation invisible for the control system.

This is a structural problem that can only be solved by using other signals as feedback signals or by relocating the loads.

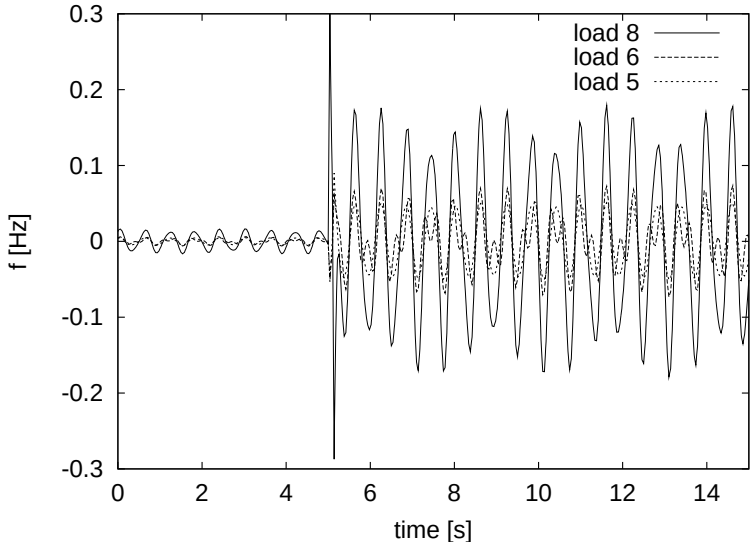

Figure 6.2: Load frequency deviation with no additional damping.

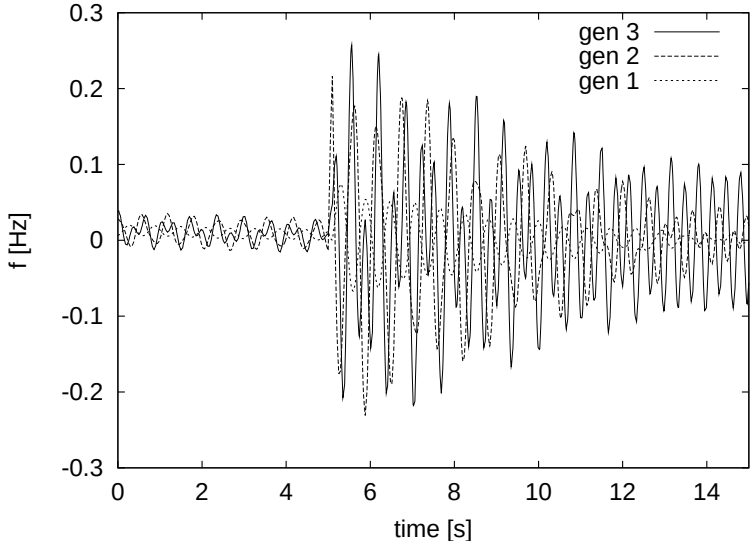

Figure 6.3: Generator frequency deviation with damping by load control.

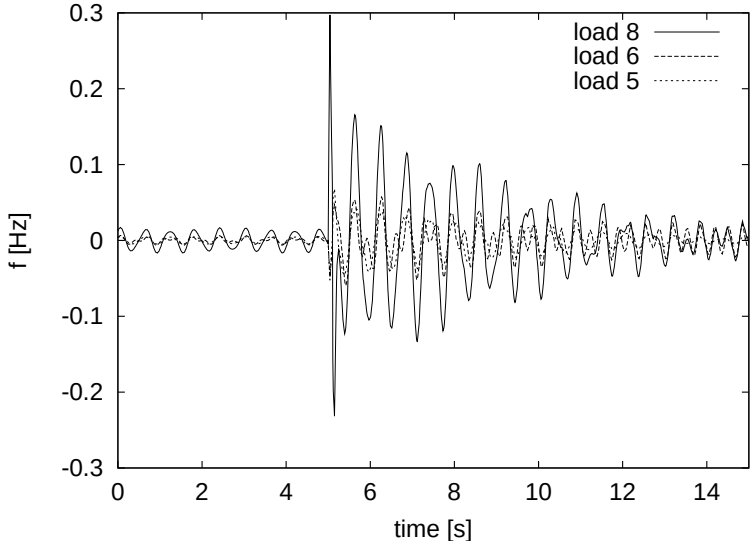

Figure 6.4: Load frequency deviation with damping by load control.

The sensitivity to reactive covariation for this system seems to be limited. In Samuelsson et al. (1995) it is shown that a two-machine system is most sensitive for reactive power modulation when the point of injection is located at the (mass-weighted) centre of the swing. This is obviously not the case here. A possible explanation is that in Samuelsson et al. (1995) there was a transfer of reactive power through the injection point for the damping power whereas the injection points in this simulation imports reactive power from both ends.

16-Machine system

This system is the simplified model of the NORDEL power system (Figure 6.5) developed in Akke (1989). This model differs from many other models in that the reactive loads are small (10 MVar) compared to the active loads (1-5 GW) Although unusual it is not improbable to have such a situation. In NORDEL the TSOs have the right to demand that the reactive power drawn from the transmission network should be zero.

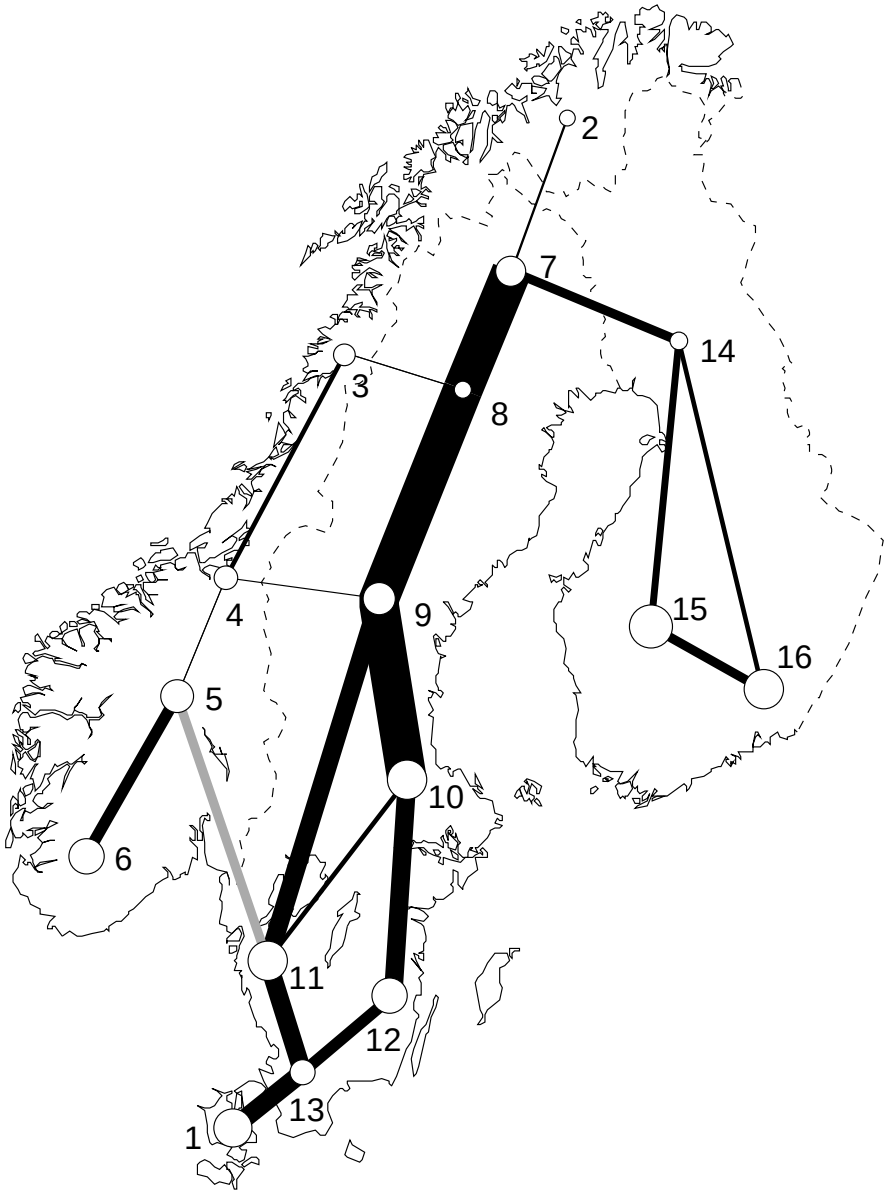

Figure 6.5: The 16-bus NORDEL test system. The area of the busses corresponds to the amount of stored energy in the generators connected to that bus. For each of the lines, the width of the line corresponds to the admittance of that line; thick line = short electrical distance.

Simulation setup

The generators are described by third order models. All generators are equipped with voltage controllers but PSSs are turned off in order to get a more oscillatory system. All loads are equipped with load control using local frequency as input. The amount of load used for control is 2% or 4% of the active load at each load bus. The reactive variation is 0, 25%, 50% or 75% of the active variation. From Chapter 5 we find that for small deviations, the change in apparent power has a direction of $5 - 15°$. With 50% reactive covariation, corresponding to the change in apparent power having an angle of $28°$ this should be more than enough to cover a worst case scenario.

The system is excited at 10s by a fault on the line between bus 5 and bus 6 (southern Norway). The fault is removed after 0.1s and the power on the line between bus 5 and bus 11 (grey in Figure 6.5) is studied.

Analysis

In Figure 6.6 (top) it is seen that the damping is increased considerably when using only 2% of the load power for damping enhancement. It can also be seen that the system is sensitive to reactive covariation. For the studied case, the reactive covariation deteriorates the performance compared to a case without reactive covariation. Comparing the results from the case without additional damping and additional damping with reactive covariation, we notice that the result with reactive covariation is still superior to the case without additional damping.

Increasing the amount of damping power to 4% of the total load the damping is further increased. Comparing 4% active load and 50% reactive covariation with 2% active load and no reactive covariation (Figure 6.6 bottom) it is seen that the increased damping is only visible during the first 4 swings. After this the two cases behave quite similarly. Keeping the reactive covariation small is thus an important goal as it will allow the controller to use a smaller amount of power.

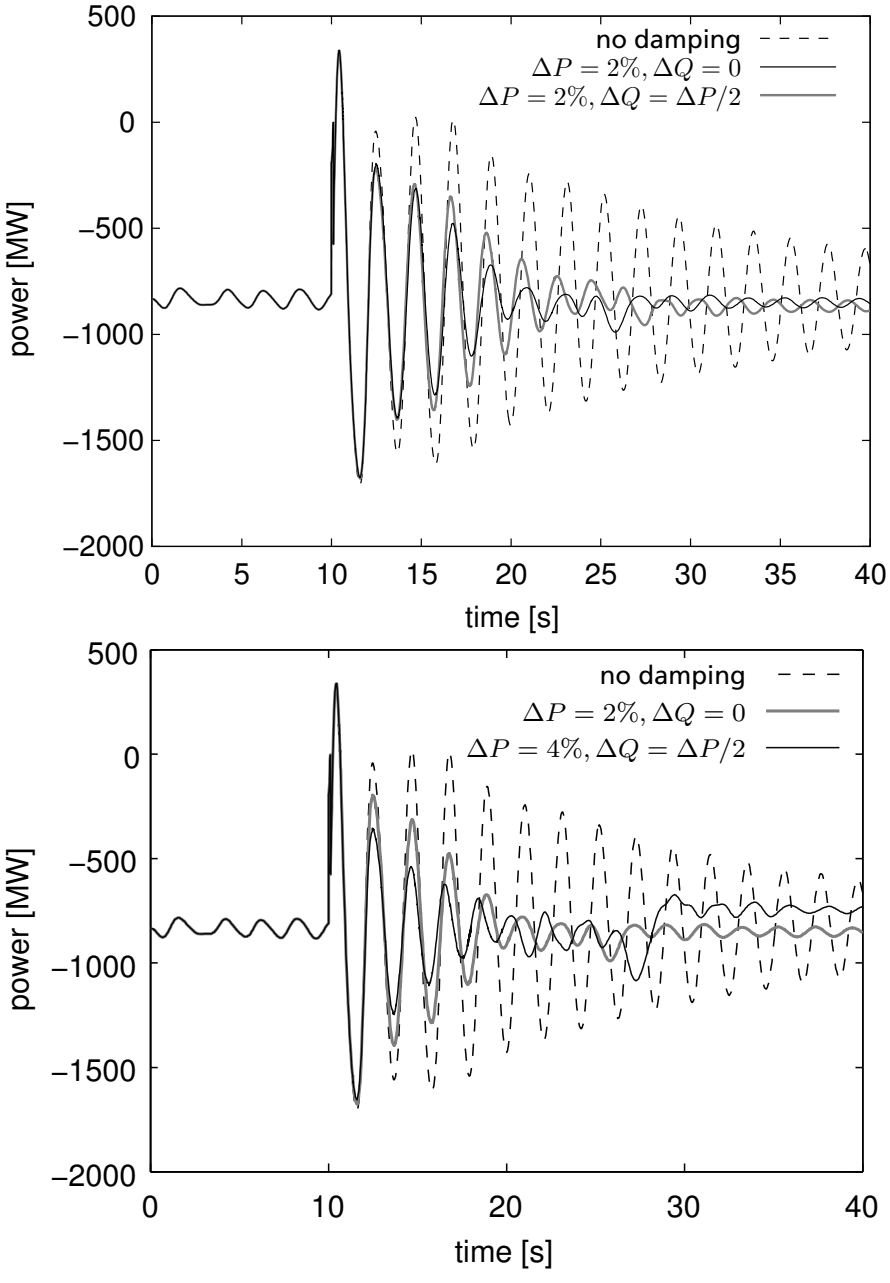

Figure 6.6: Power oscillations on one connection between Sweden and Norway.

6.3 Conclusions

It has been shown that applying load control based on local frequency measurements increases the damping in the two test cases. The influence of reactive covariation is largely dependent on network topology and load location. The practical influences of the reactive covariation is governed by the cost of damping power and control equipment in that low-cost power and equipment reduces the need of small reactive covariation. When small reactive covariation is required, local control is infeasible as prediction of reactive covariation requires local system knowledge and thus communication. Actuator location is also important for reactive covariation. In Samuelsson (1997) it is argued that the dampers should be located as close as possible to the swinging generators. In case this is unfeasible actuator location can be studied by the method described in Smed (1993).

Controller interaction is not studied. Although it is highly probable that better damping can be achieved by only using a few dampers, the results obtained with dampers at all nodes is superior to the poorly damped cases.

The use of load control is only useful for damping enhancement. The influence on transient stability is non existent due to the amount power used for damping is much smaller than the power in the swings.

Implementation of one of the proposed schemes depends largely on what payback one can expect and what kind of load that is chosen. For residential loads, a variant with a controller at the closest transformer is probably the cheapest. The controller will then send two different frequencies on top of the fundamental frequency, one frequency to turn on load and one to turn off load. The expensive part will then be in the transformer station whereas the additional cost for the appliances to be controlled can be held low.

Chapter 7

Concluding remarks

The topic of this thesis is power system oscillations and more precisely, how to minimize the effects of the oscillations. Oscillations are studied in different timescales, each one requiring its own treatment. First a summary of the obtained results is given. Second, some topics for future research in the area of power system oscillations are provided.

7.1 Summary of results

Detection

Swing detection strives to answer the question; is the present situation due to a power swing? Detection of power swings is a slow process since a power swing is a slow phenomenon compared to faults. For fast response it is often feasible to rephrase the question into; is the present situation caused by a fault? In this context, a power swing is regarded as a normal albeit undesirable operating condition. Based on this, a new idea for distinguishing faults from power swings in distance protection relays is presented. The principle is based on a change of coordinate system to a system that is more suitable for distinguishing faults from power swings. It should be noted that the proposed method only works for large power swings, that is, when there is a risk to mix up faults with power swings. The new detector performs well for low impedance faults in a line. In

case of parallel lines and low impedance faults the detector on the faulted line will indicate a fault. The detector on the parallel healthy line will, however, not always detect the situation as a fault. This is due to the location and impedance of the fault together with source impedances.

Estimation

Estimation of the frequency and damping for the electro-mechanical modes in a power system can be performed on data from large disturbances, ring down analysis, or from data collected during normal operation, ambient analysis. Benefits with ambient analysis is the possibility to get information about the system without probing it. This can be used for planning studies and model calibration. The use of ambient analysis also makes real-time monitoring of oscillation frequency and damping possible. Detection of low damping can then alarm operators or enable special protection schemes. A drawback with ambient analysis is that the system might be poorly excited making it difficult to estimate the parameters.

It is shown in case studies on measured data that real-time monitoring of electro-mechanical oscillation frequency and damping is possible, at least for single mode systems. It is also discussed that the interpretation of the results are often easier to perform in the frequency domain rather than using pole locations. For very lightly damped systems it is, however, possible to evaluate the system from the pole locations only. Using spectral estimates does, however, contribute a lot to the general understanding of the system behaviour.

Damping estimation can be done from any system wide measured quantity. For load-control it interesting to use local frequency as an indicator of poorly damped dynamics. Limits on resolutions are derived and compares well to measurements.

Control

Control of active power on end-user loads in order to enhance the damping of lightly damped electro-mechanical modes in a power system is pursued. For the control to be effective, the variation of reactive power at the transmission level

should be kept small while the variation of active power should be large. The distribution network will, however, contribute with some change in reactive power when active end-loads are changed.

The change in reactive power contributed by the distribution network is studied. In the timescale of a power swing, admittance type load behaviour can be expected. For this case it is shown that the angle between the positive sequence voltages at the load and the feeding bus is a good measure of the reactive covariation. It is also shown when this approximation is valid for constant power type loads. When evaluated on a test system, the accuracy for changes at least up to 10% is good.

The results derived above are used to mimic the behaviour of distribution networks subject to end-load control when simulating transmission system behaviour. Two systems are investigated, a three-machine test system and a 16-machine system derived from the NORDEL system. For both cases, the damping is considerably enhanced when using load modulation based on local bus frequency.

The three-machine system is relatively insensitive to variations in reactive power. The sensitivity to variations in active power is, however, also limited. The latter behaviour is due to the location of the loads being close to the (mass-weighted) centre of the swing modes. This also reduces the mode observability.

The 16-machine system is sensitive to reactive variation, the performance is, however, not severely deteriorated. The sensitivity to active variations is high which can be seen from the fact that using only 2% of the available active load for load modulation enhances the damping significantly. Even when the reactive covariation is increased to unreasonable levels, the performance compared to the case without load modulation is superior.

7.2 Future work

The detection algorithm is derived under the simplified assumption that the apparent impedance moves on a circle. As seen in the case studies it works well even on multiple circles and “close to circles” (poleslipping). The performance needs, however, to be evaluated on more realistic data. The detector today is

only a fault/non-fault detector. The possibility to predict out-of-step conditions should be investigated. This can be done by using the angle formed by the lines between the origin and the circle centre and the circle centre and the impedance. This angle is a measure of the angle between the generator and the centre of inertia. The angle and its derivative could then be used in the same way as generator angle and speed to predict a pending loss of synchronism.

The techniques used to estimate frequency and especially damping can be described as brute force methods. As shown here and in Wies et al. (2003) determination of damping is difficult, especially when damping is high or excitation is low. Fundamental limits on when damping estimation is possible would prove useful and will possibly give insight to better methods to estimate damping. The driving forces for small oscillations, that is the random load variations, should be investigated. So far white noise has been assumed which probably is a poor assumption. More work in the spirit of Johansson and Martinsson (1986) needs to be done in order to tune the estimators. Estimators using more than one input signal should be investigated in order to see what benefits that can be gained in accuracy and estimation speed.

Load control is simulated with loads mimicing the behaviour of an aggregated load subject to load modulation. More detailed analysis should be performed in order to verify the behaviour of the aggregated load. This should also include dynamic loads as the dynamics of loads can influence the damping substantially which can be seen in Hiskens and Milanovic (1997). For local control the need of high precision frequency measurements where the signal is subjected to phase jumps needs to be addressed.

Bibliography

PES Winter Meeting (2000). *IEEE Power Engineering Society Winter Meeting. Conference Proceedings*. 140, 142

Akaike, H. (1974). A new look at the statistical model identification. *IEEE Transactions on Automatic Control*, vol. 19, no. 6, pp. 716–723. 53

Akke, M. (1989). Power System Stabilizers in Multimachie Systems. Lic Thesis, Dept of Automatic Control, Lund University, Sweden. 121, 130

Anderson, P. M. and Fouad, A. A. (1993). *Power System Control and Stability*. IEEE. 121, 127

Bendat, J. S. and Piersol, A. G. (1980). *Engineering Applications of Correlation and Spectral Analysis*. John Wiley & sons. 42

Bounou, M., Lefebvre, S. and Malhame, R. (1992). A spectral algorithm for extracting power system modes from time recordings. *IEEE Transactions on Power Systems*, vol. 7, no. 2, pp. 665–683. 60

Cao, L. and Schwartz, H. M. (2000). A directional forgetting algorithm based on the decomposition of the information matrix. *Automatica*, vol. 36, no. 11, pp. 1725–31. 30, 65, 66, 82, 87

Centeno, V., de la Ree, J., Phadke, A., Michel, G., Murphy, R. and Jr., R. B. (1993). Adaptive out-of-step relaying using phasor measurement techniques. *IEEE Computer Applications in Power*, vol. 6, no. 4, pp. 12–17. 21

Centeno, V., Phadke, A., Edris, A., Benton, J., Gaudi, M. and Michel, G. (1997). An adaptive out-of-step relay [for power system protection]. *IEEE Transactions on Power Delivery*, vol. 12, no. 1, pp. 61–71. 21

Chui, C. K. and Chen, G. (1999). *Kalman Filtering with Real-Time Applications*. Springer Series in Information Sciences.Vol. 17. Springer. 67

Claesson, I., Eriksson, P., Mandersson, B. and Salomonsson, G. (1990). *Analog Circuits and Signals*. Studentlitteratur. In Swedish. 48

Clarke, E. (1945). Impedances Seen by Relays during Power Swings with and without Faults. *AIEE Transactions*, vol. 64, pp. 372–384 +471–472. 14, 21

Cutsem, T. V. and Vournas, C. (1998). *Voltage Stability of Electric Power Systems*. Kluwer Academic Publishers. 111

Dash, P. K., Pradhan, G. P. A. K., Routray, A. and Duttagupta, B. (2000). An extended Kalman filter for frequency measurement of distorted signals. In PES Winter Meeting (2000). 67

Dous, G. L. (1999). Voltage stability in power systems. Lic Thesis, Dept of Electric Power Systems, Chalmers Göteborg Sweden. 101

Goodwin, G. C. and Payne, R. L. (1977). *Dynamic System Identification, Experiment Design and Data Analysis*. Academic Press. 26

Haner, J., Laughlin, T. and Taylor, C. (1986). Experience with the R-Rdot out-of-step relay. *IEEE Transactions on Power Delivery*, vol. PWRD-1, no. 2, pp. 35–39. 12, 17

Hansson, M. and Salomonsson, G. (1997). A multiple window method for estimation of peaked spectra. *IEEE Transactions on Signal Processing*, vol. 45, no. 3, pp. 778–781. 58

Hauer, J., Demeure, C. and Scharf, L. (1990). Initial results in prony analysis of power system response signals. *IEEE Transactions on Power Systems*, vol. 5, no. 1, pp. 80–9. 41

Hauer, J., Hughes, F. J., Trudnowski, D., Rogers, G., Pierre, J., Scharf, L. and Litzenberger, W. (1998). *A Dynamic Information Manager for Networked Monitoring of Large Power Systems*. Tech. Rep. WO 8813-01, EPRI. 42

Hemmingsson, M. (2001). *Estimation of Electro-Mechanical mode parameters using frequency measurements*. Tech. Rep. TEIE-7141, Dept of Industrial Electrical Engineering & Automation, Lund University, Sweden. 6

Hemmingsson, M., Samuelsson, O., Pedersen, K. O. H. and Nielsen, A. H. (2001). Estimation of electro-mechanical mode parameters using frequency measurements. In *IEEE Power Engineering Society Winter Meeting. Conference Proceedings*. 6

Hill, D. J. (1993). Nonlinear dynamic load models with recovery for voltage stability studies. *IEEE Transactions on Power Systems*, vol. 8, no. 1, pp. 166–176. 101

Hiskens, I. and Milanovic, J. (1997). Locating dynamic loads which significantly influence damping. *IEEE Transactions on Power Systems*, vol. 12, no. 1, pp. 255–262. 4, 138

Ilar, F. (1981). Innovations in the detection of power swings in electrical networks. *Brown Boveri Review*, vol. 68, no. 2, pp. 87–93. 15

Ilar, F. and Metzger, F. (1984). European patent no 0 057948 b1, us patent 4,426,670. 15

Johansson, K. and Martinsson, B. (1986). *Measurement and Validation of Load-Variations*. Master's thesis, Dept of Electric Power Systems, Chalmers Göteborg Sweden. in Swedish. 43, 49, 50, 97, 138

Johansson, R. (1993). *System Modeling and Identification*. Englewood Cliffs, N.J. Prentice Hall. 98

Jonsson, M. and Daalder, J. (2001). A new protection scheme to prevent maltrips due to power swings. In *2001 IEEE/PES Transmission and Distribution Conference and Exposition*, vol. 2, pp. 724–730. IEEE. 17

Julier, S. J. (1997). *Process Models for the Navigation of High-Speed Land Vehicles*. Ph.D. thesis, University of Oxford, England. 67

Karlsson, D. and Hill, D. J. (1994). Modelling and identification of nonlinear dynamic loads in power systems. *IEEE Transactions on Power Systems*, vol. 9, no. 1, pp. 156–166. 49, 101

Kautz, W. H. (1951). Transient synthesis in time domain. *IRE Transactions on Circuit Theory*, vol. 1, no. 3, pp. 29–39. 56

Kosterev, D. N., Taylor, C. W. and Mittelstadt, W. A. (1999). Model validation for the august 10, 1996 wscc system outage. *IEEE Transactions on Power Systems*, vol. 14, no. 3, pp. 967–979. 89, 95, 97

Kumaresan, R. and Tufts, D. W. (1982). Estimating the parameters of exponentially damped sinusoids and pole-zero modeling in noise. *IEEE Transactions on Acoustics, Speech, and Signal Processing*, vol. 30, no. 6, pp. 833–40. 52, 53

Lacoss, R. (1971). Data adaptive spectral analysis methods. *Geophysics*, , no. 36. 57

Larsson, M. (2001). *Coordinated Voltage Control in Electric Power Systems*. Ph.D. thesis, Dept of Industrial Electrical Engineering & Automation, Lund University, Sweden. http://www.iea.lth.se/publications. 108, 125

Ledwich, G. and Palmer, E. (2000). Modal estimates from normal operation of power systems. In PES Winter Meeting (2000), pp. 1527–31. 43, 79

Lee, K. and Poon, K. (1988). Analysis of transient swings in large interconnected power systems by Fourier transformation. *IEEE Transactions on Power Systems*, vol. 3, no. 4, pp. 1573–1579. 62

Lee, K. and Poon, K. (1990). Analysis of power system dynamic oscillations with beat phenomenon by Fourier transformation. *IEEE Transactions on Power Systems*, vol. 5, no. 1, pp. 148–153. 62

Ljung, L. and Söderström, T. (1983). *Theory and Pratice of Recursive Identification*. The MIT Press Cambridge, Massachusetts. 65, 98

Machowski, J. and Nelles, D. (1992). Deutsches patent de 41 00 646 a1. 15

Machowski, J. and Nelles, D. (1997). New power swing blocking method. In *Sixth International Conference on Developments in Power System Protection*. IEE. 15

Middleton, R. and Goodwin, G. (1990). *Digital Control and Estimation, -a Unified Approach*. Prentice Hall. 56

Minakawa, T., Sato, M., Ichikawa, Y. and Ishihara, Y. (1999). A new method for detecting loss of synchronism using power and current measured on a line. *IEEE Transactions on Power Delivery*, vol. 14, no. 1, pp. 68–73. 19, 20

Moore, P. and Johns, A. (1996). New method of power swing blocking for digital distance protection. *IEE Proceedings Generation, Transmission and Distribution*, vol. 143, no. 1, pp. 19–26. 16

Murthi, M. N. and Rao, B. D. (2000). All-pole modeling of speech based on the minimum variance distortionless response spectrum. *IEEE Transactions on Speech and Audio Processing*, vol. 8, no. 3, pp. 221–239. 57

Nishiyama, K. (1997). A nonlinear filter for estimating a sinusoidal signal and its parameters in white noise: On the case of a single sinusoid. *IEEE Transactions on Signal Processing*, vol. 45, no. 4, pp. 970–981. 67

on Load Representation for Dynamic Performance, I. T. F. (1993). Load representation for dynamic performance analysis. *IEEE Transactions on Power Systems*, vol. 8, no. 2, pp. 472–482. 101

on Load Representation for Dynamic Performance, I. T. F. (1995). Bibliography on load models for power flow and dynamic performance simulation. *IEEE Transactions on Power Systems*, vol. 10, no. 1, pp. 523–538. 101

O'Shea, P. (2000). The use of sliding spectral windows for parameter estimation in power system disturbance monitoring. *IEEE Transactions on Power Systems*, vol. 15, no. 4, pp. 1261–1267. 62

O'Shea, P. (2002). A high-resolution spectral analysis algorithm for power-system disturbance monitoring. *IEEE Transactions on Power Systems*, vol. 17, no. 3, pp. 676–680. 62

Parkum, J. E. (1992). *Recursive Identification of Time-Varying Systems*. Ph.D. thesis, Dept of Informatics and Mathematical Modelling, Technical University of Denmark. 65, 66

Pierre, D., Trudnowski, D. and Hauer, J. (1992). Identifying linear reduced-order models for systems with arbitrary initial conditions using prony signal analysis. *IEEE Transactions on Automatic Control*, vol. 37, no. 6, pp. 831–5. 41

Pierre, J. W., Trudnowski, D. J. and Donnelly, M. K. (1997). Initial results in electromechanical mode identification from ambient data. *IEEE Transactions on Power Systems*, vol. 12, no. 3, pp. 1245–51. 41

Poage, F. C., Streifud, C. A., McGregor, D. M. and George, E. E. (1943). Performance Requirements for Relays on Unusually Long Transmission Lines. *AIEE Transactions*, vol. 62, pp. 275–283. 14, 21, 23

Proakis, J. G. and Manolakis, D. G. (1988). *Introduction to Digital Signal Processing*. New York Macmillan. 52, 74

Rao, B. D. (1988). Perturbation analysis of an svd-based linear prediction method for estimating the frequencies of multiple sinusoids. *IEEE Transactions on Acoustics, Speech, and Signal Processing*, vol. 36, no. 7, pp. 1026–35. 54

Redfern, M. and Checksfield, M. (1995). A new pole slipping protection algorithm for dispersed storage and generation using the equal area criterion. *IEEE Transactions on Power Delivery*, vol. 10, no. 1, pp. 194–202. 18, 19

Redfern, M. and Checksfield, M. (1998). A study into a new solution for the problems experienced with pole slipping protection [of synchronous generators]. *IEEE Transactions on Power Delivery*, vol. 13, no. 2, pp. 394–404. 18, 19

Rissanen, J. (1978). Modeling by shortest data description. *Automatica*, vol. 14, no. 5, pp. 465–71. 53

Romero Navarro, I. (2002). Dynamic load models for power systems. Lic Thesis, Dept of Industrial Electrical Engineering & Automation, Lund University, Sweden http://www.iea.lth.se/publications. 101, 103

Rovnyak, S., Taylor, C. and Sheng, Y. (2000). Decision trees using apparent resistance to detect impending loss of synchronism. *IEEE Transactions on Power Delivery*, vol. 15, no. 4, pp. 1157–1162. 18

Samuelsson, O. (1997). *Power System Damping, Structural Aspects of Controlling Active Power*. Ph.D. thesis, Dept of Industrial Electrical Engineering & Automation, Lund University, Sweden. http://www.iea.lth.se/publications. 6, 83, 121, 123, 134

Samuelsson, O. (1999). *Wide Area Measurements of Power System Dynamics; The North American WAMS Project and its Applicability to the Nordic Countries*. Tech. Rep. 99:50, Elforsk. 3

Samuelsson, O. and Eliasson, B. (1997). Damping of electro-mechanical oscillations in a multimachine system by direct load control. *IEEE Transactions on Power Systems*, vol. 12, no. 4, pp. 1604–9. 121

Samuelsson, O., Eliasson, B. and Olsson, G. (1995). Power oscillation damping with controlled active loads. In *Stockholm Power Tech International Symposium on Electric Power Engineering*, vol. 5, pp. 275–279. IEEE. 130

Sanchez-Gasca, J. J. and Chow, J. H. (1999). Performance comparison of three identification methods for the analysis of electromechanical oscillations. *IEEE Transactions on Power Systems*, vol. 14, no. 3, pp. 995–1002. 41

Scala, B. F. L. and Bitmead, R. R. (1996). Design of an extended Kalman filter frequency tracker. *IEEE Transactions on Signal Processing*, vol. 44, no. 3, pp. 739–742. 67

Scala, B. F. L., Bitmead, R. R. and Quinn, B. G. (1996). An extended Kalman filter frequency tracker for high-noise environments. *IEEE Transactions on Signal Processing*, vol. 44, no. 2, pp. 431–434. 67

Smed, T. (1993). Feasible eigenvalue sensitivity for large power systems. *IEEE Transactions on Power Systems*. 134

Taylor, C., Haner, J., Hill, L., Mittelstadt, W. and Cresap, R. (1983). A new out-of-step relay with rate of change of apparent resistance augmentation. *IEEE Transactions on Power Apparatus and Systems*, vol. PAS-102, no. 3, pp. 631–639. 12, 17

Taylor, C. W. (1994). *Power System Voltage Stability*. McGraw-Hill. 111

Thomson, D. J. (1982). Spectrum esimation and harmonic analysis. In *Proceedings of the IEEE*, vol. 70, pp. 1055–1096. 58

Wahlberg, B. (1991). Identification of resonant systems using Kautz filters. In *Proceedings of the 30th IEEE Conference on Decision and Control*, vol. 2, pp. 2005–2010. IEEE. 56

Welfonder, E., Hall, B. and Neifer, R. (1994). Influence of the frequency and voltage dependence of load part systems on the control behaviour of power systems during emergency conditions. In G. Goodwin and R. J. Evans, eds.,

Proceeding of the 12th Triennial World Congress of the International Federation of Automatic Control, 1993, vol. 6, pp. 259–266. 103

Welfonder, E., Weber, H. and Hall, B. (1989). Investigations of the frequency and voltage dependence of load part systems using a digital self-acting measuring and identification system. *IEEE Transactions on Power Systems*, vol. 4, no. 1, pp. 19–25. 103

Wies, R. W., Pierre, J. and Trudnowski, D. (2003). Use of ARMA block processing for estimating stationary low-frequency electromechanical modes of power systems. *IEEE Transactions on Power Systems*, vol. 18, no. 1, pp. 167–173. 138

Appendix A

Abbreviations

$AR(p)$	AutoRegressive model $y(k) = a_1 y(k-1) + \ldots + a_p y(k-p) + e(k)$
$ARMA(p,q)$	AutoRegressive MovingAverage model $y(k) = a_1 y(k-1) + \ldots + a_p y(k-p) + c_0 e(k) + \ldots + c_q e(k-q)$
λ	Eigenvalue or forgetting factor
σ	real part of eigenvalue or singular value of a matrix
ω	imaginary part of eigenvalue
θ	Vector of estimated parameters or voltage angle
P	Active power
$P(\omega)$	Power spectrum estimate
$\mathbf{P}$	Approximate covariance for parameters in RLS methods
$\mathbf{R}$	Covariance matrix for a signal
AVR	Automatic Voltage Regulator
EKF	Extended Kalman Filter
EM	Electro-Mechanical

FFT	Fast Fourier Transform
HVDC	High Voltage Direct Current
LP	Linear Prediction
LS	Least Squares
NORDEL	Co-opertion council for the transmission operators in Denmark, Finland, Iceland, Norway and Sweden.
PMU	Phasor Measurement Unit
PSS	Power System Stabilizer (add-on to AVR)
RLS	Recursive Least Squares
SNR	Signal to Noise Ratio
SVC	Static Var Compensator
SVD	Singular Value Decomposition
TSO	Transmission System Operator
WECC	Western Electricity Coordinating Council, formerly known as WSCC
WSCC	Western Systems Coordinating Council, transmission system on the west coast of North America